EFFECT OF HYPERLIPIDEMIA

ON DRONEDARONE DISPOSITION

By

YOUSEF ABDULLAH M BIN JARDAN

A thesis submitted in partial fulfillment of the requirements for the degree of

Doctor of Philosophy

in

Pharmaceutical Sciences

Faculty of Pharmacy and Pharmaceutical Sciences

University of Alberta

Abstract

The pharmacokinetics of dronedarone, effect of hyperlipidemia on dronedarone disposition and dronedarone tissue distribution in normolipidemic (NL) and hyperlipidemic (HL) rats were studied. Novel and sensitive HPLC-UV and LC-MS reverse phase assay methods were developed. Rat plasma (100 μL) was subjected to a one-step liquid-liquid extraction followed by separation of the residues after injection into C18 analytical columns. Both methods had excellent linear relationships between peak height ratios and plasma concentrations. The lower limit of quantification of HPLC-UV (dronedarone and desbutyldronedarone) and LC-MS (dronedarone) based on 100 μL of rat plasma were 25 ng/mL and 5 ng/mL, respectively. The HPLC method was then used to characterize the pharmacokinetic profile of dronedarone in the rat. Single doses were administered to rats intravenously (4 mg/kg), orally (55 mg/kg) and intraperitoneally (65 mg/kg). To induce hyperlipidemia (HL), some of the rats to be given oral dronedarone were administered intraperitoneal doses of poloxamer 407 (P407). Dronedarone was found to possess a high volume of distribution and moderate clearance in the rat. The drug showed poor bioavailability (<20%) after oral and intraperitoneal administration. HL increased dronedarone plasma concentrations measured by area under the plasma concentration vs. time curve. Tissue distribution and hepatic microsomal metabolism experiments were conducted to explore the cause of these changes in HL. After oral single doses of dronedarone, rats were anesthetized and plasma and tissue specimens (heart, lung and liver) were collected. Liver and intestinal microsomal proteins from control, P407 and dietary induced obese rats were harvested and used to measure velocity of desbutyldronedarone (metabolite) formation from dronedarone. HL increased the geometric mean area under the concentration vs. time curves of dronedarone by 2.3 to 5-fold. In tissues (heart, liver and lung), however, concentrations of drug selectively increased or decreased. Heart, the

site of action of the drug, had the highest levels of dronedarone. Reductions in liver and intestinal metabolic efficiency (intrinsic clearance) were observed in rats with increased serum lipids (P407 and dietary induced obese) rats compared to controls. The data suggested down regulation in enzymes involved in dronedarone metabolism occurs in the presence of increased lipid levels in the serum, which may explain the higher plasma concentrations in rats given P407.

Preface

This thesis is an original work by YOUSEF ABDULLAH M BIN JARDAN. The research project, of which this thesis is a part, received research ethics approval from the University of Alberta Research Ethics Board, Project Name "The Influence of lipids on the pharmacokinetics and pharmacodynamics of some representative lipoprotein binding drugs", No. AUP227 and A25. The method of dronedarone analysis in Methods and Materials section 2.2.1 was published as **Jardan YA**, Gabr RQ, Brocks DR., "Pharmacokinetics of dronedarone in rat using a newly developed high-performance liquid chromatographic assay method". Biomedical Chromatography. 2014 Aug;28(8):1070-4. Also, dronedarone pharmacokinetic study in section 2.4 was published as **Jardan YA**, Brocks DR.," The pharmacokinetics of dronedarone in normolipidemic and hyperlipidemic rats". Biopharmaceutics Drug Disposition. 2016 Sep;37(6):345-51. I was responsible for the experiments, data generation and collection as well as the manuscripts preparation. The rest of work has not been previously published.

Dedication

To my parents, Abdullah and Nourah

To my lovely wife and son Tagreed and Fahad

To my brothers and sisters

Acknowledgements

First of all, I would like to thank my supervisor Dr. Dion Brocks for his continuous guidance, help and support throughout the PhD program and my supervisory committee Dr. Ayman El Kadi and Dr. Arno Siraki for their guidance and support during the PhD program. Especially, Dr. Ayman for his help and guidance with microsome studies and for the unlimited accessibility of his laboratory facilities.

Also, I would like to thank my lab mates Dr. Raniah, Hetal, Mohammad, Ali, Marwa and Hamdah for having a friendly work environment in the lab.

Special thanks to Saudi Cultural Bureau, King Saud University for their financial support for my PhD research.

Lastly, I would like to deeply thank my wife (Tagreed) for her sincere encouragement, and emotional support throughout my study. Also, I am very grateful to my parents for their prayers and emotional support.

Contents

List of Tables

List of Figures

List of abbreviations and symbols

α	Level of significance
ºC	Celsius
µg	Microgram
µM	Micromolar
µL	Microliter
AM	Amiodarone
ANOVA	Analysis of variance
AV	Atrioventricular
AUC	Area under the curve
BMI	Body mass index
CETP	Cholesteryl ester transfer protein
CHOL	Cholesterol
CL	Clearance
CLint	Intrinsic clearance
CL/F	Oral Clearance
CM	Chylomicrons
Cmax	Maximum plasma drug concentration
CuSo4	Cupric sulfate
CV	Coefficient of variation
CYPs	Cytochrome P450
C18	Octadecylsilane column

DBD	Desbutyldronedarone
DR	Dronedarone
g	G-force
F	Oral bioavailability
fu	Unbound fraction
H2SO4	Sulfuric acid
HCl	Hydrochloric acid
HDL	High-density lipoprotein
HFCS	High fructose corn syrup (Group or liquid used)
HFD	Group provided high fat diet 45% kcal of fat and normal water
HFD/HFCS	Group provided high fat diet (45% kcal fat) with 13%w/v HFCS
HMG-CoAR	3-hydroxy-3-methylglutaryl coenzyme A reductase
HL	Hyperlipidemia
H_2O	Water
HPLC	High performance liquid chromatography
IBW	Ideal bodyweight
IDL	Intermediate density lipoprotein
ip	Intraperitoneal
IS	Internal standard
iv	Intravenous
KCl	Potassium chloride

Kg	Kilogram
Ki	The inhibition constant for inhibition
Km	The affinity constant
KH_2PO_4	Potassium dihydrogen phosphate
Kp	The tissue-to-plasma concentration ratios
L	Liter
LBW	Lean body weight
LCMS	Liquid chromatography-Mass spectrometry
LDL	Low-density lipoprotein
LDL-R	Low density lipoprotein receptor
Log *p*	Logarithm value of octanol/water partition coefficient
LOQ	Lower limit of quantification
LP	Lipoprotein
LPL	Lipoprotein lipase
Mate	Multidrug and toxin extrusion protein transporter
Mdr	Multiple drug resistance protein
MRT	Mean residence time
mg	Milligram
min	Minutes
mL	Milli liter
mRNA	Messenger RNA
m2	Square meters
Na2CO3	Sodium carbonate

NAPDH	Nicotinamide adenine dinucleotide phosphate tetra sodium
ng	Nanogram
NL	Normolipidemic
Oct	Organic cationic transporters
PCSK9	Proprotein convertase subtilisin/kexin type 9
PPAR	Peroxisome proliferator–activated receptor
PK	Pharmacokinetics
PD	Pharmacodynamics
PL	Phospholipids
Rpm	Rotations per minute
SA	Sinoatrial
SD	Standard deviation
t ½	Terminal elimination phase half-life
TBW	Total body weight
VLDL	Very low density lipoprotein
VLDL-R	Very low density lipoprotein receptor
TG	Triglycerides
Tmax	Time to reach maximum concentration
UV	Ultra-violet
Vd	Volume of distributuon
Vdss	Volume of distributuon at steady state
Vmax	The maximal rate of formation (capacity)
Vs	Versus

WHO	World Health Organization

Chapter1: Introduction

1.1. Lipid and lipoproteins

Lipid is an essential component in the normal mammalian diet. There are many forms of lipid, which is mainly composed of triglycerides (TG); phospholipids (PL); and cholesterol (CHOL). The main lipid part of both TG and PL is fatty acid. CHOL on the other hand possesses the sterol nucleus which is formed from catalysis of fatty acid molecules. All lipids have a structural role in the cells of the body. TG are also used for energy production by the body. While PL and CHOL mostly possess intracellular functions [1]. Triglycerides in food are absorbed from the intestines, metabolized to di and monoglycerides, then reprocessed by the Golgi bodies of enterocytes into chylomicrons (CM). Then, CM are transferred in the thoracic duct and gain access to the venous blood where they can be transported to adipose and liver [2].

Lipoproteins are classified based on the density and content of lipid, protein and apoprotein into CM, Very Low Density Lipoproteins (VLDL), Intermediate Density Lipoproteins (IDL), Low Density Lipoproteins (LDL) and High-Density Lipoproteins (HDL)[3-5]. Lipoproteins are mainly produced by the liver except CM which is synthesized by the enterocytes [1,5].

Table 1: Characteristics of plasma lipoproteins

Lipoprotein	Density(g/mL)	Size(Å)	Protein %	Lipid %		
				TG %	CHOL %	PL %
CM	0.95	800–5000	1	88	4	7
VLDL	0.95–1.006	300–800	8	54	22	16
LDL	1.019–1.063	180–280	20	11	46	22
HDL	1.063–1.210	50–120	50	4	20	26

Adapted from [3].

Table 2: Mean normal levels of Triglyceride and Cholesterol in human and rat

Species	Triglyceride (mmol/L)	Cholesterol (mmol/L)
Human	1.04	3.72
Rat	1.23	1.47

Adapted from [6].

The LDL receptor (LDL-R) group consists of more than ten receptors [7]. Five of these are known to bind to lipoproteins including very low density lipoprotein receptors (VLDLR). They are synthesized by the Golgi bodies and transported to the cell membranes by vesicles. Once recognition of their substrates occurs, the receptors bind and capture the substrates intracellularly by vesicles [7,8]. After that, the vesicle formed will transported into lysosomes and disrupted. This allows for the release of the lipids into the cytoplasm. The receptors simultaneously will return to the cell membrane to bind another substrates (Figure 1) [7]. These receptors have different

distributions within tissues. For example, LDL-R is found in almost all tissues except thyroid, adipose and salivary gland. On the other hand, VLDL-R is rich in heart, muscle, adipose, macrophages and brain but not expressed in liver [7].

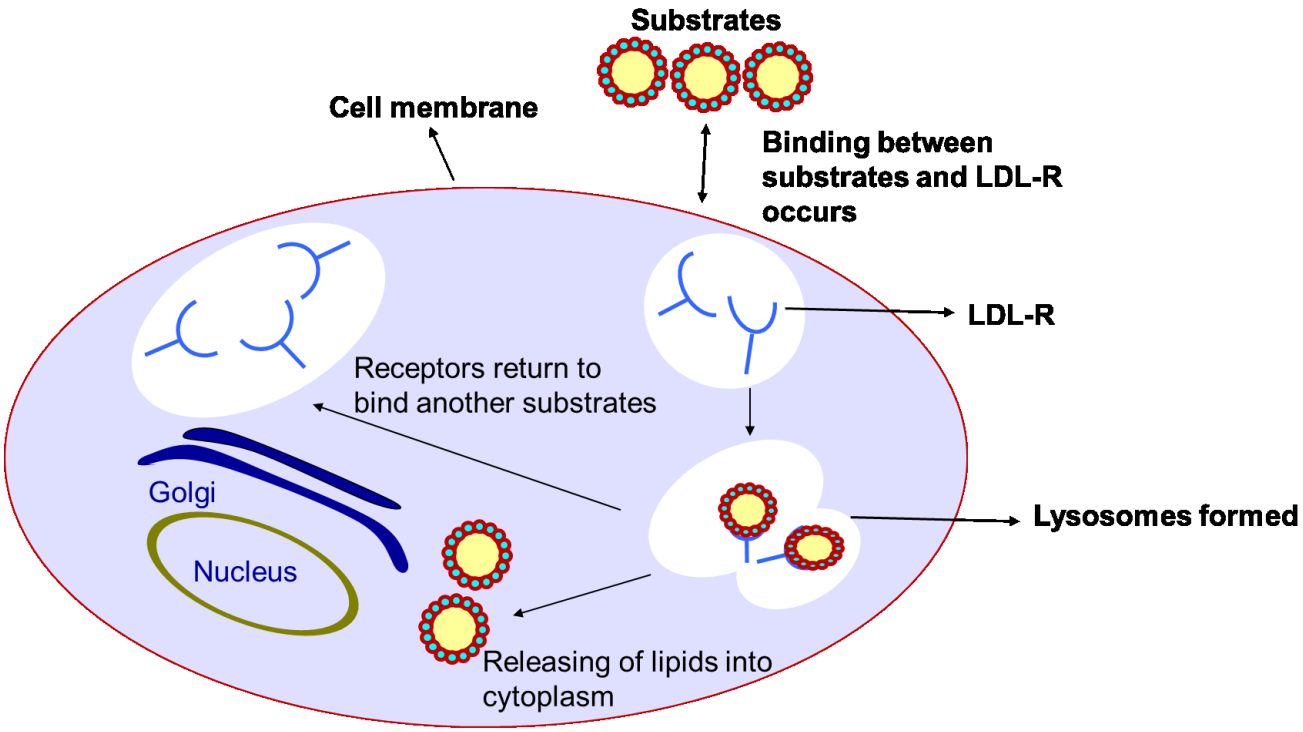

Figure 1: An illustration explained LDL-R binding with substrates.

1.2. Hyperlipidemia

Hyperlipidemia (HL) is a condition distinguished by elevation of plasma lipoproteins in the bloodstream. It is caused by either genetics (familial or primary hyperlipidemia) or from non-healthy diet, diseases, and drugs (secondary hyperlipidemia). According to the Fredrickson classification, familial or primary HL is classified based on the pattern of separation of lipoproteins after ultracentrifugation or electrophoresis.[3,9-12]. There are many medical conditions which are associated with HL including pregnancy, diabetes mellitus, hypothyroidism, malaria, HIV/AIDS, and obesity [3,13] . Moreover, HL can be developed by using some medications such as corticosteroids, estrogens, birth control pills, isotretinoin, beta blockers, anti-HIV medications, immunosuppressants and some diuretics [3,13]. HL is considered as a major risk factor of atherosclerosis and ischemic heart disease [13-15]. Atherosclerosis (Figure 2) is caused mainly through a sequence of events starting with alteration of low density lipoproteins (LDL) in arterial walls by oxidation and nonenzymatic glycation. The mildly oxidized LDL (OxLDL) recruits monocytes in the arterial endothelium, which causes transformation of the monocytes into macrophages. Macrophages accelerate LDL oxidation; alter the regulation of LDL receptors, Apo lipoprotein B accumulation and making them insensitive to the increase in cellular levels of cholesterol (CHOL). Moreover, OxLDL induces plasminogen inhibitor levels accelerating coagulation, inducing vasoconstrictor endothelin expression, and inhibiting nitric oxide expression. These reactions lead to heavy accumulations of CHOL and formation of CHOL-laden cells which called foam cells which form the fatty streaks. As the fatty streaks increased, the surrounding smooth and fibrous muscle tissues proliferate and form larger plaques, a process aggravated by release of inflammatory substances from macrophages [1,13,16].

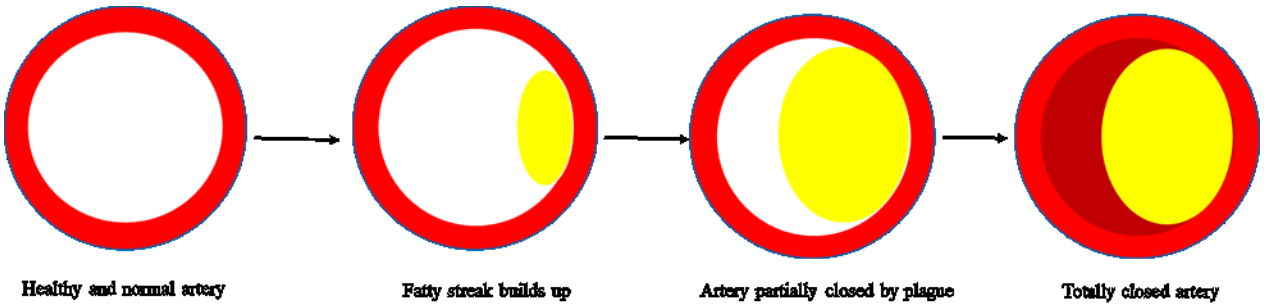

Figure 2: An illustration detailing progression of atherosclerosis in blood vessels.

1.2.1. Animal models used to assess the effects of hyperlipidemia

Many animal models have been used to induce HL. HL can be induced by high fat diet [17,18] administrating compounds like poloxamer 407 (P407) or Triton to the animals [19-21] and by genetic manipulation of animal species [22,23]. The feeding of high fat diet to rats or hamsters has been widely used as an experimental model to induce HL [17]. High fat diet may consist of lard cholesterol, sodium cholate and pulverized food given for 4 weeks or 33.0% (cal) fat given for 8 weeks [17,24]. The major practical disadvantage of high fat models is that animals must be fed for four or up to eight weeks to reach higher serum lipid levels. Many animal species are also relatively resistant to the development of HL. High fat diet may cause chronic inflammation to the animal which increases liver function enzymes (aspartate aminotransferase (AST) and alanine aminotransferase (ALT) [18,21]. This may present a confounding variable that might have to be considered in evaluating results from the use of the model (given most HL patients do not have liver damage).

Injection of a surfactant like Triton is another model to induce HL, Triton works by inhibiting lipoprotein lipase (LPL) enzymes, which are responsible for triglyceride metabolism [21] A single dose of Triton effectively elevates lipid levels by to about 10-fold. Levine et al found that Triton WR 1339 (polyoxyethylene ether of alkyl phenol) required more than twice weekly injections to get high serum cholesterol and triglycerides levels [21]. Unfortunately, toxicity (hemolysis) has been reported with Triton-W1339 which limit its use for investigational purposes [25]. Chemicals and biological agents such as isotretinoin, nicotine, polychlorinated biphenyls, estrogen, tumor necrosis factor, copper, pertussis toxin, histamine receptor agonists, carbon disulfide and ethanol have also been used to induce HL [26-28]. P407 is known to induce experimental HL in many species including rabbit [29], rat [20], and mouse [30]. Another method that might be used to induce and increase the lipids is by giving lipid directly to the systemic circulation as infusion.

P407, widely used in drug delivery applications, is a block copolymer consisting of repeated polyoxypropylene and polyoxyethylene units [31]. Injection of P407 intraperitoneally (ip) into rodents quickly (within 24 h) causes a profound state of HL . The P407 model is reversible in nature, dose-dependent and an inert model of HL [32]. After injection of a single dose increased concentrations of lipoprotein cholesterol, total cholesterol (TC) and triglyceride (TG) occurs [32,33].

Table 3: Different experimental animal models of HL

Model	Treatment	Duration
Poloxamer P407 1g/kg	Single 1g/kg	36 h post dose
Triton WR1339	Single 250mg/kg	24 h post dose
Poloxamer P407	Single 0.4 g/kg	24 h post dose
High fat diet	Food consist of lard, cholesterol, sodium cholate and pulverized food	for 4 weeks
High fat diet	33.0% (cal) fat	for 8 weeks

1.2.2. P407- induced HL

P407 induces HL directly by inhibiting LPL, an enzyme which prompts the hydrolysis of TG . Also, P407 stimulates indirectly 3-hydroxy-3-methylglutaryl coenzyme A reductase (HMG-CoAR) which is essential for the biosynthesis of cholesterol [29,34].Moreover, P407 increases the activity of cholesteryl ester transfer protein (CETP). When CETP activity is increased, more small dense atherogenic LDL particles are produced. At the same time, activity of hepatic lipase which is involved in the metabolism of TG, is inhibited significantly in P407 treated rats [35].

The P407 model is reversible , One interesting feature of the model is that the lipid levels increase to such an extent that one can visually see the changes in the plasma over time. Within 24 h the plasma becomes milky-white in appearance. From 48 to 72 h after dosing the plasma starts to return to its native clear-yellow consistency. The levels of plasma lipids have been followed after a single dose of P407 of 0.5 and 1 g/kg to the rats, concentrations of TG, TC and HDL were determined to be diminishing within 12-24 h after dose [32]. Nevertheless, LDL was still rising and the other lipid levels were still higher than baseline levels up to 48 h after the agent was given [33].

.

1.3. HL and link to obesity

A medical condition associated with HL is obesity. Obesity is defined as an excessive or abnormal accumulation of adipose tissue associated with medical problems such as hypertension, HL, insulin resistance, Type 2 diabetes and atherosclerosis [36]. It has been reported that more than 20% of ischemic heart disease and 40% of diabetes cases are due to obesity-related complications (28). Body Mass Index (BMI) is used as a measure of obesity severity by incorporating body weight and height. BMI categorizes people overweight if BMIs range from 25 to 29.9 kg/m^2, and obese if equal or greater than 30 kg/m [37]. Obesity causes changes in cardiac output, regional blood flow, hormonal release [38], and expressions pro-inflammatory cytokines [39,40]. As result of these changes, pharmacokinetics of medications parameters may be changed [41].

1.4. Diet-Induced Obesity (DIO) Models

Induction of obesity through dietary manipulation is one of the most common models to induce obesity, and is another fundamental approach towards creating a state of HL. This model simulates the most common cause of human obesity. Most commonly the animals are fed a diet composed of high fat and carbohydrate for a long period of time. In this model, animals which were fed with high fructose corn syrup (HFCS) or a high fat diet had higher body weights and adipose tissue compared to control animals which were fed normal diet [42-44]. The differences in the food composition and the length of feeding period can lead to different severities of obesity and biological and physiological changes in the animal models. Also, there is a model of diet-induced obesity which involves feeding breeding animals with dietary obesity models which results in obesity generation [45].

1.5. Genetic models of obesity

This approach involves removing or impairing specific genes in the animal. It may include mutations of leptin signaling and/or leptin receptors. The leptin signaling mutation models are caused by mutation in the ob gene which stops leptin secretion (this model is called "ob/ob" mouse) or by defective leptin receptors which causes a morbidity-associated obesity (this is called the leptin receptor deficient "db/db" mouse and leptin receptor-deficient rats "fa/fa Zucker rat"). Furthermore, the leptin signaling mutation models are associated with hyperinsulinemia, hyperglycemia, hyperphagia and hypothyroidism [45]. In leptin receptor mutations, researchers can target gene codes by knocking them out to develop different models of obesity [45].

1.6. Treatment options for HL

It is important to monitor and control lipid levels by adapting a healthy lifestyle, and taking proper medication or a combination of both [4,46].

1.6.1. Lifestyle changes

It is recommended that patients with high levels of lipid change their daily diet routine and exercising to reach the optimal healthy weight. The change in the diet should involves eating a low-fat diet rich in vegetables and fruits.

1.6.2. Pharmacological treatment

There are many pharmacological treatment choices available to treat HL and elevated levels of triglycerides [4]. Some examples follow.

1.6.2.1. Statins or (HMG CoAR) inhibitors

Statins are the most powerful and effective choices for reducing high LDL cholesterol levels. Moreover, they are effective choice to prevent cardiovascular disease, heart attack and stroke [47]. Statin medications include simvastatin, pravastatin, lovastatin, fluvastatin, rosuvastatin and atorvastatin. They work mainly by inhibiting HMG-CoAR, a rate-limiting enzyme of cholesterol biosynthesis pathway, which reduces the production of cholesterol in the body. Also, it has been reported that statins is lowering the level of cholesterol in plasma indirectly by upregulating LDL-R [48,49]. Statins are associated with myopathy or rhabdomyolysis which should be considered in clinical practice [47].

1.6.2.2. Proprotein convertase subtilisin/kexin type 9 (PCSK9) inhibitors

This is a newer class of medication for treatment of LDL cholesterol levels. PCSK9 is an enzyme which decreases the LDL-R on the surface of hepatic cells by degradation. Inhibition of this enzyme then would cause an increase in LDL-R and a decrease in the plasma concentration of LDL, cholesterol and apoprotein B. These inhibitors include alirocumab and evolocumab. They are given by injection every two to four weeks [50].

1.6.2.3. Bile acid sequestrants

This class works to decrease the amount of cholesterol absorbed from foods by binding and attaching to intestinal bile acids, consequently also stopping their enterohepatic reabsorption. The non-absorbed cholesterol will be used for the formation of bile acids and reduced the plasma concentration of LDL cholesterol in the plasma[50]. They are colestipol, colesevelam and

cholestyramine. This class is recommended for patient with mild to moderate LDL cholesterol levels [50].

1.6.2.3. Ezetimibe

This agent works by diminishing the body's ability to absorb cholesterol produced inside the body as well as cholesterol coming from the food [50].

1.6.2.4. Nicotinic acid (Niacin)

Niacin is recommended for patients with elevated cholesterol levels who are not responding to statins [50]. These agents are working by both reducing the hepatic synthesis of VLDL and inducing of LPL enzyme activity [51]. It has possible side effects which include flushing, itching, nausea, numbness and tingling. This medication may cause damage to the liver.

1.6.2.5. Fibrates

Fibrate can lower triglyceride levels and raise HDL cholesterol. They work by activating the nuclear receptor, peroxisome proliferator–activated receptor (PPAR), which increases the free fatty acid oxidation process in the liver and decreases triglyceride synthesis. Moreover, PPAR activation prompts the expression of LPL [50]. Examples include gemfibrozil, fenofibrate and fenofibric acid. Fibrates have been reported to cause muscle toxicity (rhabdomyolysis) [47,48,50].

1.7. Treatment approach in obesity

As outlined above, obesity is often associated with increases in serum lipids. Treatment of obesity therefore can coincidentally treat HL in obese patients. Obesity can be managed by changing lifestyle, pharmacological treatment and surgical treatment.

1.7.1. Lifestyle changes

Changing lifestyle is important to reduce the severity of obesity. Obese subjects should manage their weight by decreasing the daily calories required and being physically active. Ideally, it is beneficial to have a complete medical team to help supervises and support obese subjects in their weight management plan [52,53].

1.7.2. Pharmacological treatment

Pharmacological treatment can be used with lifestyle modification. Pharmacological treatment of obesity is advised for patients with BMI ≥30 kg/m^2 and for patients who have had obesity-related illness with BMI ≥27 kg/ m^2. Obesity treatment medications include diethylpropion, phentermine, phendimetrazine, benzphetamine, orlistat, liraglutide and lorcaserin [54,55]. These work by a variety of mechanisms.

1.7.3. Surgical treatment

Surgery could be one of the options in morbidly obese patients (BMI>35). As it is a surgical procedure it is associated with a number of risks and untoward effects. At present, the most successful and widely used surgical interventions for weight loss are sleeve

gastrectomy(removing portion of stomach by surgery), the Roux-en-Y gastric bypass (attaching the stomach pouch directly to part of the small intestine) and adjustable gastric banding (a device attached to the upper portion of the stomach which reduce consumption and amount of food)[56].

1.8. Effect of HL and obesity on drug disposition

The levels of drugs in the blood are affected by various factors such as rates and extents of drug input, clearance (CL, drug elimination from the body) and volume of distribution (Vd). The Vd plays an direct role in the determination of drug loading dose, and because of its effect on half-lifer, the dosing intervals. Vd depends on the degree of binding to plasma and tissue protein, physiochemical properties of the drug, and tissue blood flow [57].

Clearance can be affected by metabolizing enzyme activity, glomerular filtration (influenced by plasma protein binding), renal tubular reabsorption and secretion (both of which can be influenced by drug transport proteins) [57,58].

HL can influence the pharmacokinetics, pharmacodynamics and toxicity of lipophilic drugs. A major reason for the change in drug pharmacokinetics in HL is an increase in drug binding to lipoprotein. HL may also cause changes in pharmacokinetics by directly altering drug metabolizing enzymes and transporter protein expression. P407-induced HL has proven to be a widely-used model to study the effect of HL on many lipophilic drugs. In most studies, pharmacokinetic changes were reported within 36 hours from the dosing of P407 injection. In some cases, HL was seen to also influence the pharmacodynamic relationships of the drug. For example, it was found that HL enhances the QT interval prolonging effects compared to normolipidemic (NL) controls. This was of interest because a prolongation in QT intervals

increases the risk of ventricular arrhythmias [59,60]. Aliabadi et al found that cyclosporine A in HL rats caused microscopic lesions associated with nephrotoxicity, along with higher drug concentrations in blood, plasma and liver. The increase in cyclosporine A concentration appeared to be caused by high lipoprotein binding, but also decreases in CL as a result of the HL inhibitory effect on CYP enzyme activity [3,61,62]. The uptake of cyclosporine A in liver and kidney could be due to the increase in LDL-bound drug and subsequent uptake of the drug-LDL complex into cells by the action to LDL receptors. Another drug, fluvoxamine, exhibited changes in protein binding and higher AUC in HL rats with lower brain concentrations in HL compared to NL rats[63]. Moreover, docetaxel and clomipramine were reported to have higher plasma protein binding and AUC in HL rats due to a reduction in hepatic metabolism in HL rats [64,65].

It has been reported that obesity can cause significant changes in the pharmacokinetics and pharmacodynamics of drugs [66]. These changes may be due to changes in total body fat, cardiac output, hepatic blood flow, hormonal production, drug metabolizing enzymes and transporter proteins [66]. The CL along with bioavailable drug dictates the average dose rate to be used in a dosage regimen.

Obesity could change drug absorption by accelerating gastric rate emptying, increasing gastric perfusion, speeding cardiac output, and altering enterohepatic recirculation. Nonetheless, there are no significant differences in rate and extent of absorption of propranolol and dexfenfluramine given orally between obese and non-obese subjects [67,68]. Absorption processes are not only involved in drug uptake from the oral route. In this light, the absorption of a subcutaneous injection of insulin was not different between obese and non-obese patients [69]. On the contrary,

Sanderink et al reported that the absorption of subcutaneous injection of enoxaparin was slower in obese than in non-obese subjects and the absorption extent was complete in both group [70].

Drug transporters have an impact on absorption processes as well. As they are found and distributed in the small intestine, they can alter the absorption by influxing or effluxing drug across cell membrane. It has been reported that the absorption of intraduodenal dose of nelfinavir was increased significantly in obese compared to control rats. The increase was associated with low expression of an efflux transporter (P-glycoprotein) [71]. Moreover, drug distribution is affected by many factors in the body which include drug chemical structure, the physicochemical properties of a drug, heart output, capillary permeability, blood flow, drug uptake by receptors and protein binding [72]. Volume of distribution (Vd) can be used as a measure to estimate the extent to which a drug distributes into tissues. Lipophilic drugs, with a high partition (octanol/ water) coefficient value, mostly have an enhanced ability to penetrate adipose tissue compared to hydrophilic drugs. So, for obese subjects, it is expected that lipophilic drugs will have larger Vd in obese compared to non-obese people. It has been reported that the Vd of piperacillin and tazobactam were significantly higher in obese subjects compared to a control group [73]. Also, protein binding of drugs can be affected in obese patients as a result of increased levels of α1 acid glycoprotein which alters the unbound fraction of basic drugs in plasma and affects their tissue distribution. Most obesity cases associated with HL, or at least increases in serum lipids. It has been reported that HL increases the lipoprotein levels in plasma which decreases the unbound fraction of drug and decrease the Vd [6,74,75]. Drug metabolism is classified into phase I and phase II, each of which involves different enzyme systems (Figure 3) [72]. Phase I metabolism processes involve a group of chemical reactions where the xenobiotic is usually modified by introducing a

polar function group. These chemical reactions include oxidation, reduction and hydrolysis. The major phase I reactions happen via cytochrome P450 (CYPs). CYP enzymes are a superfamily of heme-containing enzymes for oxidative metabolism of xenobiotics. they are found in the smooth endoplasmic reticulum of liver, heart, brain, lung, and kidney [76]. CYP enzymes have been classified into many families and subfamilies based on their similarities in amino acid sequence. The most important CYP families in human for drug metabolism are CYP1, CYP2, and CYP3 families [77].

Phase II enzymes consist of different families of conjugating enzymes (glutathione-S-transferases, UDP-glucuronosyltransferases or UGT, sulfotransferases, N-acetyltransferases, methyltransferases and amino acid conjugation). They facilitate conjugation between the xenobiotic's functional group or phase I metabolism product with an endogenous substrate like a glucuronic acid, a sulfate, or an amino acid group [72]. It has been reported that the expression of CYP3A4 in obese guinea pig is decreased compared to control [78]. Moreover, the level of protein expression of cyp3a11 was decreased in genetically obese mice (ob/ob mouse) [78]. Kim et al revealed that the expression of mRNA levels of 1A1, 1A6, 2B1 and UGTs were lower in livers of obese Zucker rats compared to lean rats [79]. In contrast to many CYP, Chaudhary et al reported that the glucuronidation processes were increased in obese Zucker rats compared to non-obese rats [80]. Sugioka et al. reported that due to reduction in CYP3A2 expression in obese Wistar rat livers, the AUC of nelfinavir was increased [71]. In addition, Abernethy et al claimed that the CL of triazolam and alprazolam were lower in obese subjects due to the decrease in CYP3A4 activity

[81]. Abdussalam et al studied liver and kidney mRNA and protein for selected CYP enzymes and transporters and found induction of the protein of CYP3A1/2 and CYP2C11 in liver of high-fat-fed rats, no changes noted for CYP1A1 at either levels of mRNA or protein and a decrease in the expressions of Oct1/2 and Mate1 with no change in Mdr1 [44]. Alteration of enzymes expression might affect drugs metabolism and pharmacokinetic in the body.

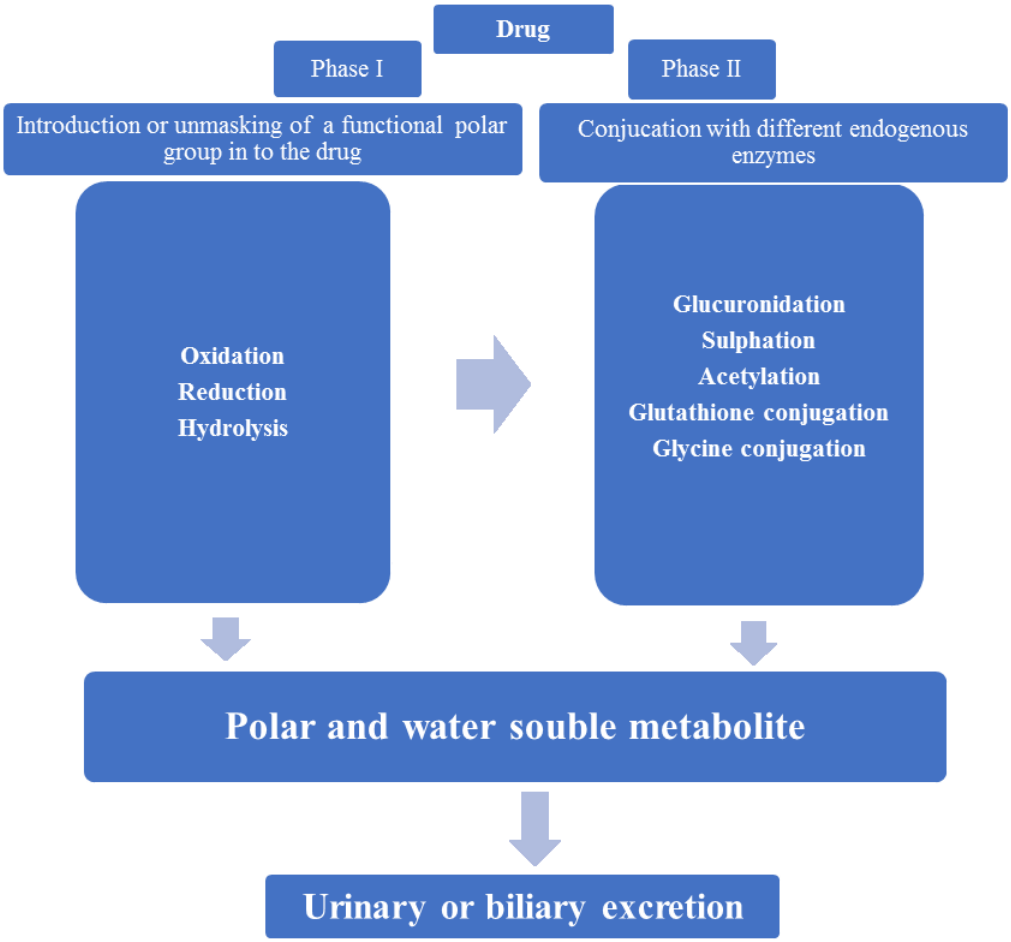

Figure 3: Overview of phase I and phase II metabolism of drugs.

1.9. Cardiac Arrhythmia

Obesity and HL are both associated with the onset of atherosclerosis, which can progressively lead to increased risk of myocardial infarction with disturbances in cardioelectrophysiological and hemodynamic function. Cardiac arrhythmia is a serious medical condition characterized by irregular rate and/or rhythm of the heartbeat. In arrhythmia, the heart beats too fast (more than 100 beats per minute), too slow (less than 60 beats per minute), or with an irregular rhythm. When the heart beats too fast, this is called tachycardia but when the heart beats too slow this is called bradycardia. The heart in arrhythmic patients is not able to pump adequate blood to the body organs which may diminish organ function. There are many factors that cause arrhythmia like, coronary artery disease, cardiomyopathy, hypertension, diabetes, hyperthyroidism, hypothyroidism, smoking and stress. Stroke and heart failure are the main complications of untreated arrhythmia. Arrhythmia are diagnosed by performing different heart-monitoring tests specific to arrhythmias. These may include: Electrocardiogram (ECG) sensors (electrodes) that detect the electrical activity of the heart when attached to the patient's chest), Holter monitor (a portable ECG device which can be worn for a specific time period like a day or more to record the heart's activity during patient's daily routines) and Echocardiogram (a non-invasive transducer) placed on the chest to produce images of the heart's size, structure and motion) [4,82].

1.10. Cardiac electrophysiology

The heart electric system controls all episodes that occur when the heart is pumping blood to the body organs. It consists of sinoatrial (SA) node in the right atrium of the heart, the atrioventricular (AV) node on the interatrial septum close to the tricuspid valve, and the His-Purkinje system along the walls of the heart's ventricles (Figure 4). A heartbeat is a cycle of relaxation and

contraction of the heart chambers. The cycle consists of the opening and closing of the valves in the right and left ventricles. During diastole, the atria and ventricles relax and start to fill up with blood. After that, the heart atria contract and pump blood into the ventricles. Then, the atria start to relax. Ventricles will contract and pump the blood out of the heart. In a healthy heart, every beat starts with a signal from the SA node (natural pacemaker). The heart rate is the number of signals which the SA node produces per minute. The signal is initialized when the vena cava fills the right atrium of the heart with blood which comes from all parts of the body. After that, the signal goes across the right and left atria cells. Then, the atria will start to contract and pump the blood by opening the valves from the atria into both ventricles. At the AV node near the ventricles, the signal slows to allow the right and left ventricles of the heart to fill with blood. Once finished, the signal moves through the Bundle of His which is in the walls of the heart ventricles. In the Bundle of His, the signal divides into right and left bundles through the Purkinje fibers and both ventricles contract. The left ventricle of the heart contracts and pushes the blood through the aortic valve to the rest of the body. The right ventricle pushes the blood through the pulmonary valve to the lungs. Once the signal is finished, the walls of the ventricles relax and prepare for another signal. This process continues as the blood refills the atria and further signals are received from the SA node [4,82].

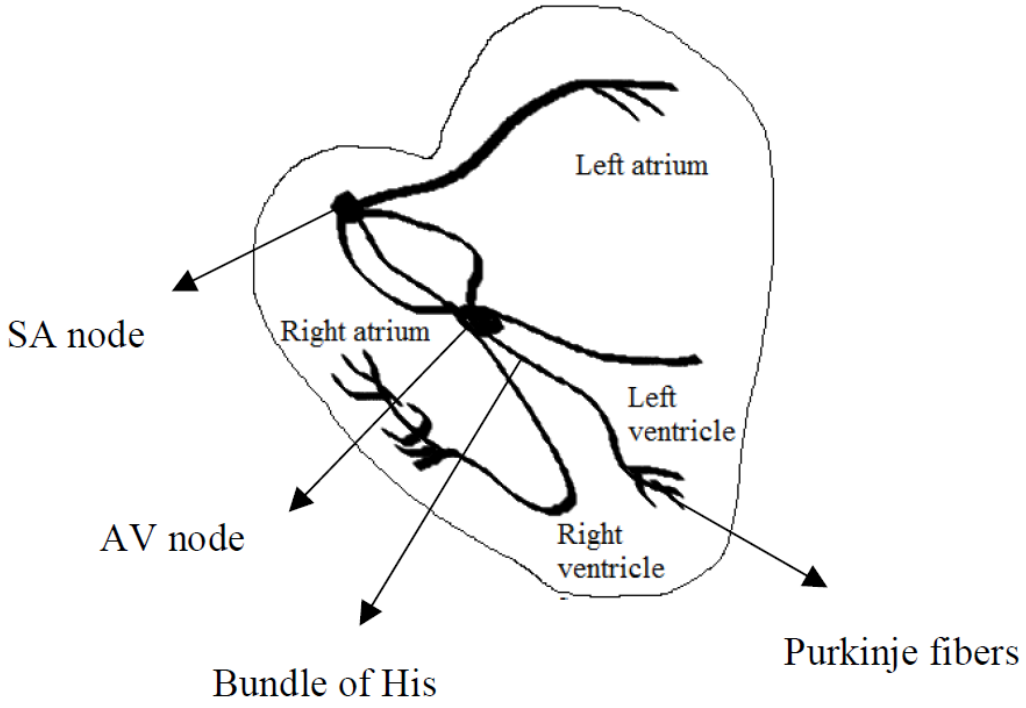

Figure 4: The cardiac conduction cycle.

The cycle starts from the SA node where the impulses generated, eventually reaches the AV node. After that, a quite delay happens so the contraction of atria process has enough time to pump and fill all the blood into the ventricles. When the atria are totally contracted, the valves between the atria and ventricles close. Now, the atria start to refill and the electrical cycle goes through the AV node and Bundle of His into the Purkinje fibers.

1.11. Type of cardiac arrhythmias

There are four main types of arrhythmia, namely premature (extra) beats, supraventricular arrhythmias, ventricular arrhythmias, and bradyarrhythmias [4,82].

1.11.1. Premature (Extra) Beats

They are the most common type of arrhythmia. They are harmless and are not associated with any symptoms. They usually feel like fluttering or a missing heartbeat in the chest. In general, premature beats do not require any treatment in healthy people.

When the premature beats occur in the atria (the upper chambers of the heart), they are called premature atrial contractions. On the other hand, when premature beats occur in the ventricles (the lower chambers of the heart), they are called premature ventricular contractions. Premature beats happen naturally in most cases. Nonetheless, some heart diseases may cause premature beats. Also, they might happen as a result of stress, smoking and/or overtraining [4,82].

1.11.2. Supraventricular Arrhythmias

They are tachycardias (the heart beats at fast rates) which start in the atria or atrioventricular (AV) node (a group of cells located between the atria and the ventricles). There are four types of Supraventricular Arrhythmias; Atrial fibrillation (AF), atrial flutter, Wolff-Parkinson-White (WPW) syndrome, and paroxysmal supraventricular tachycardia (PSVT) [4,82].

1.11.3. Atrial Fibrillation

It is the most common type of serious arrhythmia that is characterized by a very fast and irregular contraction of the atria. In AF, the electrical signals start in another part of the atria or pulmonary veins instead of the SA node. The signals travel in the atria in a very irregular way. Thus, the atria are not pumping the blood into the ventricles perfectly. AF can cause stroke and heart failure as two major complications. AF is the result of other medical conditions that affect the heart, such as heart diseases, hypertension, and an overactive thyroid gland [4,82].

1.11.4. Atrial Flutter

It has similar symptoms and complications to AF. But, the electrical signals of the heart spread through the atria in a rapid and regular rhythm. Atrial flutter cases are less common than AF[4,82].

1.11.5. Paroxysmal Supraventricular Tachycardia (PSVT)

PSVT is characterized by a very rapid heart rate that starts and ends suddenly. It happens due to issues in electrical connection between the atria and the ventricles. The electrical signals that begin in the atria and go to the ventricles may re-enter the atria, which causes extra heartbeats. It

is not dangerous and happens in young people in most cases during vigorous physical activity. There is a special type of PSVT called Wolff-Parkinson-White syndrome. In Wolff-Parkinson-White syndrome, The electrical signals of the heart travel on a longer pathway from the atria to the ventricles. [4,82].

1.11.6. Ventricular Arrhythmias

In ventricular arrhythmias, arrhythmias begin in the ventricles. They are very dangerous and require urgent medical care. They include ventricular tachycardia and ventricular fibrillation. Coronary heart disease, heart attack, a weakened heart muscle, and other problems can cause ventricular arrhythmias [4,82].

1.11.7. Ventricular Tachycardia

It is a rapid and regular beating of the ventricles that lasts for a couple of seconds or more. It is not a serious arrhythmia but it may turn into a serious arrhythmias called ventricular fibrillation [4,82].

1.11.8. Ventricular Fibrillation

In ventricular fibrillation, non-organized electrical signals make the ventricles not pump blood in normal way that may cause sudden cardiac arrest and death. To prevent sudden death, ventricular fibrillation requires immediate treatment with electric shock via heart defibrillator. There is another type of ventricular fibrillation called Torsades de pointes (where the cardiac death occurs as a result of QT interval prolongation) [4,82].

1.11.9. Bradyarrhythmia

Bradyarrhythmia happens when the heart rate is slower than normal. In severe cases, the slow heart rate may cause a coma because of insufficient blood traveling to the brain. In healthy adults, a heart rate lower than 60 beats per minute is defined as a bradyarrhythmia. Some people normally have slow heart rates, especially very physically fit people. Bradyarrhythmia is caused by: Heart attacks, underactive thyroid gland, aging and some medications such as beta blockers, calcium channel blockers, and digoxin [4,82].

1.12. Treatment approaches

Antiarrhythmic drugs were the primary therapy until the late 1960s when surgical therapy was developed. Catheter ablation (a procedure involves destroying the source of rhythm irregularity in the heart) was developed in the 1980s. It is largely used instead of surgery and pharmacological therapy for supraventricular tachycardia (SVT) and ventricular tachycardia (VT) patients [4,82]. Pharmacological drug therapy for arrhythmias has been used widely for the treatment of different kinds of arrhythmias [4].

The antiarrhythmic drugs are classified according to their actions on sodium, potassium, or calcium channels and their action on drug receptors. The commonly used classification is the Vaughan Williams classification (Table 2). According to the Vaughan-Williams classification, class I agents are sodium channel blockers, class II are beta blockers, class III are potassium channel blockers and class IV are calcium channel blockers. The class I agents are classified into class Ia (sodium and potassium channel blockage), for example procainamide, quinidine and dispopyramide. The class 1b agents are pure sodium channel blockers; this class includes

tocainide, mexiletine and lidocaine. Class Ic comprises strong sodium channel blockers; it includes flecainide, propafenone and moricizine. Class II antiarrhythmic medicines are beta-blockers, blocking the impulses that may cause an irregular heart rhythm and interfering with hormonal influences on the heart. Examples of beta blockers are: atenolol, acebutolol, metoprolol, nadolol, bisoprolol and propranolol. The class III agents are drugs that work mainly by blocking potassium channels. The class includes sotalol, dofetilide, ibutilide, amiodarone and bretylium [4].

Class IV agents are calcium channel blockers which prevent calcium from entering heart's cells and blood vessel walls. Calcium channel blockers are also called calcium antagonists and includes amlodipine, diltiazem, felodipine, isradipine, nicardipine, nifedipine, Nisoldipine and verapamil. The pharmacokinetic profile of antiarrhythmic drugs varies with each drug (Table 5). amiodarone has the longest half-life compared to other drugs whereas lidocaine is the shortest one [4].

Table 4: Vaughan-Williams classification.

Class	Mode of Action
Class I	Blocking Na^{+} Channels
Class II β-block	Blocking β-Channels
Class III	Blocking K^{+} Channels
Class IV	Blocking Ca^{2+}Channels

Table 5: Pharmacokinetic Parameters of some of the antiarrhythmic drugs[4].

Drug	**Oral Bioavailability F (%)**	**V_{dss} (L/kg)**	**Protein Binding (%)**	**$t_{1/2}$ (h)**
Disopyramide	70–95	0.8–2.0	50–80	4–8
Procainamide	75–95	1.5–3.0	10–20	2–6
Quinidine	70–80	2.0–3.5	80–90	5–9
Lidocaine	–	1–2	65–75	1–3
Mexiletine	80–95	5–12	60–75	7–20
Flecainide	90–95	8–10	35–45	10–20
Propafenone	11–39	85–95	85–95	3–25
Amiodarone	22–88	70–150	95–99	15–100
Dofetilide	85–95	2.5–3.5	60–70	6–10
Dronedarone	4 (fasting) 15 (with food)	20	>98	13–19
Ibutilide	–	6–12	40–50	3–6
Sotalol	90–95	1.2–2.4	30–40	10–20
Diltiazem	35–50	3–5	70–85	4–10
Verapamil	20–40	1.5–5.0	95–99	4–12

Adapted from [4].

1.13. The benzofuran antiarrhythmics

1.13.1. Amiodarone

AM is an important and often used antiarrhythmic agent (classified as a Vaughan-Williams class III). It is a benzofuran compound (Figure 5). It has a weak sodium channel–blocking activity, non-competitive inhibition of α- and β-adrenergic receptors, and calcium channel–blocking effects as well [83,84]. AM is widely used as first-line therapy for the treatment of patients with arrhythmia [83,85,86] . AM is a highly lipophilic drug, with Log *p* value of 9, which is responsible to its complex PK properties [83,87]. It binds extensively to plasma proteins of both humans and rats, with a significant binding to lipoproteins [88]. It possesses low and unpredictable oral bioavailability (F) with erratic absorption[89]. It has a large Vd and long terminal phase half-life (t½) and extensive tissue uptake[90]. AM is extensively metabolized via five pathways namely N-deethylation, hydroxylation, O-dealkylation, deiodination, and glucuronidation. N-Dealkylation is the most important pathway in humans and rats, yielding DEA [91]. There are different enzymes which are responsible for DEA formation in liver and intestine. CYP3A4, CYP1A1 and CYP2C8 are the main isoenzymes for the metabolism in humans [92-94]. On the other hand, CYP1A1, 3A2, 3A1, 2D1 and 2C11are the major enzymes involved in rat [94-96].

HL causes an increase in the plasma levels of AM due to significant decreases Vd, CL and unbound fraction of drug. Also, it causes a decrease in the metabolism of AM in liver microsomes and a reduction in the expression of CYP P450 enzymes which are involved in the metabolism of AM. Moreover, HL shows a tissue-specific difference in AM levels in different tissue in rats [62].

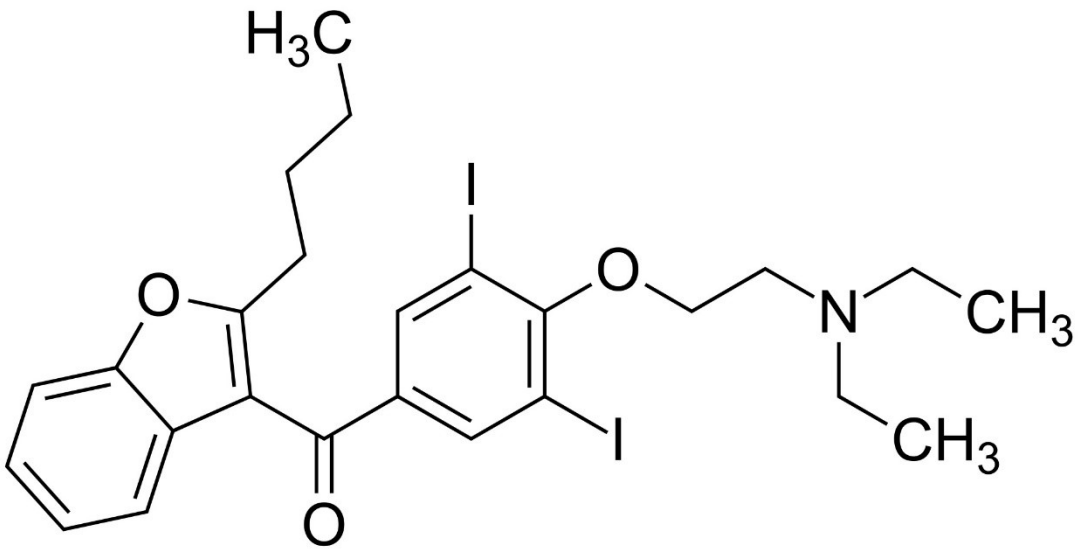

Figure 5: Chemical structure of amiodarone.

1.13.2. Dronedarone

Dronedarone (Figure 6) is a recently approved antiarrhythmic agent used mainly for the treatment of cardiac arrhythmias [97]. Dronedarone is a benzofuran derivative that was developed in an attempt to reduce the toxicity profile associated with its widely used structural analog, amiodarone. Although amiodarone is a commonly used drug, its use is hampered by several troublesome toxicities involving the thyroid, lung and liver. For example, the thyroid disturbances associated with amiodarone are associated with its iodine content, which was removed in the dronedarone structure [98-100]. Dronedarone is capable of reducing arrhythmias by blocking multiple channels (potassium currents, sodium currents and calcium currents).

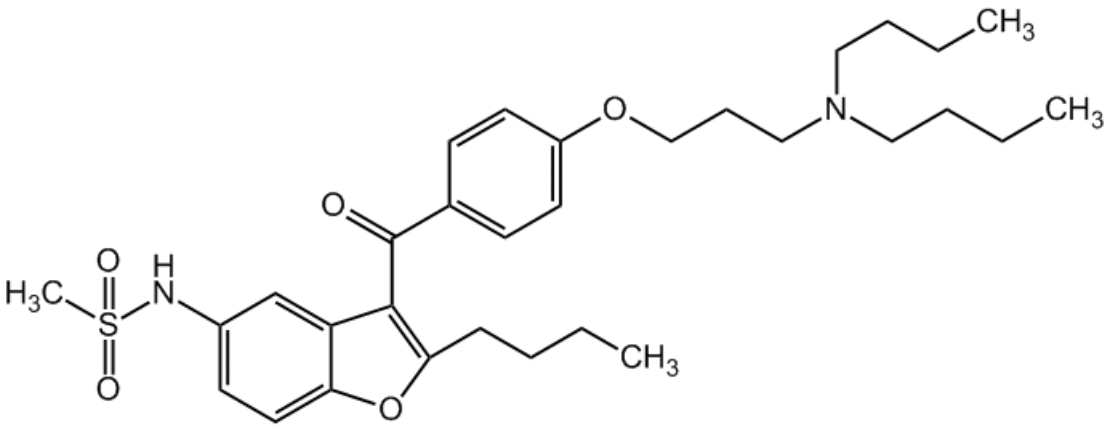

Figure 6: Chemical structure of dronedarone.

1.13.2.1. Absorption

It is well absorbed, with 70% to 94% of dronedarone accessing the portal circulation after oral ingestion with only 4% bioavailability. The bioavailability increases up to 3-fold with food. It is recommended to take dronedarone tablets with a meal.

1.13.2.2. Distribution

Dronedarone has high plasma protein binding (99.7%) with a relatively high Vd (17-20 L/kg), resulting in approximately 24 to 30 hours terminal elimination half-life after a single dose in healthy human volunteers.

1.13.2.3. Metabolism and Excretion

Dronedarone has a rapid and extensive metabolism primarily by hepatic CYP3A4/5 [97]. Desbutyldronedarone is a mono-N-dealkylated metabolite of dronedarone with less antiarrhythmic effect than its parent compound [97,99,101]. After an oral dose of dronedarone as (^{14}C-labeled), 6% of the administered dose was excreted in urine and 84% in feces as metabolites.

As HL causes an increase in plasma lipoproteins and can affect the PK, PD and toxicity of lipoprotein-bound medications. AM is a lipophilic compound of Log *p* 9 with capability to bind to lipoproteins. It has been reported that HL increases AM AUC, decreases both CL and Vd with increased heart uptake of AM in the P407 HL rat model after a single dose of AM [62,74]. Also, repeated doses of AM in HL rats produced similar increase of AM plasma and heart concentrations with increased in echocardiogram intensity. The higher concentration of AM in HL rat hearts could be a result of VLDL-R mediated uptake of AM. Moreover, in liver and intestinal microsomal preparations, HL causes a decrease in AM metabolism which is associated with an inhibition and downregulation of selective expression of some of the CYP isoforms CYP3A1/2 and CYP2C11. Tissue distribution studies of AM revealed that the increase in plasma concentration of AM in HL rat is not associated with decreases in all other tissue which suggest that HL has a tissue-specific effects.

1.14. Rationale, Hypotheses, Objectives

1.14.1. Rationale

Currently the published pharmacokinetic information on dronedarone is sparse; most comes from internal unpublished company studies. Moreover, there are several cases reports and *in vitro* studies beginning to appear showing that dronedarone is associated with some of the same serious side effects as amiodarone, including toxic hepatitis in elderly patients and pulmonary toxicity [97,102-106]. Studies in animals may help shed light on why the drug causes these same toxicities as amiodarone, but one cannot rule out a pharmacokinetic explanation either. To date, there are few analytical methods reported for the measurement of dronedarone in biological specimens from humans, and none in animal species.

The PK of amiodarone are profoundly influenced in an animal model of HL [10]. It is PD properties are also influenced by this model [107]. Patients with cardiovascular disease who might be prescribed a benzofuran antiarrhythmic drug are likely to be afflicted with HL, which is a condition predisposing to atherosclerosis and coronary heart disease. HL can also affect the pharmacokinetic behavior of lipophilic drugs *in vivo* by reducing unbound fraction (fu) or by facilitating lipoprotein receptor-mediated drug tissue uptake [62,75]. Dronedarone has a log octanol/water partition coefficient (Log *p*) of 6.46, which might predispose it for binding to serum lipoproteins, and hence altered pharmacokinetics in HL.

1.14.2. Hypotheses

Given its benzofuran structure and similarity to AM, dronedarone will:

I. Have pharmacokinetic properties in rat similar to human, and similar to those of AM (moderate CL, high Vd, and long terminal phase half-life)

II. Exhibit differences in pharmacokinetics in NL and HL rats

III. Display different tissue distribution and drug metabolic properties in normolipidemic and HL rats.

1.14.3. Objectives

Based on the mentioned rationale, this thesis has the following specific objectives:

1. Develop a sensitive and validated reverse phase HPLC-UV assay for the determination of dronedarone in rat plasma.
2. Develop a sensitive and validated liquid chromatography-mass spectrophotometry (LC-MS) assay for the determination of dronedarone in rat plasma.
3. Study the PK of dronedarone in normolipidemic and hyperlipidemic (P407-treated) rats.
4. To assess the effect of HL (P407-induced and DIO) on the tissue distribution and microsomal metabolism of dronedarone.

Chapter 2. Materials and Methods

2.1. Materials and reagents

Dronedarone HCl and ethopropazine HCl were obtained from Sigma-Aldrich (St. Louis, MO, USA). Desbutyldronedarone HCl was purchased from TLC PharmaChem Inc (Aurora, ON, Canada). Methanol, acetonitrile, hexane, tert-butyl methyl ether and water (all HPLC grades), triethylamine, sodium phosphate (mono and dibasic), potassium phosphate (monobasic) and sulfuric acid were purchased from Caledon Laboratories Ltd (Georgetown, Ontario, Canada). Nicotinamide adenine dinucleotide phosphate tetrasodium (NADPH), sodium chloride, sodium bromide, sodium thiocyanate, P407, NaOH and bovine serum albumin (BSA) were purchased from Sigma-Aldrich (St. Louis, MO). Potassium dihydrogen orthophosphate (KH_2PO_4), dipotassium hydrogen orthophosphate, KCl, $MgCl_2.6H_2O$, sucrose, and $CaCl_2.2H_2O$ (all analytical grades) were obtained from BDH (Toronto, ON, Canada). Polyethylene glycol (PEG) 400 (analytical grade) was purchased from Fisher Scientific (Fair Lawn, NJ, USA). Isoflurane USP was purchased from Halocarbon Products Corporation (River Edge, NJ, USA). Heparin sodium injection, 1000 U/mL and 10000 U/mL, were obtained from Leo Pharma Inc. (Thornhill, ON, Canada). Enzymatic assay kits for measurement TC of and TG in plasma were obtained from Sckisui diagnostics (P.E.I, Canada). The calibrator for the TG and TC kit was purchased from Sckisui diagnostics (P.E.I, Canada).

2.2. Methods

2.2.1. Development of a reverse phase HPLC-UV assay of dronedarone in rat plasma.

2.2.1.1. Instrumentation and chromatographic conditions

The chromatographic system consisted of a Waters (Milford, MA, USA) 600E multi-solvent delivery system pump, auto sampler with variable injection valve (Waters 717) and UV–visible tunable absorbance detector (Waters 486). The chromatograms were recorded using EZStart software (Scientific Software, Pleasanton, CA, USA) in a Windows-based computer system for data collection and processing. Separation of dronedarone and ethopropazine were performed on a 150×4.6 mm i.d., 5 μm particle size Alltima C18-column (Alltech, Deerfield, IL, USA). The mobile phase consisted of acetonitrile: [25 mM KH_2PO_4:3 mM sulfuric acid: 3.6 mM triethylamine] in a combination of 48:52 v/v. The mobile phase was prepared daily and degassed by filtration using a 0.45 μm nylon filter. The mobile phase was pumped at an isocratic flow rate of 1 ml/min at room temperature. The UV detection wavelength was set at 254 nm. At 7 min post-injection, the UV detector was programmed to switch to a wavelength of 290 nm. The wavelengths of 254 and 290 nm represented the UV maximum absorption of ethopropazine and dronedarone, respectively. Total analytical run time was 20 min.

2.2.1.2. Standard and stock solutions

A stock drug solution was prepared by dissolving 5.3 mg of dronedarone HCl in 49.7 mL of methanol, representing 100 μg/mL of dronedarone base. A stock solution of desbutyldronedarone was prepared by dissolving 5.36 mg of desbutyldronedarone HCl in 50 mL of methanol, representing 100 μg/mL of desbutyldronedarone base. The working standard solutions were

prepared daily from the stock solution by serial dilution with methanol to give final concentrations of 10000, 1000 and 100 ng/mL dronedarone. The internal standard (I.S.) stock solution was prepared by dissolving 5 mg of ethopropazine HCl in 100 mL of methanol (50 µg/mL). All solutions were stored at -20°C between uses. For construction of standard curve, samples of plasma (0.1 mL) were prepared by adding dronedarone equivalent to 25, 50, 100, 250, 500 and 1000 ng/mL.

2.2.1.3. Extraction procedure

Dronedarone was extracted from rat plasma using a one-step liquid–liquid extraction. A 10 µL volume of IS solution was added to 0.1 mL of rat plasma. Plasma proteins were precipitated by the addition of 300 µL of acetonitrile, and then the tubes were vortex mixed for 5 s, then centrifuged for 2 min at high speed (3000 g). The supernatant was transferred to new glass tubes using clean Pasteur pipets. Volumes of 300 µL HPLC water and 6 mL hexane were then added, the tubes were vortex mixed for 30 s and centrifuged at 3000 g for 3 min. The organic solvent layer was transferred to new tubes and evaporated to dryness *in vacuo*. The residues were reconstituted using 200 µL of mobile phase with up to 150 µL being injected into the chromatographic system.

For extraction from tissues, approximately 300 mg of each blotted, thawed tissue was homogenized in distilled water (1:3 w/w) with a variable speed hand-held tissue homogenizer run at high speed (Branson product, VWR Scientific, Danbury, CT, USA). An aliquot of 400 uL of homogenate of each tissue (equivalent to 100 mg of wet tissue) was transferred to a glass tube and 50 µL of IS and 1 ml of acetonitrile were added to each tube. The tubes were vortex mixed

(10 s) and centrifuged for 5 min in order to precipitate the protein content. The supernatant layers were transferred to new tubes and 8 ml of hexane were added. The tubes were then vortex mixed for 1 min and centrifuged at 3000 g for 3 min. The organic layer was transferred to new glass tubes and evaporated to dryness *in vacuo*. The residues were reconstituted and injected into the chromatographic system.

2.2.1.4. Recovery

Recovery was determined with dronedarone concentrations of 50 and 500 ng/mL of plasma, using four replicates of each concentration. The extraction efficiency was determined by comparing the extracted peak heights of analyte in the extracted samples to the peak heights of the same amounts of analyte directly injected into the HPLC, without extraction.

2.2.1.5. Calibration, accuracy and validation

Calibration curves were quantified by using peak height ratios of dronedarone (concentration range from 25 to 1000 ng/mL) to IS vs. the nominal dronedarone concentration. Intra-day validation was examined at four different concentrations (25, 50, 100 and 500 ng/mL) per day in five replicates. This step repeated on three separate days for determination of inter-day validation. For each daily run, an independent set of calibration curves samples was prepared to allow quantification of the peak height ratios of dronedarone to IS. Accuracy and precision were assessed using mean intra- or inter-day percentage error and coefficient of variation (CV%), respectively. Calibration curves were weighted by a factor of 1/concentration because of the broad range of concentrations.

Precision was determined using percentage coefficient of variation (CV %) which was calculated as

$$CV\%\ interaday = \frac{100 \times SD}{mean\ measured\ concentration},$$

and,

$$CV\%\ interday = \frac{CV\%\ run1 + CV\%\ run\ 2 + CV\%\ run\ 3}{3}$$

Bias was assessed using mean intra- or interday percentage error of the mean, which was calculated as:

$$Mean\ \%\ error\ intraday = 100 \times \frac{measured\ concentration - expected\ concentration}{expected\ concentration}$$

And

$$Mean\ \%\ error\ interday = \frac{error\%\ run\ 1 + error\ \%\ run\ 2 + error\%\ run\ 3}{3}$$

2.2.1.6. Stability of dronedarone in rat plasma

The stability of dronedarone in plasma was evaluated in triplicate using two different concentrations of dronedarone (250 and 500 ng/mL). Samples (n=3 per concentration) were incubated with rat plasma and kept in -20°C for one week and one month. Thereafter, samples were extracted and assayed to determine the recovered concentration of dronedarone.

2.2.1.7 Assay of desbutyldronedarone

The abovementioned assay was modified and used for quantitation of desbutyldronedarone in the microsomal metabolism experiments. When used in plasma, there were some differences from the dronedarone assay outlined above. Briefly, dronedarone and DBD were extracted from rat plasma using a one-step liquid–liquid extraction. A 10 µL volume of IS solution was added to 0.1 mL of rat plasma. Plasma proteins were precipitated by the addition of 300 µL of acetonitrile, and then the tubes were vortex mixed for 5 s, then centrifuged for 2 min at high speed (3000 g). The supernatant was transferred to new glass tubes using clean Pasteur pipets. Volumes of 100 µL HPLC water, 1 N NaOH and 3 mL of methyl tert-butyl ether were added, the tubes were vortex, mixed for 1 min and centrifuged at 3000 g for 3 min. The organic solvent layer was transferred to new tubes and evaporated to dryness *in vacuo*. The residues were reconstituted using 150 µL of mobile phase with up to 150 µL being injected into the chromatographic system. The mobile phase consisted of acetonitrile: [25 mM KH2PO4:3 mM sulfuric acid: 3.6 mM triethylamine] in a combination of 55:45 v/v was pumped at an isocratic flow rate of 1 ml/min at room temperature. The UV detection wavelength was set at 288 nm.

2.3. Development of a liquid chromatography-mass spectrometry (LC/MS) assay method for the quantification of dronedarone in rat plasma.

2.3.1. Instrumentation and chromatographic conditions

After development and utilization of the abovementioned HPLC-UV assay, development of an LC-MS assay for measurement of dronedarone was undertaken. An isocratic separation was performed on a reverse phase C18 column (Alltima HP, 250 × 2.1 mm) at 25°C using 70% methanol in water with 1 mM ammonium formate (pH=4.5) as mobile phase. Detection was accomplished by a mass spectrometer (Waters Micromass ZQ 4000 spectrometer) in positive-ionization mode using selected ion monitoring: m/z= 557.4 for dronedarone and m/z = 313.2 for IS. Standard, stock solutions and extraction procedures were prepared as described in the HPLC method above (Section 2.2.1.3 and 2.2.1.5)

2.3.2. Calibration, accuracy and validation

Calibration curves were quantified by using peak height ratios of dronedarone (concentration range from 5 to 1000 ng/mL) to IS vs. the nominal dronedarone concentration. Intra-day validation was examined at four different concentrations (5, 50, 100 and 1000 ng/mL) per day in five replicates. This step repeated on three separate days for determination of inter-day validation. For each daily run, an independent set of calibration curve samples were prepared to allow quantification of the peak height ratios of dronedarone to IS. Accuracy and precision were assessed using mean intra- or inter-day percentage error and coefficient of variation (CV%), respectively. Calibration curves were weighted by a factor of 1/concentration because of the broad range of concentration.

2.3.3. Assessment of matrix effect

To determine the effect of plasma on the process of ionization of the dronedarone and IS, the post-extraction spike method proposed by Matuszewski et al [108,109] was applied. Briefly, one six-replicate set of analyte-free plasma matrix were extracted and dried. In the second set, the same volume of HPLC water was subjected to extraction. After the extracts were dried, 100 µL of dronedarone (500 ng/mL) and IS was added to the tubes. The samples were injected into the LC-MS and responses recorded. The responses of the analytes in the biomatrix-containing extracts were compared with those of the samples only containing water.

2. 4. Pharmacokinetics of dronedarone in normolipidemic and hyperlipidemic rats

2.4.1. Animals and experimental procedures

All protocols for the use of male Sprague-Dawley rats were approved by the University of Alberta Health Sciences Animal Policy and Welfare Committee. Body weight ranged from 250 to 350 g and all rats were housed in temperature-controlled rooms with a 12 h light/dark per day. The animals were fed a standard rodent chow containing 4.5% fat (PicoLab® Laboratory Rodent Diet (5L0d-irradiated), LabDiet, St. Louis, MO).

The day before the experiment, the right jugular vein of rats was cannulated with sterilized Silastic laboratory tubing (Dow Corning Corporation, Midland, MI) under isoflurane delivered by anesthetic machine. The cannula was filled with sterile 100 U/mL heparin in 0.9% saline. After implantation, the animals were transferred to regular holding cages and allowed free access to water, but food was withheld overnight and until two hours after the dronedarone dose. The next morning the rats were transferred to metabolic cages and dosing was performed.

Animal groups for microsomal metabolism studies were rats given normal chow with water (Control), normal chow with high fructose corn syrup water (HFCS), 45% high fat chow (HFD) with water, Combined HFCS-HFD as previously reported [44] and P407-induced HL [110].

2.4.2. Drug administration and sample collection

Injectable solutions of dronedarone HCl (4 mg/mL and 100 mg/mL as base) were prepared in ethanol: polyethyelene glycol (PEG) 400 (1:10). Oral dronedarone HCl (100 mg base/mL) was prepared by a suspension in 1% methylcellulose. On the morning of the pharmacokinetic assessment, each assigned NL rat (n=8) was given an iv dose of 4 mg dronedarone base/kg. These doses were injected over 1 min via the implanted jugular vein cannulas, immediately followed by injection flush of approximately 1 mL of sterile normal saline solution (over 1 min). Other groups of NL and (n=8) and HL rats (n=6) received 55 mg dronedarone base/kg as a suspension of the HCL salt by oral gavage. The last group of NL rats (n=7) received an ip dose of 65 mg dronedarone base/kg of as the HCl salt. In the rats given doses iv, at the time of first sample withdrawal, the first 0.2 mL volume of blood was discarded. Thereafter blood samples (~0.2 mL) were collected from the cannula nominally at approximately 0.083, 0.33, 0.67, 1, 2, 3, 4, 6, 9, 10, 24 h after dosing. In the rats given dronedarone po and ip, blood samples (~0.2 mL) were collected from the cannula at approximately 0.25, 0.5, 1.5, 1, 2, 3, 4, 6, 9, 12 and 24 h postdose. Heparin in normal saline (100 U/mL) was used to fill the cannula after each blood sample collection. Each blood sample was collected by pre-heparinized needles and centrifuged at 2000 g for 3 min. The plasma was transferred to new glass tubes and stored at -20°C until assayed for dronedarone. HL was induced by a single ip dose of 1 g/kg of P407 (0.13 g/ml solution in normal saline) as

previously described [111]. After 18 h, the right jugular veins of these rats were catheterized. The pharmacokinetic study commenced 36 h after the ip injection of P407 [111].

2.4.3. Protein binding in plasma

An erythrocyte vs buffer or diluted plasma partitioning method was used to determine the *in vitro* plasma protein binding of dronedarone. In brief, NL and HL blood were collected into heparinized tubes by cardiac puncture. The blood was divided into two equal parts into two different tubes and the plasma was separated from blood cells by centrifugation at 2500 g for 10 min. Then, the plasma was separated; the buffy coat layers were discarded. The blood cells were washed in an equal volume of isotonic Sorensen's phosphate buffer (pH 7.4) followed by centrifugation at 2500 g for 10 min. These washing and centrifugation steps were repeated two times. After the last washing step, the volume of erythrocytes was determined in each tube and an appropriate amount of either diluted plasma or buffer was added to the tubes to yield a hematocrit of 0.3 (buffer) or 0.4 (diluted plasma)[111]. The NL plasma was diluted by a factor of 1:19, and the HL plasma was diluted by a factor of 1:29. Dronedarone as a methanolic solution was added to each tube to provide for drug concentrations of 5000 ng/ml (0.4% methanol in blood). Then, the tubes were incubated in a 37 ° C shaking water bath for 1 h. The calculation of fu in plasma was determined by a series of equations outlined by Schumacher et al[112].

The erythrocyte concentration of dronedarone in the erythrocyte–diluted plasma was determined by the following equation:

$$\mathrm{CE} = \frac{\mathrm{CB} - \mathrm{Cp}(1 - \mathrm{HCT})}{\mathrm{HCT}}$$

Where CB is the concentration of dronedarone in the blood cell–diluted plasma suspension, Cp is the concentration of dronedarone in the diluted plasma, and HCT is the hematocrit in the erythrocyte–diluted plasma sample. To estimate the erythrocyte concentration of dronedarone in the erythrocyte–buffer samples (CE*), the concentration of dronedarone in the blood cell–buffer suspension was substituted for CB, and the buffer concentration of dronedarone was substituted for Cp. The fu of dronedarone was determined by

$$fu = \frac{\alpha \cdot Pp/Pb}{1 - [\frac{Pp}{Pb} \cdot (1 - \alpha)]}$$

Where α is the plasma-dilution factor. The partition coefficients for erythrocyte: diluted plasma (Pp) or buffer (Pb) are represented by the quotients CE/Cp and CE*/Cbuffer, respectively.

2.5. Tissue distribution and microsomal metabolism of dronedarone in rat

2.5.1. Sample collection in tissue distribution studies

NL and HL rats (n= 4 per time point) were given an oral dose of dronedarone (55 mg dronedarone base/kg as a suspension of the HCL salt by oral gavage) after 1,3,6,9,12,24 h postdose, plasma, Heart, liver, and lung were collected by exsanguination of rats by cardiac puncture under anesthesia with isoflurane. The excised plasma and tissues were kept in separate tubes at -80°C and then analyzed for dronedarone by UV-HPLC method.

2.5.2. Preparation of microsomes

Livers of control, HL, HFCS, HFD and combined HFCS-HFD (N=6) rats were collected under isoflurane then washed thoroughly in cold KCl solution (1.15% W/V in distilled water). After washing, the tissue was homogenized in cold sucrose solution (0.25 M in distilled water) by using a homogenizer (5 g of tissues in 25 ml of sucrose). The tissue was centrifuged at 1000 g for 8 minutes. The supernatants were transferred to new tubes and centrifuged again at 15,000 g for 10 minutes. Centrifugation continued again by transferring supernatants to new tubes at 100,000 g for 1 hour. Then the pellets were resuspended in sucrose 0.25 M solution and stored at -80 ° C freezer.

2.6. Lowry assay for protein concentration in microsomes

The Lowry assay method for protein concentration is based on comparing the unknown concentration of protein preparation with serial standard solutions of bovine serum albumin (BSA)[113]. The following solutions had to be prepared in order to assay the concentration of protein in microsomal preparations:

Reagent A: 1mL of sodium and potassium tartrate 2% in distilled water, 1mL of CuSO4 1% in distilled water, and 20 mL of Na_2CO_3 anhydrous 10% in 0.5 M NaOH.

Reagent B: 1:10 diluted solution of Folin-phenol reagent in distilled water. Working standard solutions of BSA were prepared at the concentrations of 500, 400, 300, 200, 100, and 0 µg/mL of BSA in distilled water from the stock solution of 500 µg/mL (50 mg/100 mL H_2O). To a number of clean test tubes containing 10 µL of microsomal preparation and 240 µL of distilled water (unknown concentration of protein) or 250 µL of each standard solution, 250 µL of reagent A were added and the tubes were incubated at room temperature for 10 minutes. In the next step and

under continuous vortex mixing, 750 µL of reagent B was added to each of the test tubes and samples incubated at 50 °C for another 10 minutes. At the last step 200µl of each mixture were transferred to a well in the ELISA plate and analyzed using an ELISA reader at 600 nm.

2.7. Microsomal incubation study

Linearity of dronedarone metabolism to desbutyldronedarone was examined by incubating dronedarone with different concentration of hepatic microsomal protein ranging from 0.5 - 1mg/mL for 10 min. After optimizing selecting the optimum hepatic microsomal protein, each 0.3-ml incubate has 0.5 mg/ml protein of the microsomal preparations, 2 to 150 µM dronedarone base, 1 mM NADPH, and 5 mM magnesium chloride hexahydrate dissolved in 0.1 M potassium phosphate buffer (pH = 7.4). The substrate was added to the microsomal suspension and the oxidative reactions were started with the addition of 10 µL NADPH after a 5-min pre-equilibration period in the water-bath. All incubations were performed in triplicate in a 37°C water bath shaker for 10 min. Incubation conditions were optimized so that the rate of metabolism was linear with respect to incubation time and microsomal protein concentration. The incubation terminated by adding 0.5 ml of ice-cold acetonitrile. Methanol concentration did not exceed 0.5% in each incubation mixture. Samples were extracted and analyzed by a modified HPLC method for dronedarone and desbutyldronedarone [114].

2.8. Microsome extraction

For extraction of dronedarone and its metabolite desbutyldronedarone, a 50 µL volume of IS solution,100 µL HPLC water and 50 µL 1N NaOH were added to 0.3 mL of incubated sample. The tubes were vortex mixed for 5 s, and after that, volume of 3 mL tert-butyl methyl ether was added, the tubes were vortex mixed for 30 s and centrifuged at 3000 g for 3 min. The organic solvent layer was transferred to new tubes and evaporated to dryness *in vacuo*. The residues were reconstituted using 200 µL of mobile phase with up to 150 µL being injected into the chromatographic system.

2.9. Dronedarone depletion study

Each 1 ml incubate has 0.5 mg/ml protein of the microsomal preparations of HFCS and combined HFD-HFCS, 1 mM NADPH, and 5 mM magnesium chloride hexahydrate dissolved in 0.1 M potassium phosphate buffer (pH = 7.4). 10 µM of dronedarone base was added to the microsomal suspension and the oxidative reactions were started with the addition of 15 µL of 1 mM NADPH after a 5-min pre-equilibration period in the water-bath. All incubations were performed in quadruples in a 37°C water bath shaker. 100 µL of incubated mixture was collected at 0 ,10,20 and 30 min. The incubation reaction terminated by adding 1.5 ml of ice-cold acetonitrile. Samples were extracted and analyzed by HPLC method.

2.10. Total P450 measurement

Hepatic microsomal CYP content was measured by a difference spectrum for the carbon monoxide-reduced form as described by Omura and Sato [115]. Briefly, microsomal preparations (1 mg/mL protein content) were placed in quartz cuvette; a few milligrams of sodium thiocyanate were added to reduce the carbon monoxide-CYP complex. The baseline was recorded. Then, carbon monoxide was bubbled for 10 s into the samples to form the carbon oxide-CYP complex. The absorbance of the cuvette contents was scanned from 400 to 500 nm. CYP content was calculated by the following equation:

$$Cyp\ content\ (nmol/mg\ protein) = \frac{OD450 - OD490}{91} \times 1000$$

2.11. TG and TC measurement

The plasma concentrations of TG and TC were measured according to the manufacturer's instructions. The lipid concentrations in each sample were calculated using standards provided in the kits, taking into account any dilution factors required. Dilution of the plasma from P407-treated rats was done using deionized water. For measurement of TC, 2.5 mL of reagent was added to 25 µL of deionized water, calibrator, or plasma sample to be assayed. the mixture was mixed and incubated for 20 min. After that, the absorbance of the calibrator (As) and of each unknown (A) at 505 nm using the deionized water sample as the reagent blank were determined.

For measurement of TG, 2.5 mL of reagent was added to 25 µL of deionized water, calibrator, or plasma sample to be assayed. the mixture was mixed and incubated for 20 min. After that, the absorbance of the calibrator (As) and of each unknown (A) at 520 nm using the deionized water sample as the reagent blank were determined. The following equation were used:

$$TC\ concentration\ (mmol/L) = \frac{\text{absorbance of the unknown}}{\text{absorbance of the calibrator}} \times calibratorconcentration$$

$$TG\ concentration\ (mmol/L) = \frac{\text{absorbance of the unknown}}{\text{absorbance of the calibrator}} \times calibratorconcentration$$

2. 12. Data and Statistical analysis

2.12.1. Pharmacokinetic and tissue distribution study analysis

All compiled data were expressed as mean±SD unless otherwise indicated. Differences were assessed for significance using Student's t-test. The level of significance was set at α=0.05. Single factor ANOVA was used to assess the significance of differences between NL and HL pharmacokinetic data. Noncompartmental analysis was mostly used to characterize the pharmacokinetic parameters of the drug in the rat [116]. The elimination rate constant (λz) was estimated by subjecting the plasma concentrations in the terminal phase to linear regression analysis. The terminal elimination phase half-life ($t_{1/2}$) was calculated by dividing 0.693 by λz. The concentration at time 0 h after iv dosing was estimated by back extrapolation to time zero using the first measured log-transformed concentrations after dosing. The AUC0-∞ after dosing was calculated using the combined log-linear trapezoidal rule from time 0 h postdose to the time

of the last measured concentration, plus the quotient of the last measured concentration divided by λz.

Clearance (CL) was calculated as $\mathrm{CL} = \frac{\mathrm{Dose}}{\mathrm{AUC}_{0-\infty}}$, and steady-state volume of distribution (Vdss) was calculated as $\mathrm{Vd}_{\mathrm{ss}} = \mathrm{CL} \times \mathrm{MRT}$ where MRT is the mean residence time[116].

Nonlinear curve fitting was used to characterize the compartmental nature of the drug using the PKSolver Excel-based computer program[117].

The oral bioavailability was calculated as $\boldsymbol{F} = \frac{\boldsymbol{mean\ AUC_{oral} \cdot Dose_{iv}}}{\boldsymbol{mean\ AUC_{iv} \cdot Dose_{po}}}$: The maximum plasma concentration (Cmax) and the time at which it occurred (tmax) were determined by visual examination of the data.

For the tissue distribution study, the area under the dronedarone concentration vs. time curves (AUC) based on the mean data from each sampling time point were calculated for each of the tissues and for the plasma. As the AUC is difficult to be determined for each rat in each group due to the study design, The Bailer's method was used to perform the data analysis [118]. For this method, α was 0.05 and the critical value of Z (Z crit) for the 2-sided test after Bonferroni adjustment was 2.24, and the observed value of Z (Z_{obs}) was calculated. The maximal concentration (C_{max}) and the time to achieve it (T_{max}) were determined by visual inspection of the data. The tissue-to-plasma (Kp) concentration ratios were also calculated for the post-distributive phase in heart, liver and lung samples

2.12.2. Microsome incubation study analysis

Substrate inhibition and Michaelis-Menten equations were used to determine V_{max} and K_m [119]. The rate of desbutyldronedarone formation in both liver and intestinal microsomes was achieved by plotting the formed desbutyldronedarone at different substrate concentrations. Substrate – Inhibition, single, and multiple enzyme models for metabolism of dronedarone to desbutyldronedarone were fitted to the formation rate versus time data using Solver routine program based on Microsoft Excel (Microsoft, Redmond, WA). The Michaelis-Menten model for a single enzyme was used as follows:

$$\boldsymbol{V = \frac{V_{max} \times [Dr]}{k_m + [Dr]}}$$

The substrate-inhibition model was used as follows:

$$\boldsymbol{V = \frac{V_{max} \times [Dr]}{k_m + [Dr] + \frac{[Dr]^n}{K_i}}}$$

One of the two-enzyme models was used, consisting of a single saturable and a second linear component, as follows:

$$\boldsymbol{V = \frac{V_{max1} \times [Dr]}{k_{m1} + [Dr]} \times CL_2 + [Dr]}$$

Where V_{max} is the maximal rate of formation (capacity), K_m is the affinity constant, [DR] is the concentration of dronedarone, n is shape factor, K_i is the inhibition constant for dronedarone inhibition, K_{m1} and V_{maxi1} are the kinetic constants for a high-affinity enzyme, and CL_2 represented the V_{max} / K_m ratio for the low-affinity enzyme. To determine the V_{max}, K_m and CL_{int} parameters, we tried different enzyme kinetic models with fitting using the Solver function in Microsoft Excel GRG Nonlinear algorithm. The optimal choice of enzyme model was judged by the residual sum of squares and the Akaike Information Criterion (AIC) as a measure of the goodness of fit. Intrinsic clearance (CL_{int}) was calculated by calculating the ratio of V_{max} to K_m. Data were analyzed using a one-way ANOVA (followed by post-hoc Duncan's multiple comparison test) and unpaired-Student's t-test. Microsoft Excel (Microsoft, Redmond WA) or Sigma Plot 13 were used in statistical analysis of data. The level of significance was set at $p<0.05$.

To estimate the Clint in the depletion experiment involving microsomes from HFCS treated rats, we used the following formula [119]:

$$CL_{int} = \frac{0.693}{t_{1/2} \times [microsomal\ protein]}$$

2.12.3. Total CYP 450 measurement study analysis

Data were analyzed using a one-way ANOVA (followed by post-hoc Duncan's multiple comparison test). Sigma Plot 13 was used in the statistical analysis of data. The level of significance was set at $p<0.05$.

2.12.4. Triglyceride and cholesterol study analysis

Data were expressed as mean±SD. Unpaired Student's T-test was used to assess the significance of differences between NL and HL. The level of significance was set at $p<0.05$.

Chapter 3: Results

3.1. Development of an HPLC-UV assay for the determination of dronedarone in rat plasma

The retention times were 4.9 min for I.S. and 19.5 min for dronedarone. By calculating the asymmetry index, the peaks were found to be symmetrical (value of 1.1 calculated in spiked rat plasma). The peaks were symmetrical. The method provided specificity with a lack of interfering peaks from endogenous components in plasma (Figure 7). The mean recoveries of dronedarone from plasma were estimated to be 90 to 92% between 50 and 500 ng/mL of dronedarone in plasma. The average extraction recovery of IS was 81 %. The signal to noise ratio (S/N) was 10 at 25 ng/ml (the validated lower limit of quantification).

There were excellent linear relationships (r^2>0.999) noted between the peak height ratios and concentrations over ranges of 25 to 1000 ng/mL plasma (Figure 8). The typical r^2 for standard curves in plasma using peak height ratios of dronedarone to IS was >0.99. The CV of intra-and inter-day assessments for plasma were 18% and less than 10%. The mean error was less than 12% (Table 6).

There were no significant differences in the measured concentrations between the nominal concentrations of 250 and 500 ng/mL, nor was a difference detected between the measures at one week and one month of storage (Table 7). The confidence intervals contained the ratio 1 when comparing the measured concentration vs. the respective nominal concentrations. Further, the ratio of unity was encompassed between the confidence intervals of four weeks vs. one week measures at both concentrations.

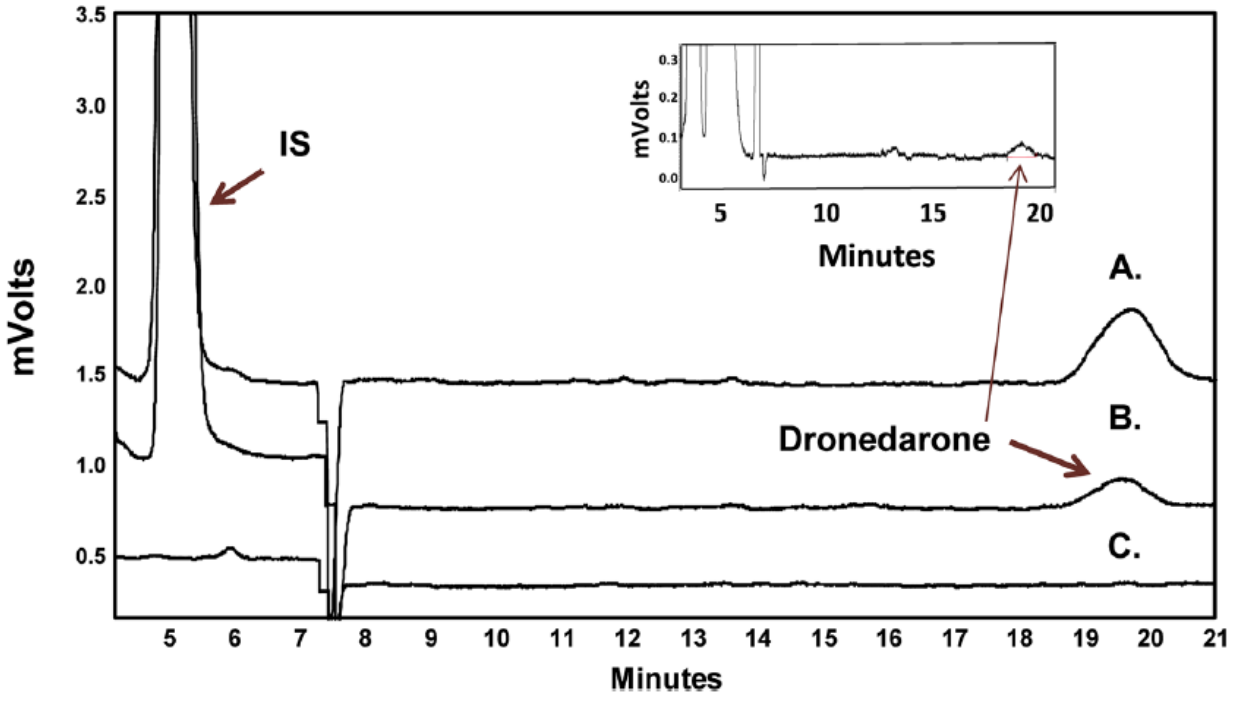

Figure 7: HPLC-UV chromatograms obtained from rat plasma given an oral dose of dronedarone (A.) rat plasma spiked with 250 ng/mL (B.) blank rat plasma(C.). The inset shows a section of a chromatogram of a rat plasma sample spiked with 25 ng/mL (the validated lower limit of quantification of the assay).

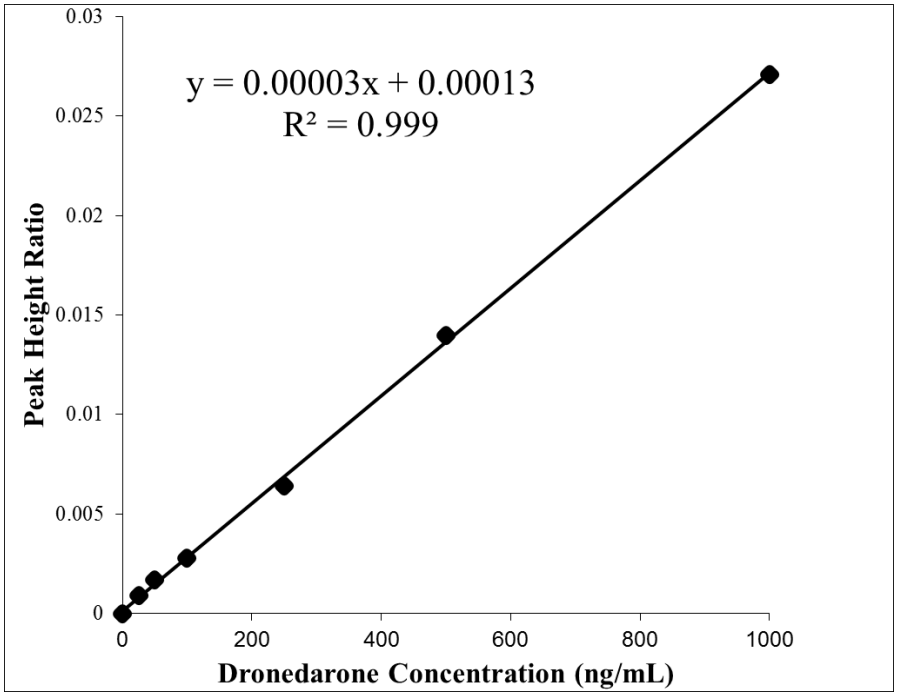

Figure 8: Representative calibration curves of dronedarone in rat plasma.

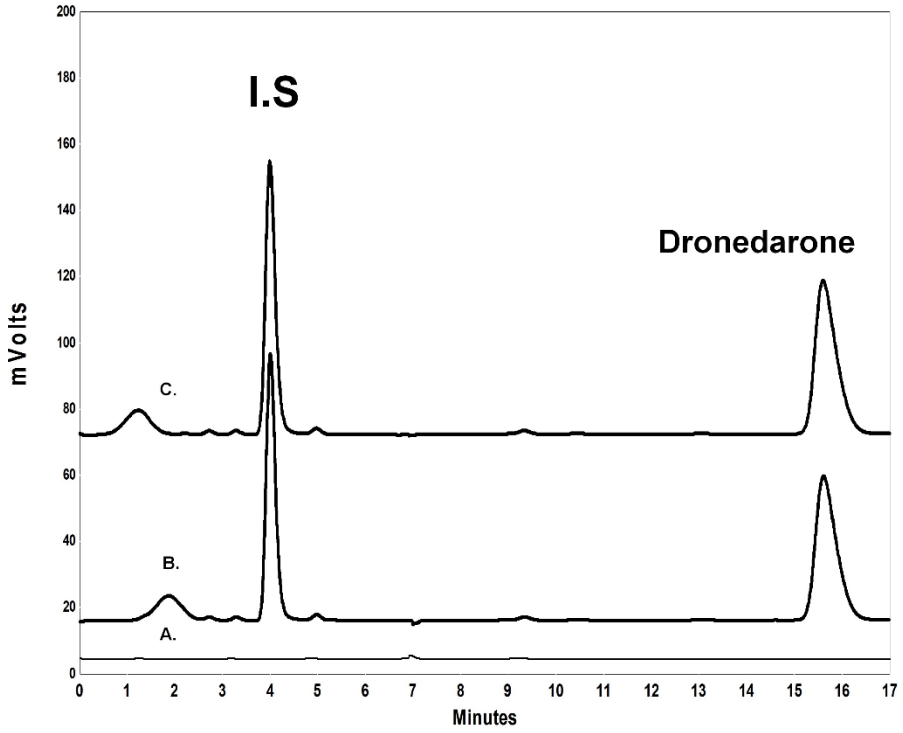

Figure 9: HPLC-UV chromatograms obtained from the assay of A.) Blank rat lung tissue, B.) Rat lung tissue 6 h after oral administration of dronedarone base, C.) Rat lung tissue spiked with 10,000ng/g tissue dronedarone.

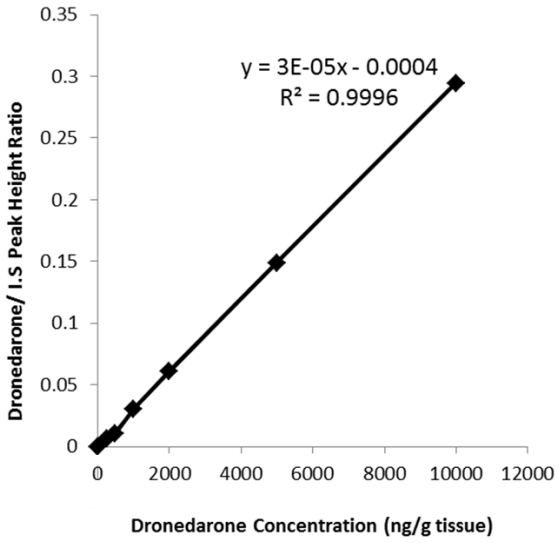

Figure 10: Representative calibration curves of dronedarone in lung tissue.

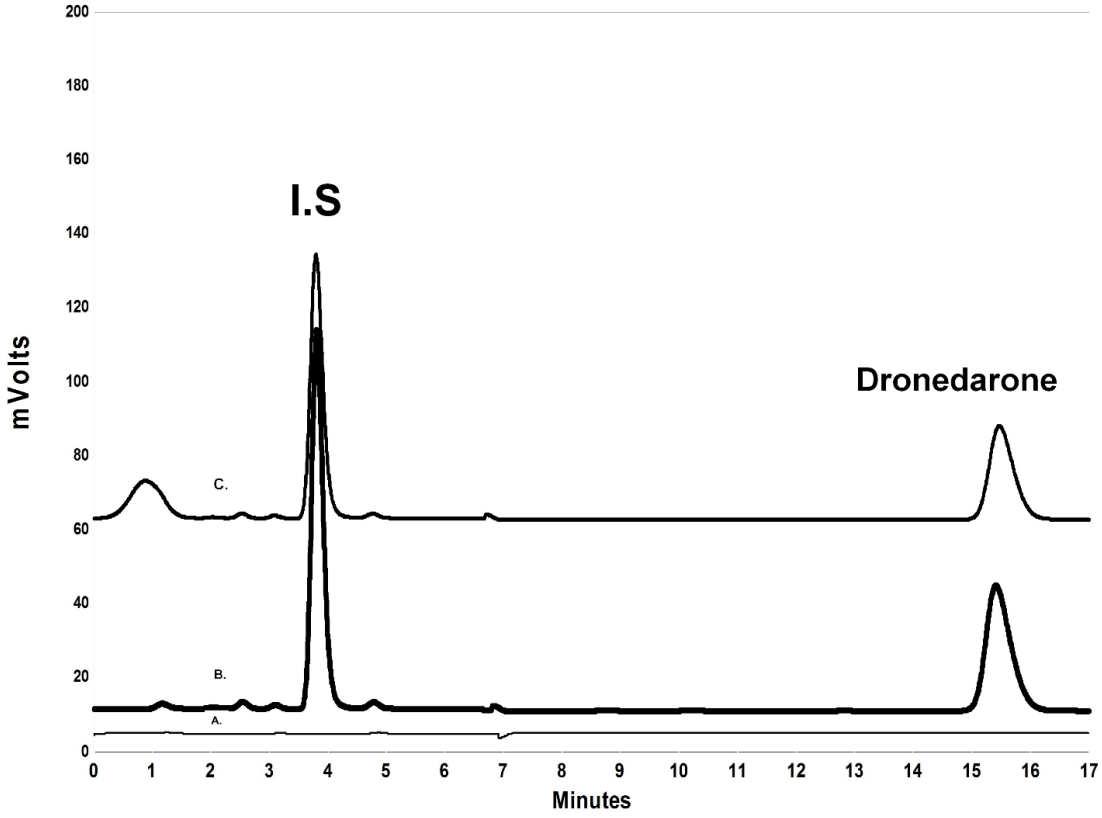

Figure 11: HPLC-UV chromatograms obtained from the assay of A.) Blank rat liver tissue, B.) Rat liver tissue 6 h after oral administration of dronedarone base, C.) Rat liver tissue spiked with 10,000 ng/g tissue dronedarone.

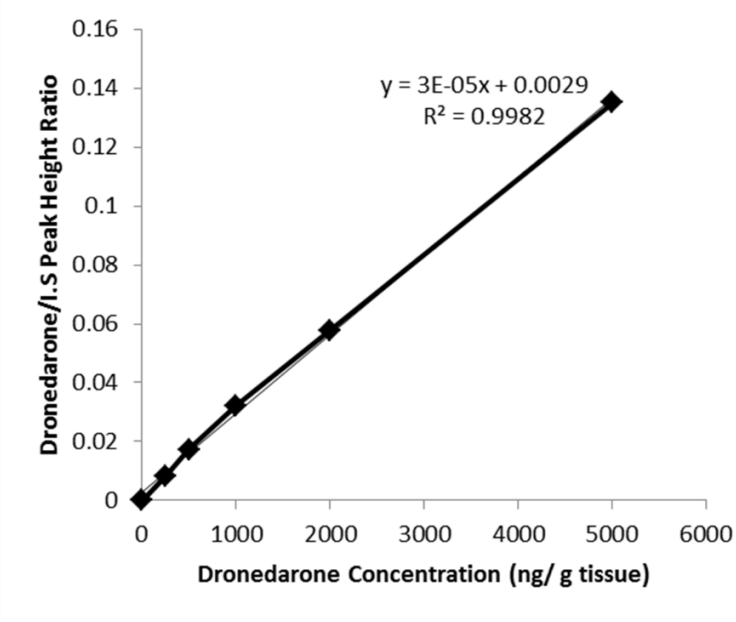

Figure 12: Representative calibration curves of dronedarone in liver tissue.

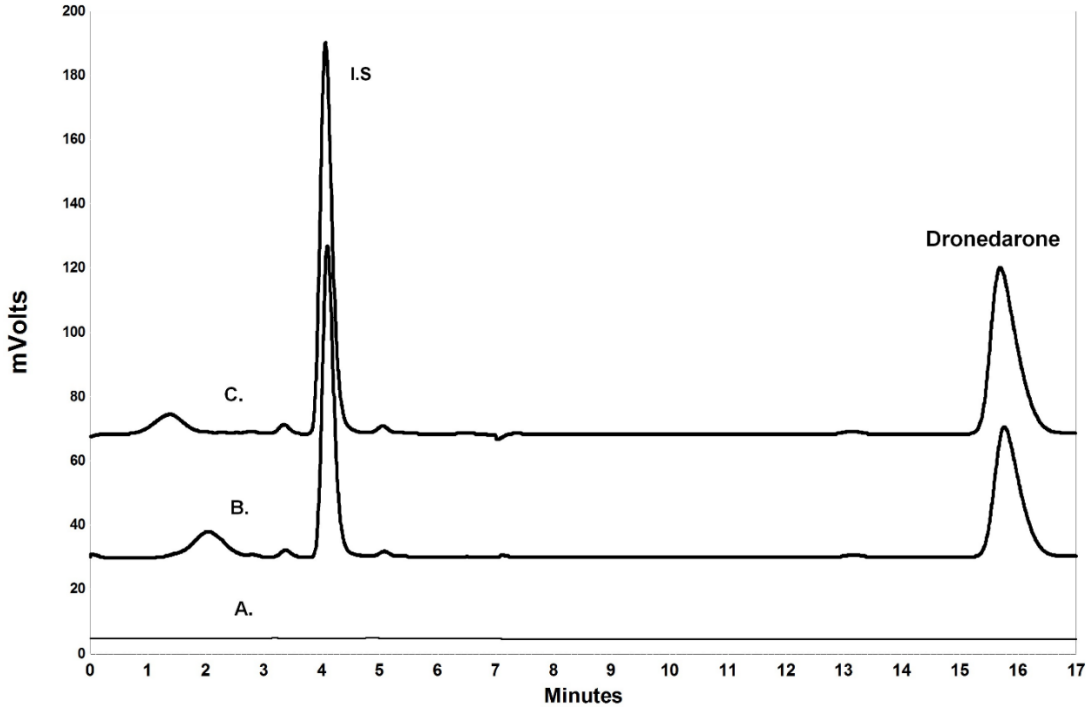

Figure 13: HPLC-UV chromatograms obtained from the assay of A.) Blank rat heart tissue, B.) Rat heart tissue 6 h after oral administration of dronedarone base, C.) Rat heart tissue spiked with 10,000 ng/g tissue dronedarone.

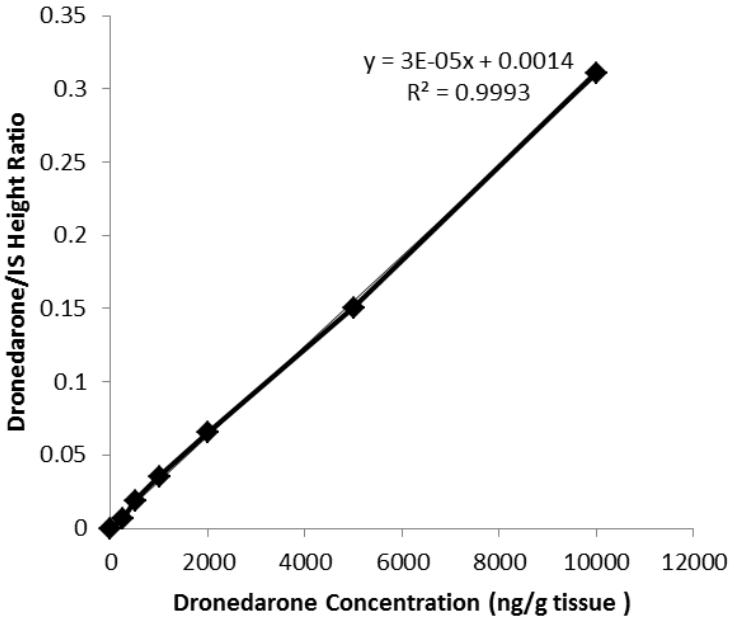

Figure 14: Representative calibration curves of dronedarone in heart tissue.

Table 6: Inter-day and intra-day validation data for dronedarone in rat plasma, n=5.

Nominal concentration, ng/mL	**Intraday**			**Interday**	
	Mean±SD, ng/mL (CV %)			**Mean±SD, ng/mL**	**Error %**
25	23.9±1.49 (6.24)	23.1±1.36 (5.89)	22.8±1.34 (5.85)	23.3 ± 0.56 (5.99)	-6.95
50	51.9±1.14 (2.19)	46.5±5.20 (11.2)	49±4.52 (9.22)	49.2±2.69 (7.53)	-1.71
100	105±5.14 (4.90)	107±6.27 (5.87)	83.9±14.9 (17.81)	98.5±12.70 (9.53)	-1.47
500	514±15.69 (3.05)	558±38.3 (6.85)	497±23.8 (4.79)	523±30.8 (4.90)	4.64

Table 7: Recovery of dronedarone after freezing of plasma for one week or one month at -20 C. Data shown are the mean±SD followed by the ratio of measured to expected and the corresponding 95% confidence intervals in square parentheses.

Nominal concentration, ng/mL	One Week	Four weeks	4 vs. 1 week
250	247±29.5 0.99 [0.69,1.28]	233±19.7 0.93 [0.74,1.13]	0.95 [0.78,1.13]
500	501±10.9 1.00 [0.95,1.06]	482±15.4 0.96 [0.89,1.04]	0.96 [0.92,1.01]

3.2. Development of a liquid chromatography-mass spectrometry (LC-MS) assay method for the quantification of dronedarone in rat plasma.

In an attempt to have in hand a more specific and sensitive assay, and attempt was made to develop an LC-MS assay for measurement of dronedarone in rat plasma. The components eluted at 8 and 13 min for IS and dronedarone, respectively (Figure 15). An excellent linear relationship was present between peak height ratios and rat plasma concentrations of dronedarone ranging from 5 to 1000 ng/mL (r^2>0.999) (Figure 16). The mass spectra of dronedarone and the internal standard, ethopropazine are shown in (Figure 17). The intraday and interday coefficients of variation (CV%) were equal or less than 11%, and mean error was <10% (Table 8). The validated limit of quantification of the assay was 5 ng/mL based on 0.1 mL rat plasma. Regarding the matrix effect, there was no significant matrix effect on the ionization of dronedarone and IS. This method can

measure the plasma concentrations of dronedarone in rat after oral single dose of 55 mg/kg (Figure 18).

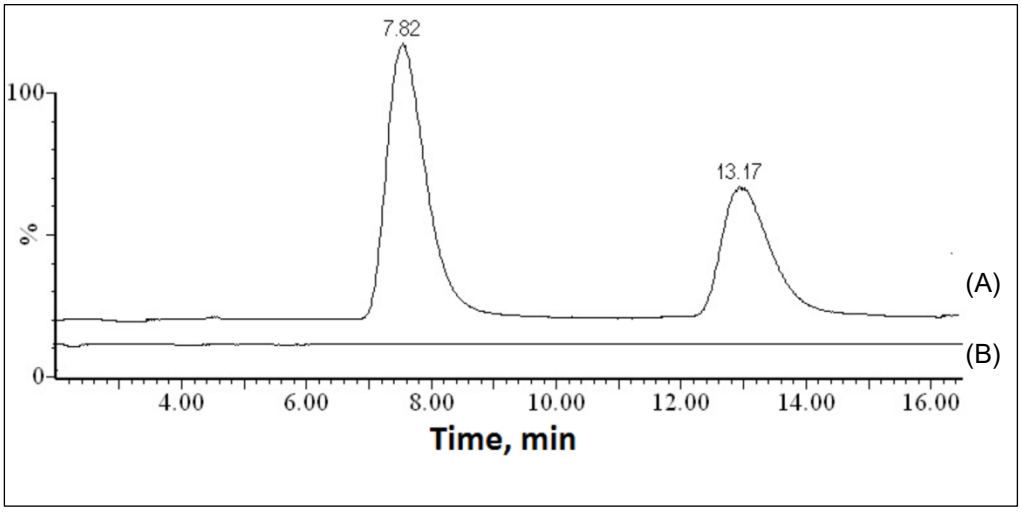

Figure 15: Selective ion chromatogram of dronedarone and ethopropazine (IS). (A) Rat plasma sample collected 6hr after an oral administration of a 55mg/kg dronedarone spiked with IS. (B) Blank rat plasma.

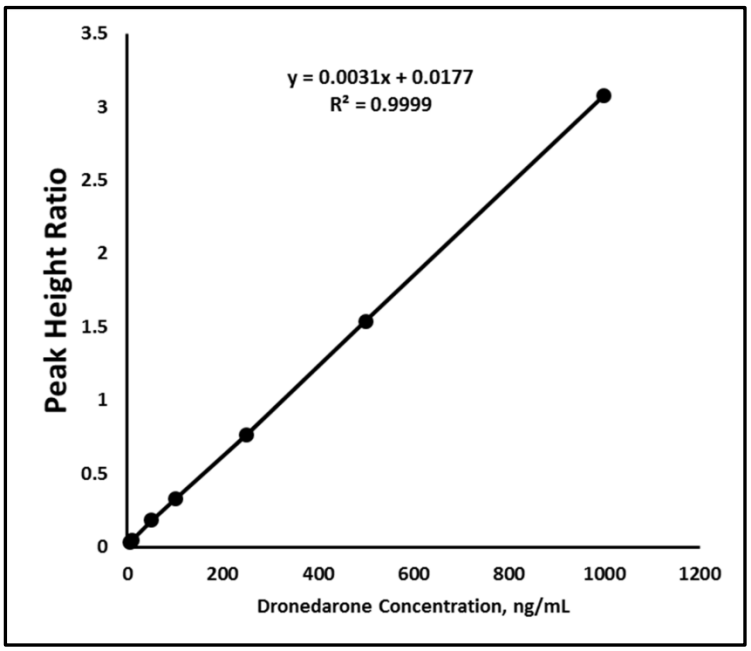

Figure 16:The assay was linear from 5 to 1000 ng/ml in plasma

Table 8: LCMS validation data for dronedarone in rat plasma, n=5.

Nominal concentration, ng/mL	**Intraday**			**Interday**	
	Mean±SD, ng/mL (CV %)			**Mean±SD, ng/mL**	**Error %**
5	4.93±0.13 (2.70)	4.59±0.44 (9.54)	5.84±1.23 (21)	5.12±0.60 (11.1)	2.38
50	58.17±4.20 (7.22)	40.27±0.44 (9.54)	40.8±1.89 (4.63)	46.41±3.25 (6.98)	-7.18
100	100.6±18.7 (18.3)	89.45±3.66 (7.93)	80.1±1.62 (2.03)	90±9.16 (9.53)	-9.95
1000	961±15.71 (3.05)	927.4±62.7 (6.77)	851.3±130 (15.3)	913.5±115 (12.6)	-8.65

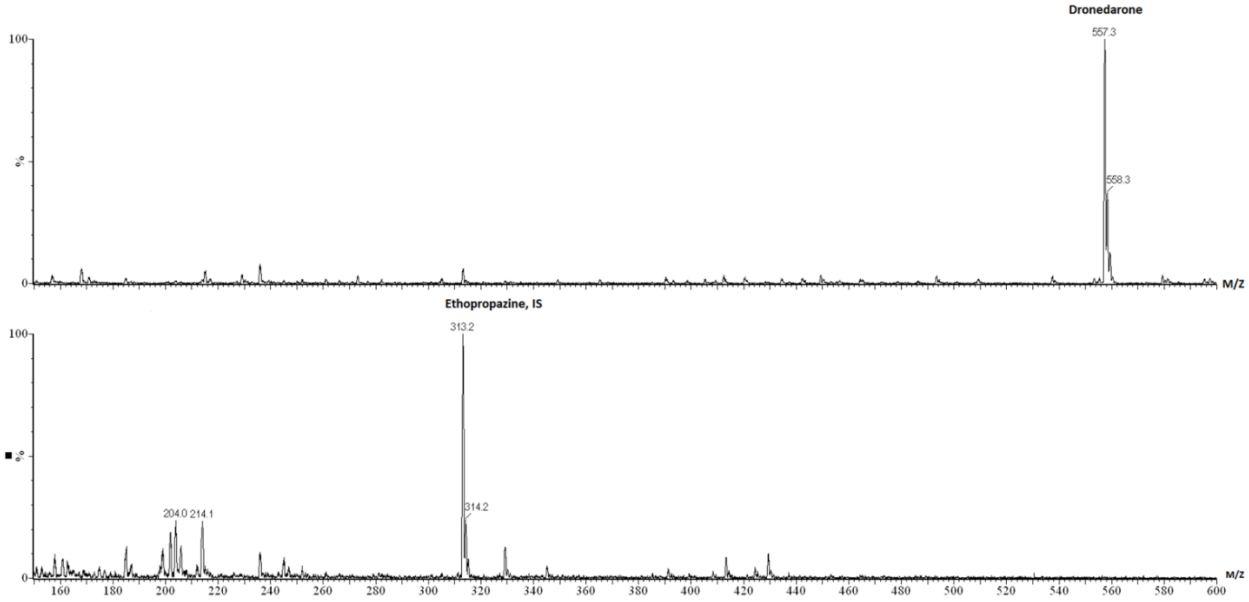

Figure 17: Mass spectra of dronedarone (upper panel) and the internal standard, ethopropazine (lower panel). The monitored ions are highlighted in the spectra.

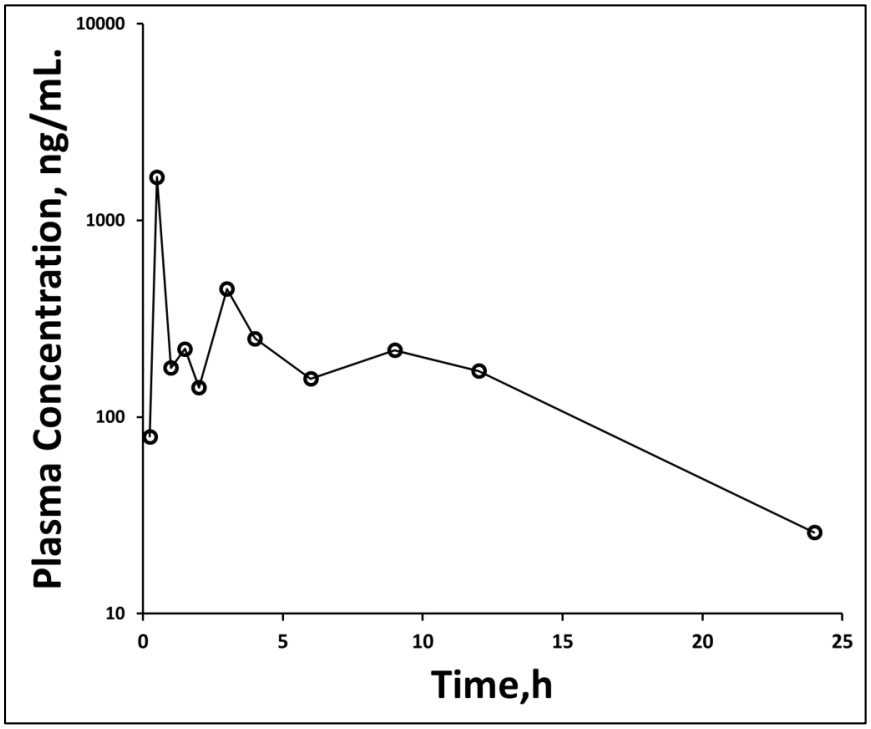

Figure 18: The plasma dronedarone concentrations after oral administration (55 mg/kg dronedarone as base) in rat.

3.2. Pharmacokinetics of dronedarone in normolipidemic rats

Data showing the pharmacokinetic data calculated from noncompartmental analysis is depicted in Table 9. Using PK Solver and statistical criteria for assessment of goodness of fit, after iv doses, the plasma concentrations of dronedarone were found to generally decline in a triphasic manner (Figure 19). The volume of the central compartment was estimated to be 1.51±2.15 L/kg, or about 14% of the Vdss, which was far greater than total body weight and total body water mass (Table 9). Individual rats pharmacokinetic profiles after iv, po, ip doses and corresponding pharmacokinetics parameters are shown in Figures 20, 21 and 22 and Tables 10,11 and 12).

After oral dosing, there were measurable amounts of drug in plasma at the time of the first post-dose blood sample (Figure 19) in each rat, and the t_{max} was generally attained by 3.5 hours after dosing. The terminal phases after po and ip dosing both closely matched that of iv dosing, indicating the lack of flip-flop kinetics. The mean F of po and ip dronedarone was estimated to be low (<20%; Table 9); statistical analysis was not undertaken because it was not a crossover design. Intraperitoneal dosing led to peak concentrations (C_{max}) being reached at approximately the same time as that of oral doses, with similar half-life. The AUC and C_{max} after ip doses were not significantly different from oral doses.

Table 9: Summary of pharmacokinetics of dronedarone in plasma of Sprague–Dawley rats. Data are expressed as arithmetic mean±SD for all parameters except t_{max}, which is expressed as median. The range is indicated in parentheses.

Parameter	**Intravenous 4 mg/kg (n=8)**	**Oral 55 mg/kg (n=8)**	**Intraperitoneal 65 mg/kg (n=7)**
AUC_{0-24}, mg·h/L	2.70±0.872 (1.73-4.18)	6.12±1.81 (3.64-9.65)	6.30±5.01 (1.56-15.7)
$AUC_{0-\infty}$, mg·h/L	2.92±0.992 (1.77-4.75)	6.64±1.99 (3.84-10.1)	7.37±5.90 (2.05-18.0)
$t_{½}$, h	6.84±2.51 (4.33-11.6)	6.03±1.88 (3.30-8.02)	8.78±2.96 (4.61-13.7)
CL, mL/min/kg	25.1±8.09 (14.1-37.6)	-	-
Vdss, L/kg	10.8±4.77 (2.87-16.5)	-	-
C_{max}, mg/L	-	1.87±1.65 (0.29-4.91)	0.816±0.611 (0.179-1.95)
t_{max}, h	-	3.50 (0.50-8.00)	3.00 (0.25-6.0)
CL/F, mL/min/kg	-	178±56.8 (107-282)	250±176 (60.4-529)
Vdss/F, L/kg	-	98.8±36.3 (47.2-163)	191±168 (43.8-534)
MRT, h	6.25±3.18 (2.11-11.6)	9.69±3.41 (6.03-14.7)	12.6±2.97 (8.26-16.9)
F, %	-	15.9	14.9

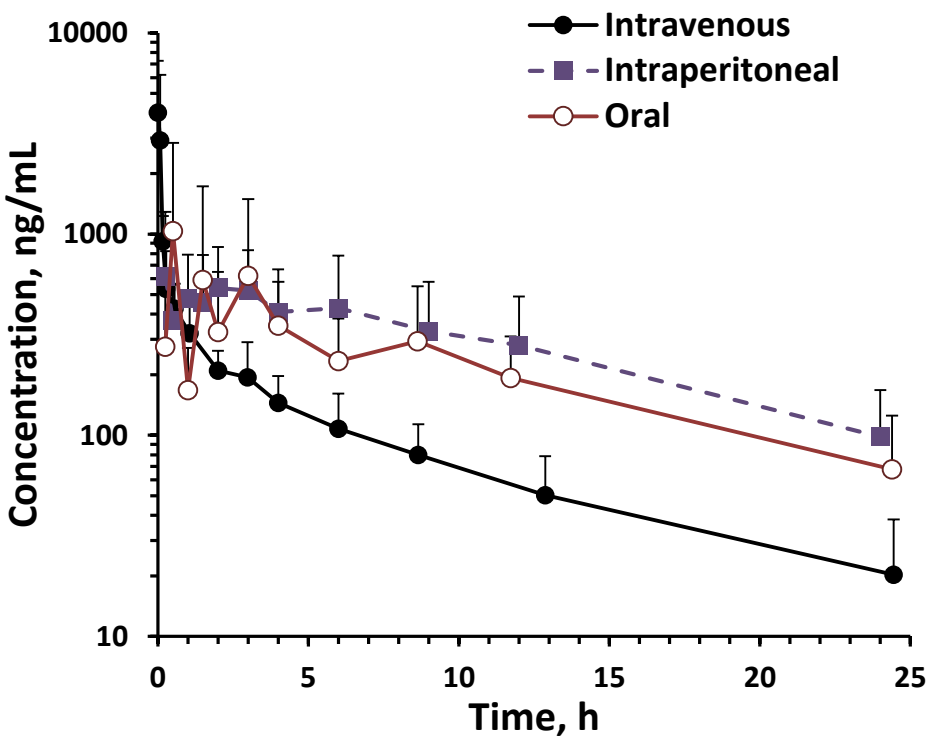

Figure 19: Mean plasma concentration (±SD) vs. time profiles of dronedarone after intravenous (4 mg/kg), oral (55 mg/kg) ip (65 mg/kg) single doses to normolipidemic Sprague-Dawley rats.

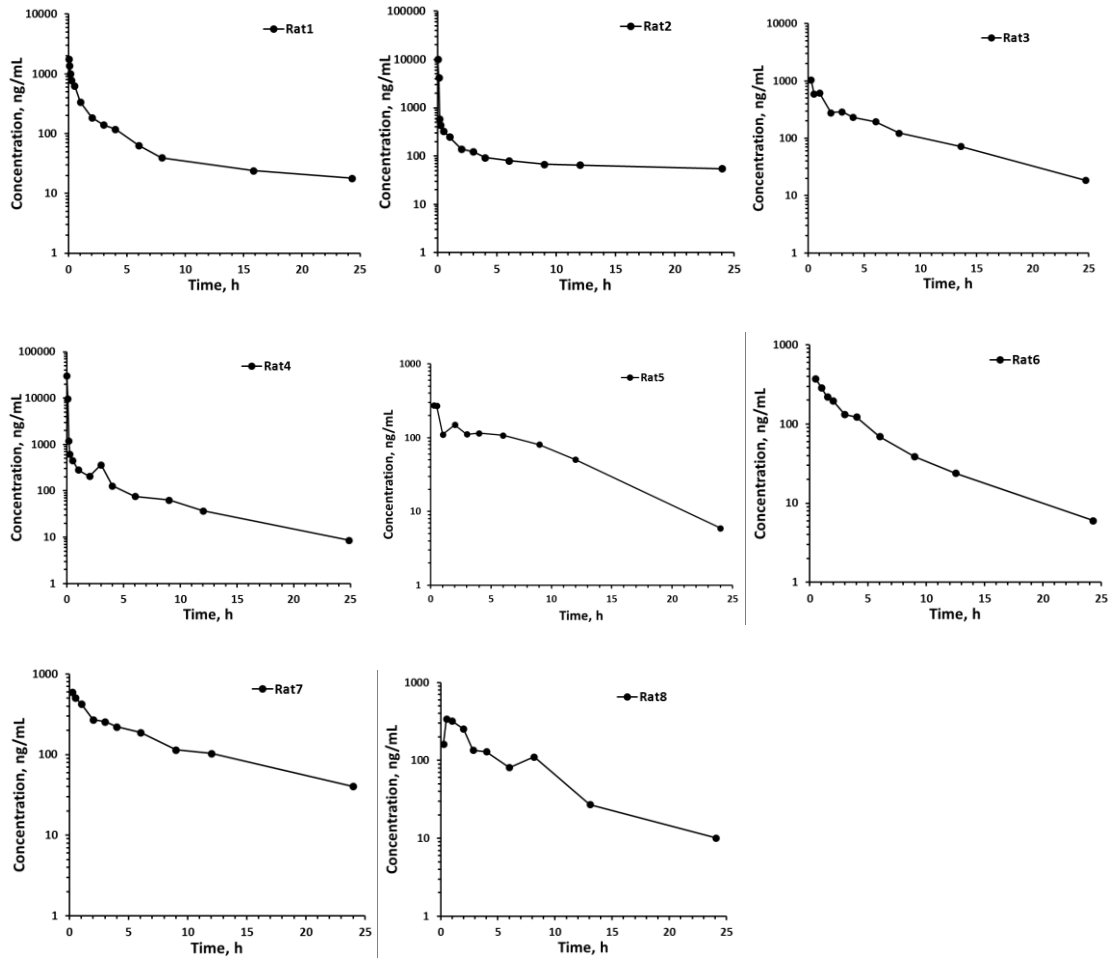

Figure 20: Individual plasma concentration versus time curves of dronedarone in eight normolipidemic (NL) rats after iv injection of 4 mg/kg of drug as base

Table 10: The individual pharmacokinetic data in eight rats after the intravenous administration of 4 mg/kg of dronedarone as base.

	AUC_{0-24}, mg·h/L	**$AUC_{0-\infty}$, mg·h/L**	**$t_{½}$, h**	**CL, mL/min/kg**	**Vdss, L/kg**	**MRT, h**
Rat 1	1.98	2.28	11.64	29.18	16.49	9.42
Rat 2	2.59	3.12	6.70	21.4	14.88	11.59
Rat 3	3.29	3.36	5.67	19.86	4.52	3.79
Rat 4	1.73	1.77	4.33	37.65	15.81	6.45
Rat 5	2.42	2.47	5.77	27.02	5.78	2.11
Rat 6	4.58	5.15	9.66	12.95	6.87	2.80
Rat 7	1.92	1.99	4.94	33.5	12.71	6.33
Rat 8	3.49	3.65	6	18.25	7.70	7.04

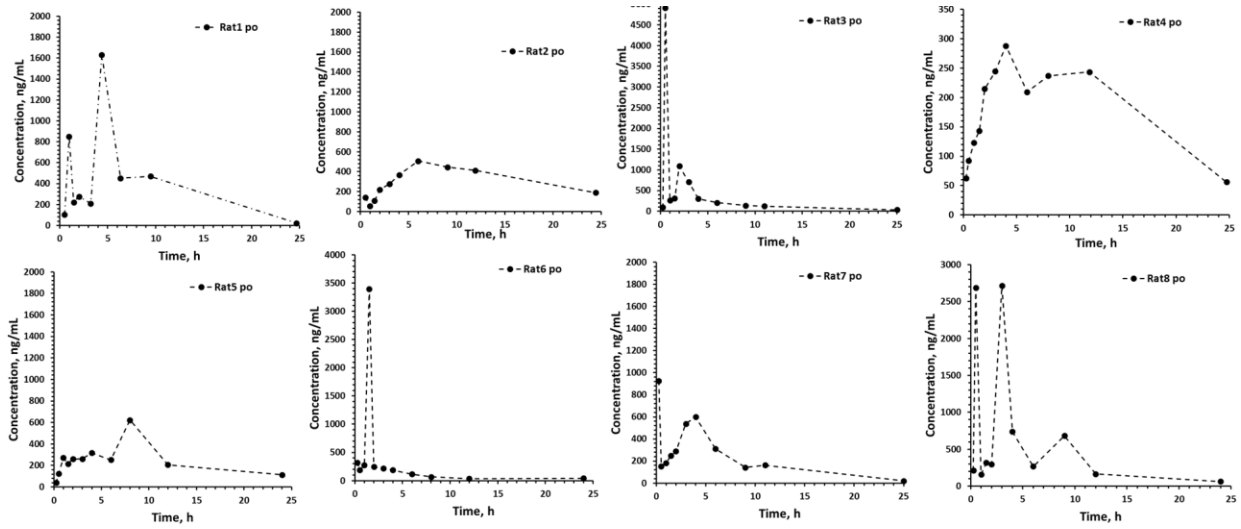

Figure 21: Individual plasma concentration versus time curves of dronedarone in eight normolipidemic (NL) rats after oral dose of 55 mg/kg of drug as base.

Table 11: The individual pharmacokinetic data in eight rats after oral administration of 55 mg/kg of dronedarone as base.

	AUC_{0-24}, mg·h/L	**$AUC_{0-\infty}$, mg·h/L**	**t½, h**	**CL/F, mL/min/kg**	**Vdss/F, L/kg**	**Tmax, H**	**MRT, h**
Rat 1	7.20	7.32	3.94	147.91	83.46	4.4	6.03
Rat 2	6.81	7.85	7.59	138.07	109.62	1.5	12.81
Rat 3	3.29	3.32	4.36	326.28	68.7	1.5	14.72
Rat 4	4.35	4.62	6.23	234.60	160.38	4	7.33
Rat 5	4.98	5.25	4.71	206.35	122.6	8	7.47
Rat 6	9.98	10.44	5.03	103.77	45.46	3	6.54
Rat 7	4.73	4.88	5.19	222.13	99.5	4	7.47
Rat 8	6.21	6.58	7.67	164.61	64.6	0.5	6.54

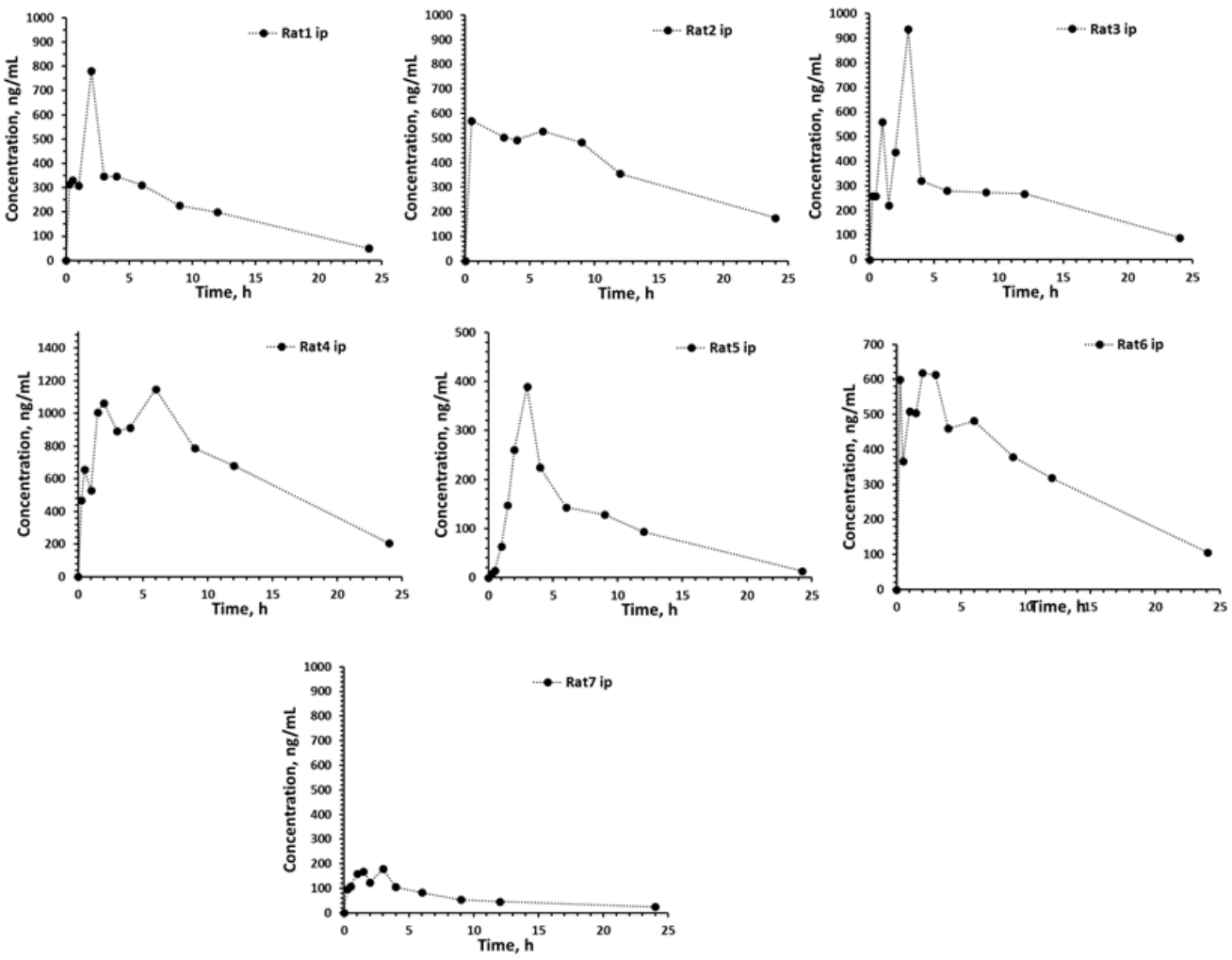

Figure 22: Individual plasma concentration versus time curves of dronedarone in seven normolipidemic (NL) rats after ip dose of 65 mg/kg of drug as base.

Table 12: The individual pharmacokinetic data in seven rats after ip administration of 65 mg/kg of dronedarone as base.

	AUC_{0-24}, mg·h/L	**$AUC_{0-\infty}$, mg·h/L**	**$t_{½}$, h**	**CL/F, mL/min/kg**	**Vdss/F, L/kg**	**Tmax, h**	**MRT, h**
Rat 1	5.329	5.801	6.59	186.74	109.45	2	9.77
Rat 2	9.701	12.396	10.65	87.39	80.72	0.25	15.39
Rat 3	6.367	7.498	8.75	144.47	110.90	3	12.80
Rat 4	15.739	17.950	7.48	60.35	43.76	6	12.10
Rat 5	2.572	2.662	4.61	406.90	201.77	6	8.26
Rat 6	1.558	2.049	13.71	528.61	534.17	3	16.8
Rat 7	2.743	3.253	9.67	333.02	254.60	0.5	12.74

Comparison of the pharmacokinetic data from orally-dosed rats (Table 13, Figure 23) revealed that the plasma concentrations in the HL rats were generally higher over the first 24 h after dosing than seen for NL rats. This was confirmed in comparing the geometric mean values, where the AUC of HL rats was significantly higher than the NL rats. In addition, the CL/F and Vd/F were significantly lower in the HL rats. No differences were seen in the other measures (C_{max}, t½ and MRT). The plasma fu of dronedarone were estimated to be 0.14±0.11% and 0.21±0.12% in the NL and HL rat plasma, respectively ($p>0.05$).

Table 13: Geometric mean pharmacokinetic parameters (CV of geometric mean in parentheses) of dronedarone after 55 mg/kg oral doses given to normolipidemic and hyperlipidemic rats.

Parameter	**Normolipidemic (n=8)**	**Hyperlipidemic (n=6)**
AUC_{0-24}, mg·h/L	5.26 (38.2%)*	12.2 (100%)
$AUC_{0-\infty}$, mg·h/L	5.58 (39.5%)*	12.7 (105%)
$t_{½}$, h	5.75 (26.0%)	5.57 (53.2%)
C_{max}, mg/L	1.13 (131%)	3.27 (257%)
t_{max}, h	2.56 (106%)	1.46 (124%)
CL/F, mL/min/kg	194 (39.5%)*	85.1 (105%)
Vdss/F, L/kg	95.7 (39.5%)*	28.9 (97.6%)
MRT, h	8.21 (39.6%)	5.66 (35.8%)
*Significantly different compared to hyperlipidemic rats (single factor ANOVA)		

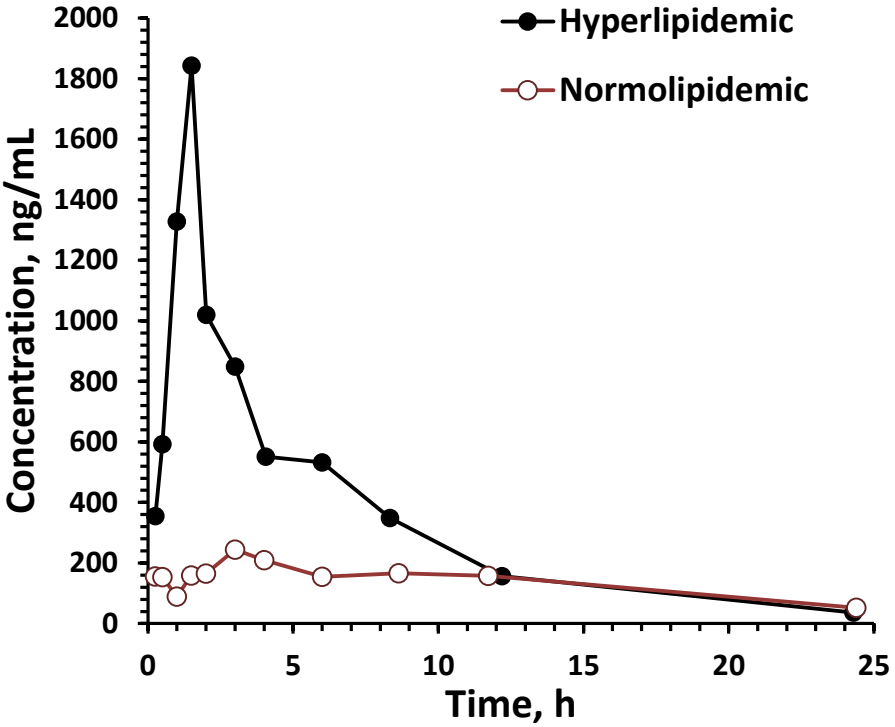

Figure 23: Geometric mean plasma concentration vs. time profiles of dronedarone after single oral doses of 55 mg/kg to normolipidemic and hyperlipidemic Sprague-Dawley rats.

3.5. Tissue distribution and metabolism of dronedarone in rat

3.5.1 Dronedarone plasma concentration

The plasma concentration of DR was higher at all measured time points in HL compared to the NL group but was only significant at 3 h. The plasma concentrations vs. time curve showed a decline in DR levels in NL after 6 hours. On the other hand, the HL group showed a decline after 9 hours at which the postdistributive phases appeared to be reached (Figure 24). The mean AUC_{0-24} was 7.92-fold higher and significant in the HL compared to NL rats (Table 14).

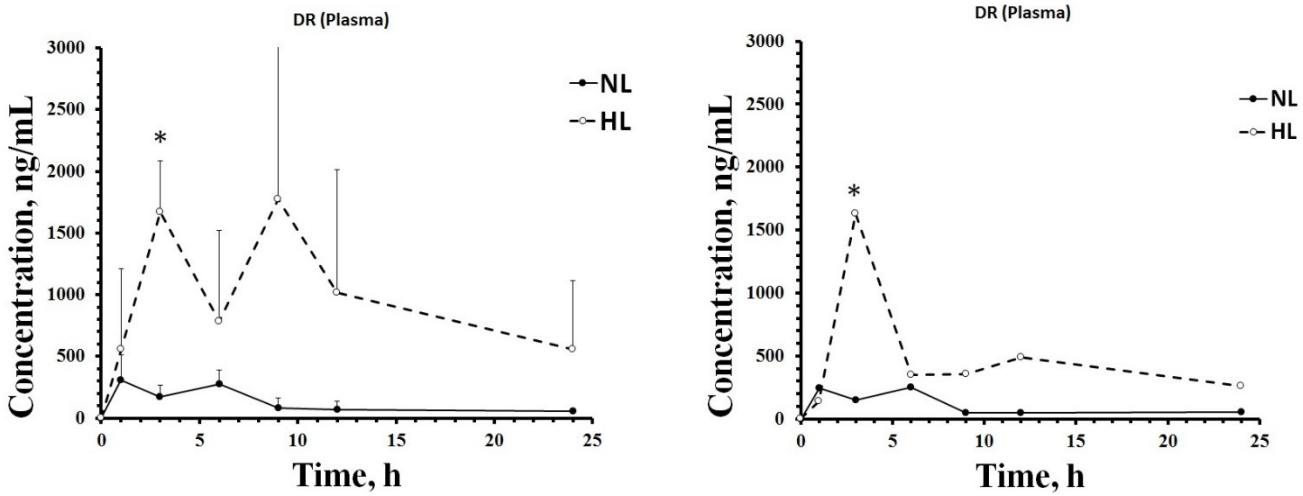

Figure 24: Mean concentration (±SD) vs. time (left), Geometric mean concentration vs. time (right) profiles of DR in the plasma following oral administration of 55mg/kg DR as base (n =24/group). Asterisks denote a significant difference in DR concentrations at that time point between NL and HL groups ($p<0.05$, unpaired t-test).

3.5.2. Dronedarone Tissue Distribution

Dronedarone (DR) was detected and measured in all specimens at quantifiable concentrations in all tissues (Figure 25 and Figure 26). The order in mean AUC from highest to lowest in NL group was heart > lung > liver > plasma. In HL group, it was lung > heart > liver > plasma (Table 14 and Figure 26). For lung, the mean AUC_{0-24} was 2.16-fold higher in the HL compared to NL rats but was not significant. In contrast, the mean AUC_{0-24} in heart was 2.1-fold higher and significant in the heart. There were no significant changes in liver concentrations between NL and HL groups. The calculated Kp values for the DR AUC in HL animals were consistently lower than those in NL animals (Table 14).

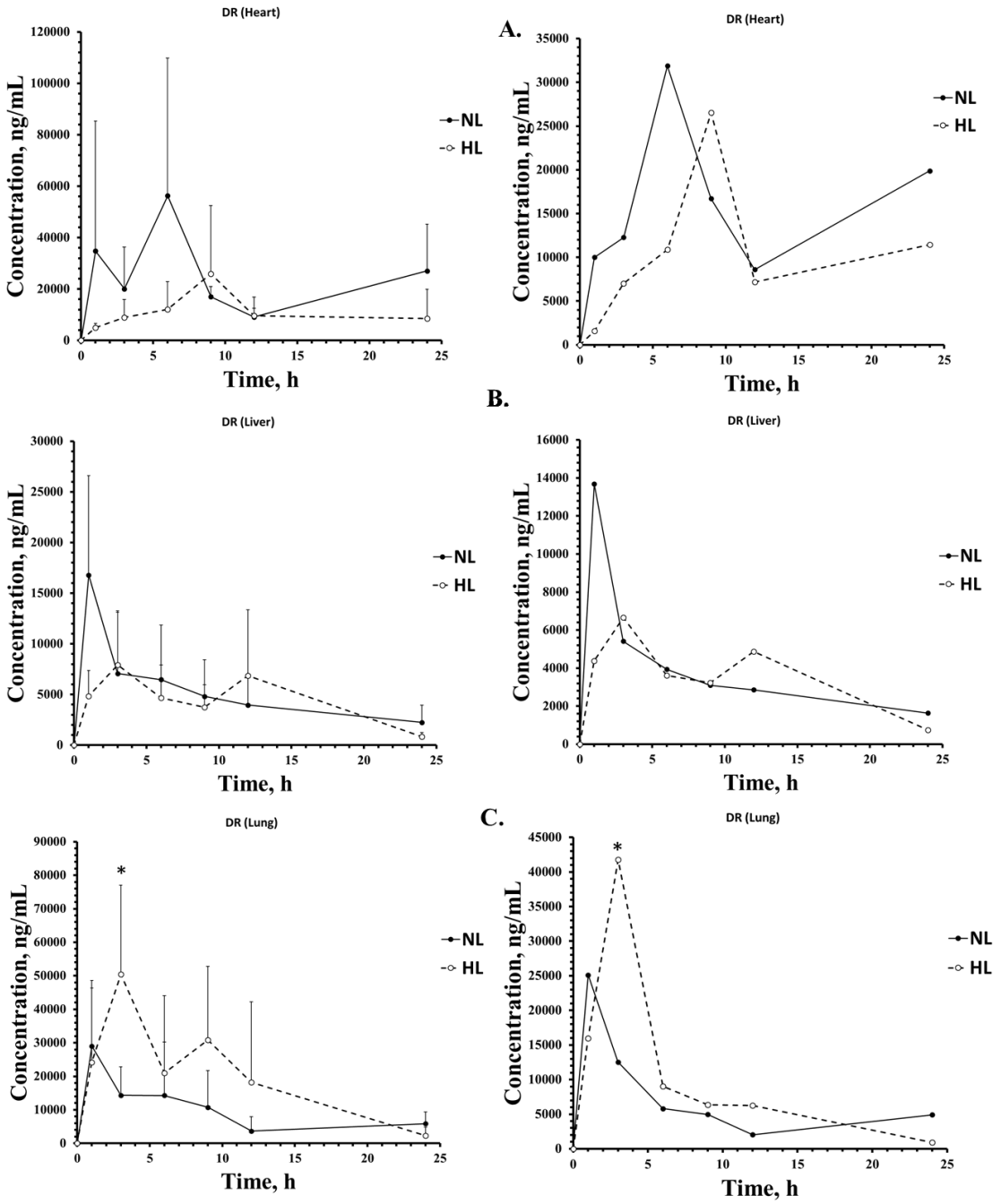

Figure 25: Mean Concentration (±SD) vs. time profiles of DR (left) and Geometric mean Concentration vs. time (right) in Heart (A.), Liver (B.) and Lung (C.) after oral administration of DR 55mg/kg as base. Asterisks denote a significant difference in DR concentrations at that time point between NL and HL groups ($p<0.05$, unpaired t-test).

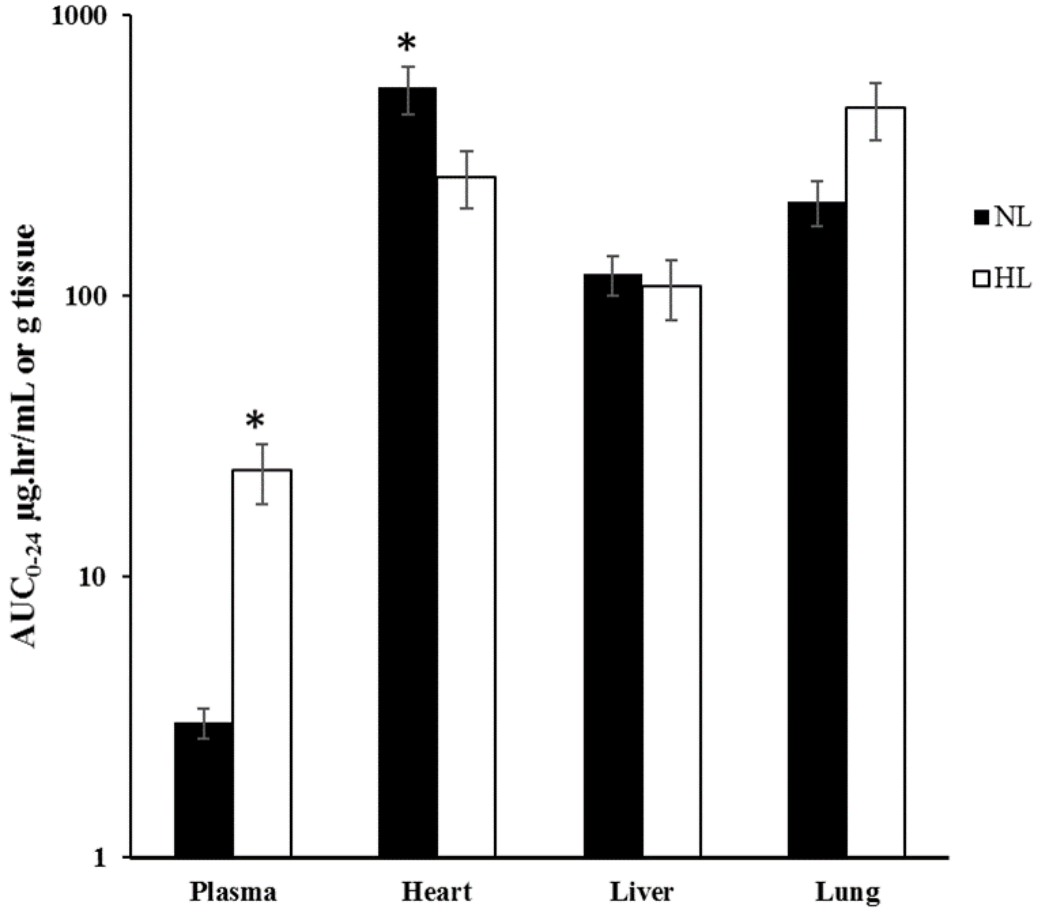

Figure 26: Mean area under the plasma and tissue concentrations (±SD) for dronedarone (µg.hr/mL or g tissue) in different tissues after oral administration of 55 mg/kg as base (n=24/group).

Table 14: Mean area under the plasma and tissue concentrations versus time curve (±SD) for DR (µg.hr/mL or g tissue) after oral administration of 55 mg/kg as base to rats (n=24/group). Asterisks Denote significant difference between two groups (using Bailer's method).

Specimen	Group		Kp	
	NL	HL	NL	HL
Plasma	3.022±0.377	23.94±5.732*	-	-
Heart	552.947±106.927*	267.035±61.957	183	11.15
Liver	119.811±19.101	108.501±26.115	39.64	4.53
Lung	216.843±38.706	468.076±109.147	71.75	19.55

3.5.3. Dronedarone microsomal incubations and metabolism to desbutyldronedarone

There was a linear increase in dronedarone metabolism rate with increasing protein concentrations from 0.25 up to 1 mg/mL suggesting that 0.5 mg/mL would be the best choice to use in the experiment (Figure 27).

In liver microsomes, the formation of desbutyldronedarone (DBD) in controls followed a pattern consistent with substrate inhibition/inactivation (the velocity curve reached the maximum and then descended as the substrate concentration increased further) (Figure 29). There was a significant difference ($p<0.05$) in V_{max}, K_m and CL_{int} values in HFD and HL groups compared to

controls (one way ANOVA) (Figure 30,Figure 31 and 32; Table 15). In the HFCS and combined HFD-HFCS groups there were linear increases in DBD formation vs. concentration profiles over the span of concentrations studied, preventing an estimation of V_{max} or K_m. The reported Cl_{int} were therefore based on the slopes of the formation rate vs. dronedarone concentrations for these two groups. Based on the CL_{int}, it was clear that the formation rates were reduced compared to controls (Figure 33 and Figure 34). The formation of DBD in liver in different groups were shown in Figure 35.

In intestine, a two-enzyme system best fit the data (one saturable, the other nonsaturable) (Figure 36, and Figure 37). A significant difference in CL_{int2} was seen for HL compared to control. The formation rate of DBD was reduced in HL compared to controls. Generally, the formation rate of DBD in intestine was much lower than in the liver in both Control and HL groups (Figure 37; Table 15).

We also tried to estimate the CL_{int} of overall dronedarone metabolism in the HFCS and HFCS-HFD groups using the enzyme depletion method (Figure 28). We found that the CL_{int} values in these 2 groups were 27.4 and 18.5 μL/min/mg protein, respectively. In comparison, the DBD formation CL values were much lower (0.074 and 0.593, respectively).

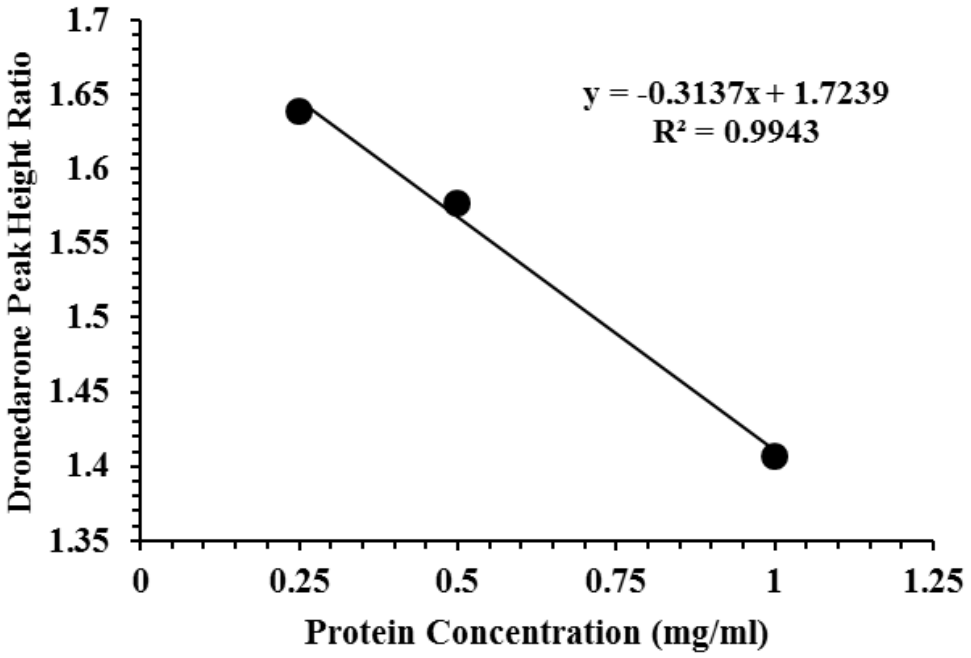

Figure 27: Linearity of dronedarone metabolism in different protein concentration of microsomes (9 µM of dronedarone was incubated with 0.25,0.5 and 1 mg/mL hepatic microsomes).

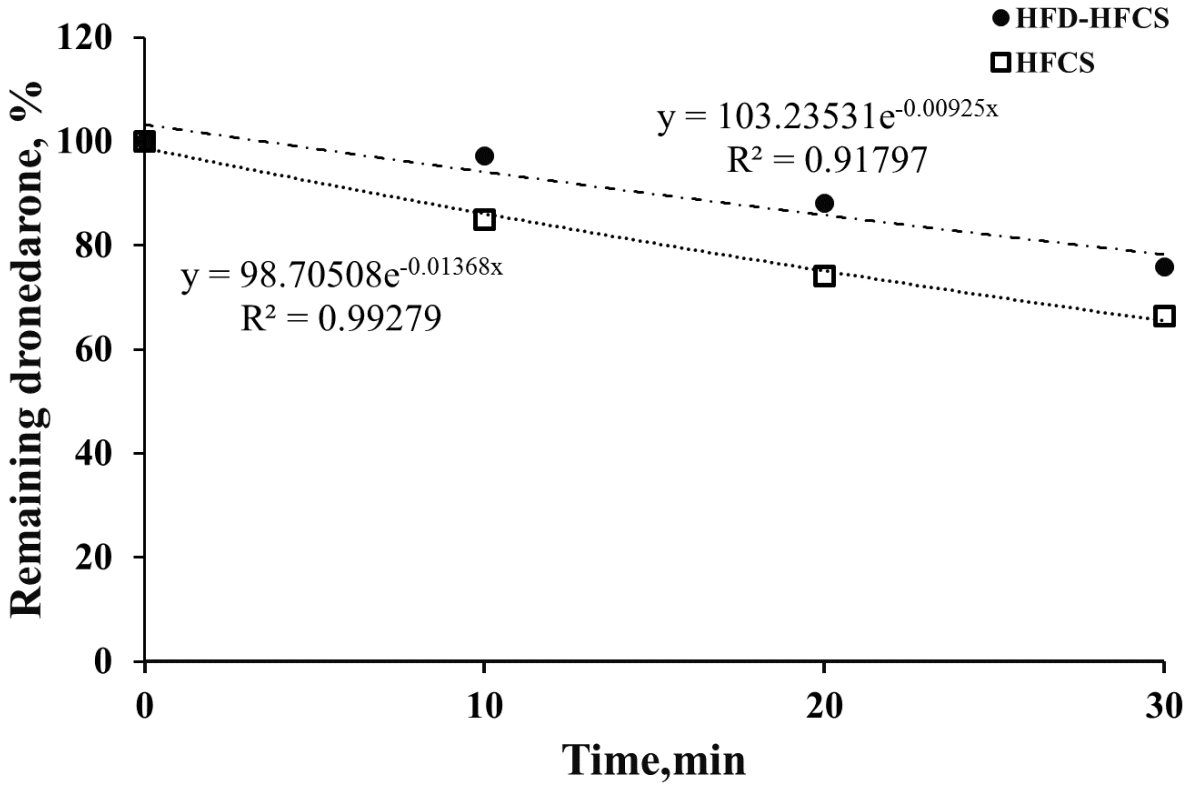

Figure 28: Dronedarone remaining (%) vs time after 10 μM was incubated with hepatic microsomal protein of HFCS and HFD-HFCS groups (n = 4/time point).

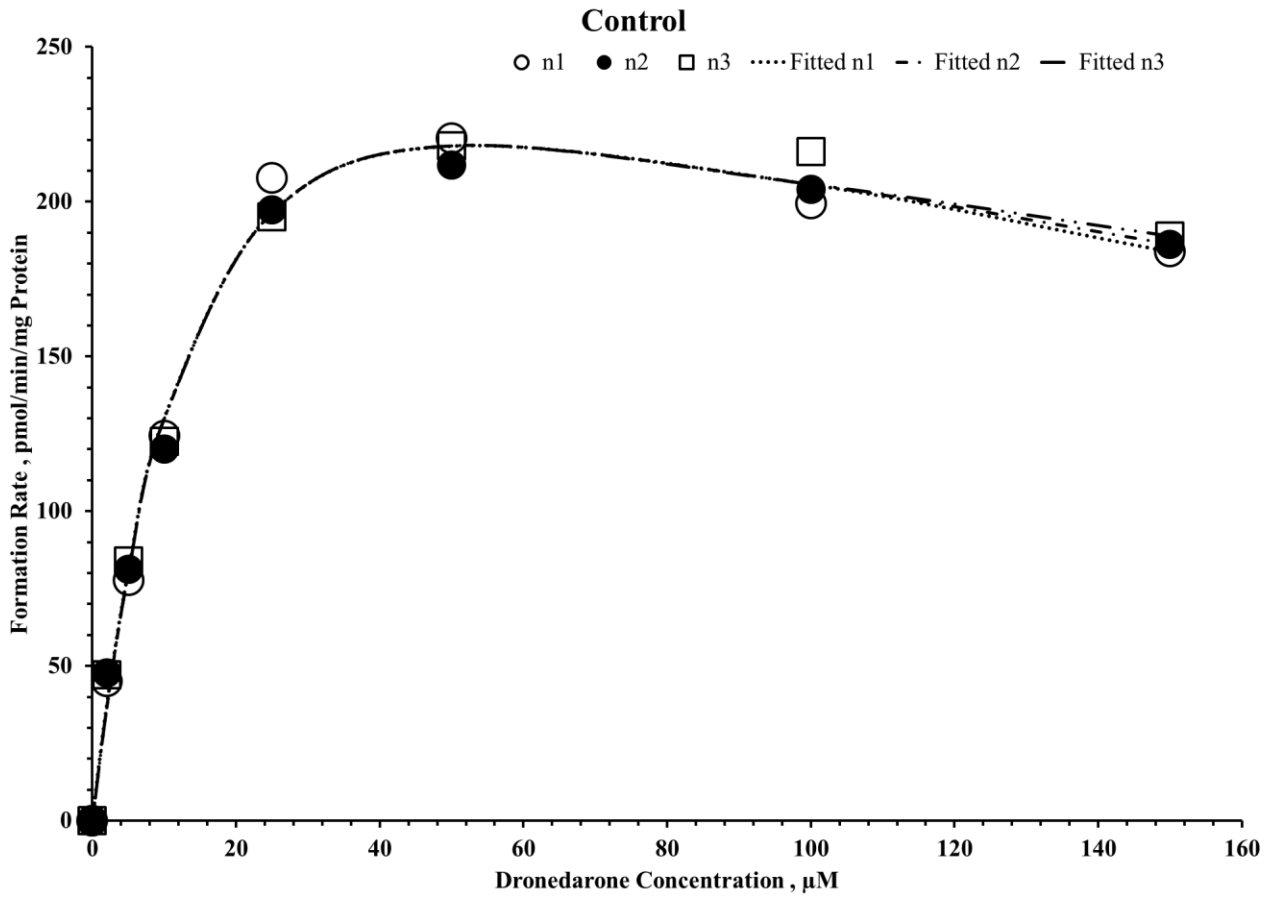

Figure 29: Velocity of DBD formation vs. Dronedarone concentration by liver microsomes in Control rat microsomes.

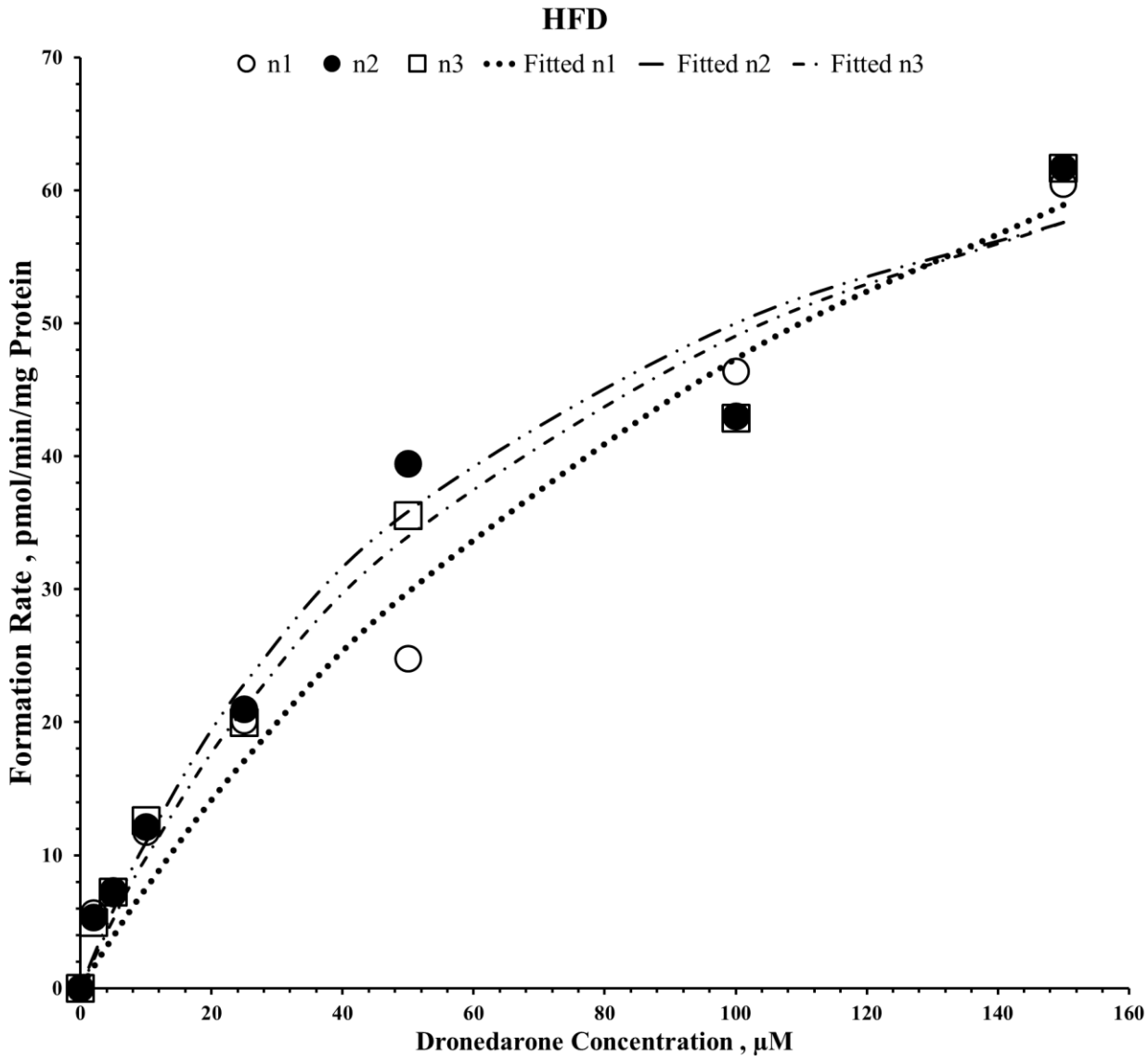

Figure 30: Velocity of DBD formation vs. dronedarone concentration by liver microsomes in HFD rat microsomes.

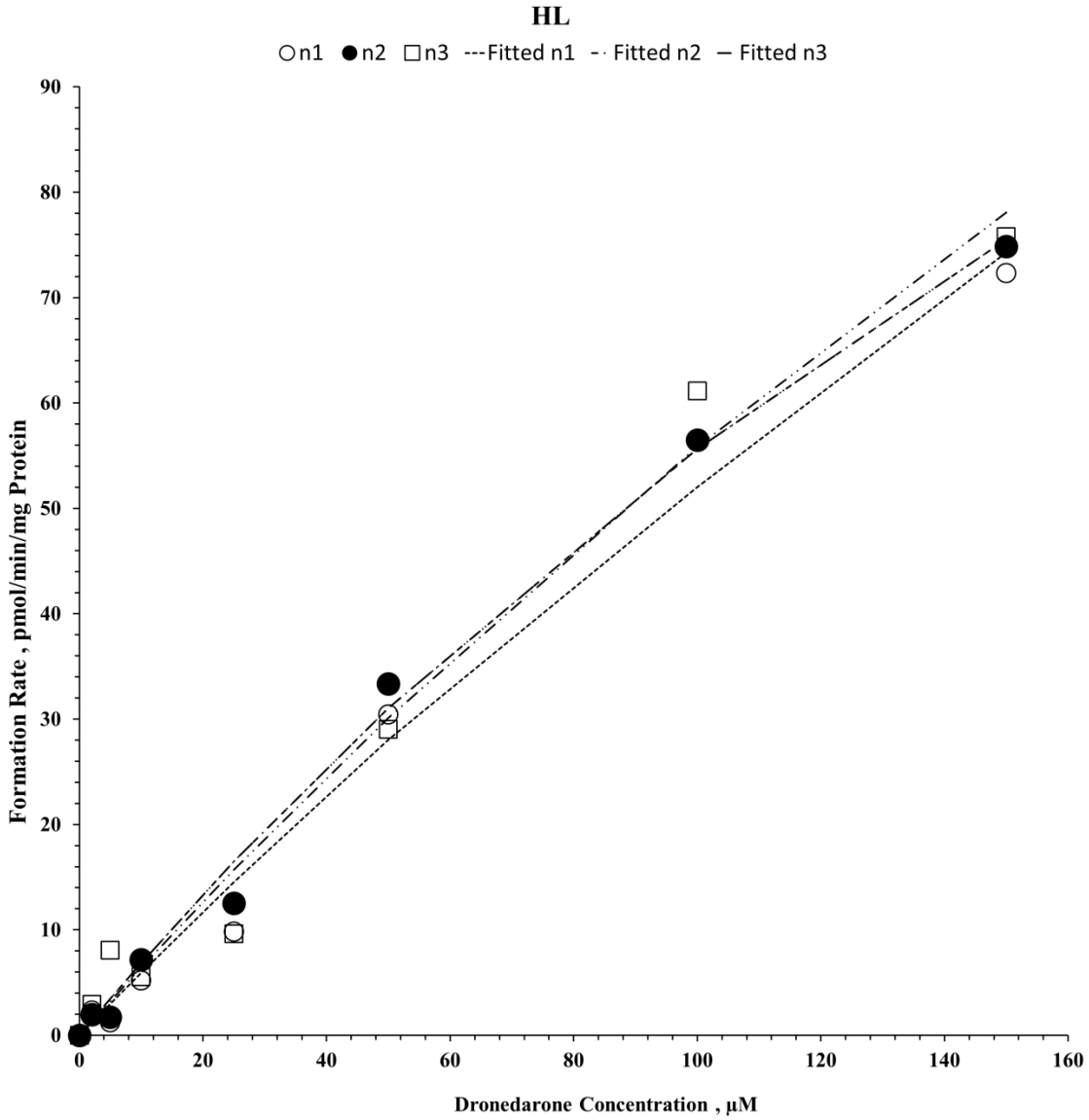

Figure 31: Velocity of DBD formation vs. dronedarone concentration by liver microsomes in HL rats microsomes.

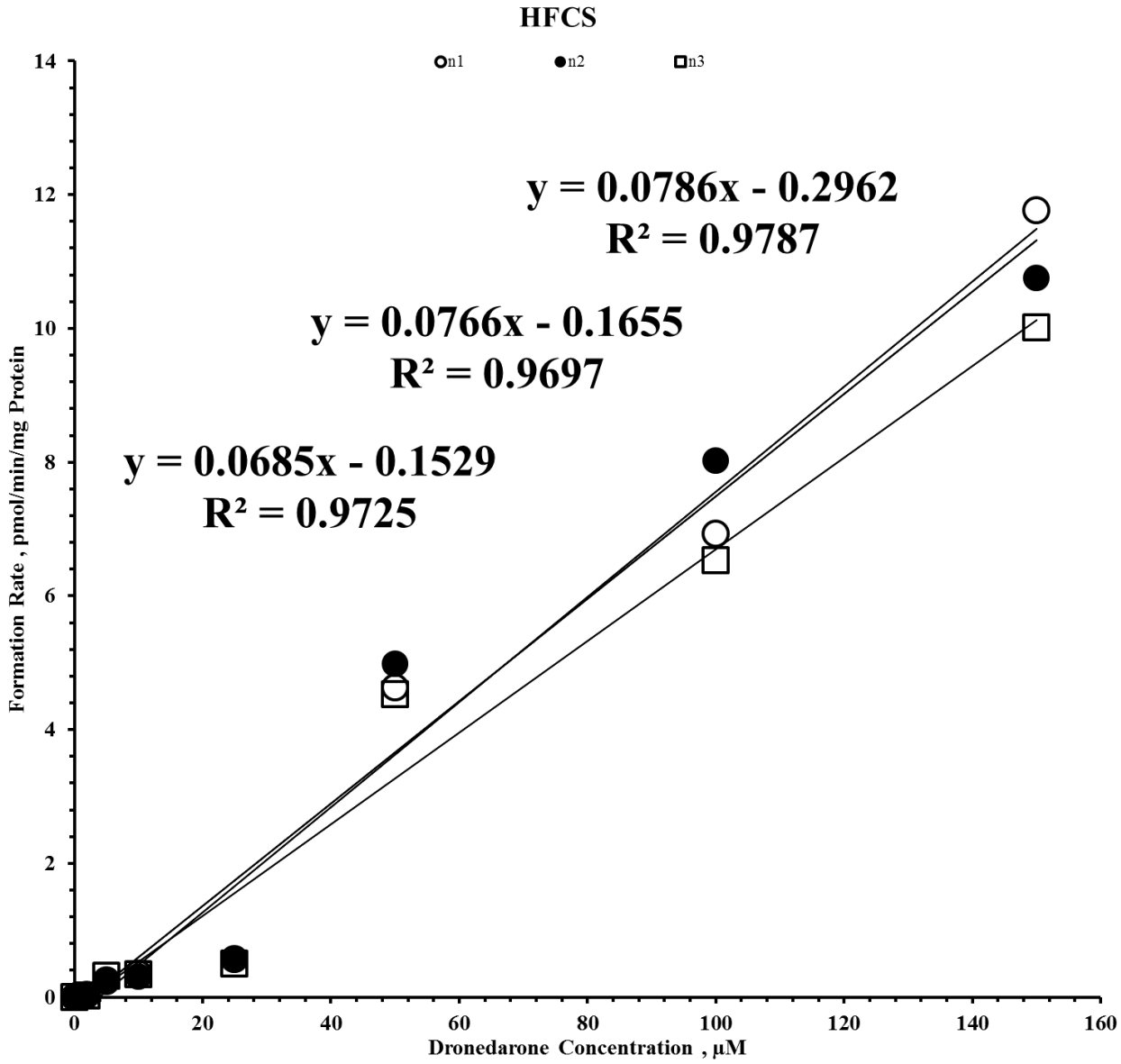

Figure 32: Velocity of DBD formation vs. dronedarone concentration by liver microsomes in HFCS rat microsomes.

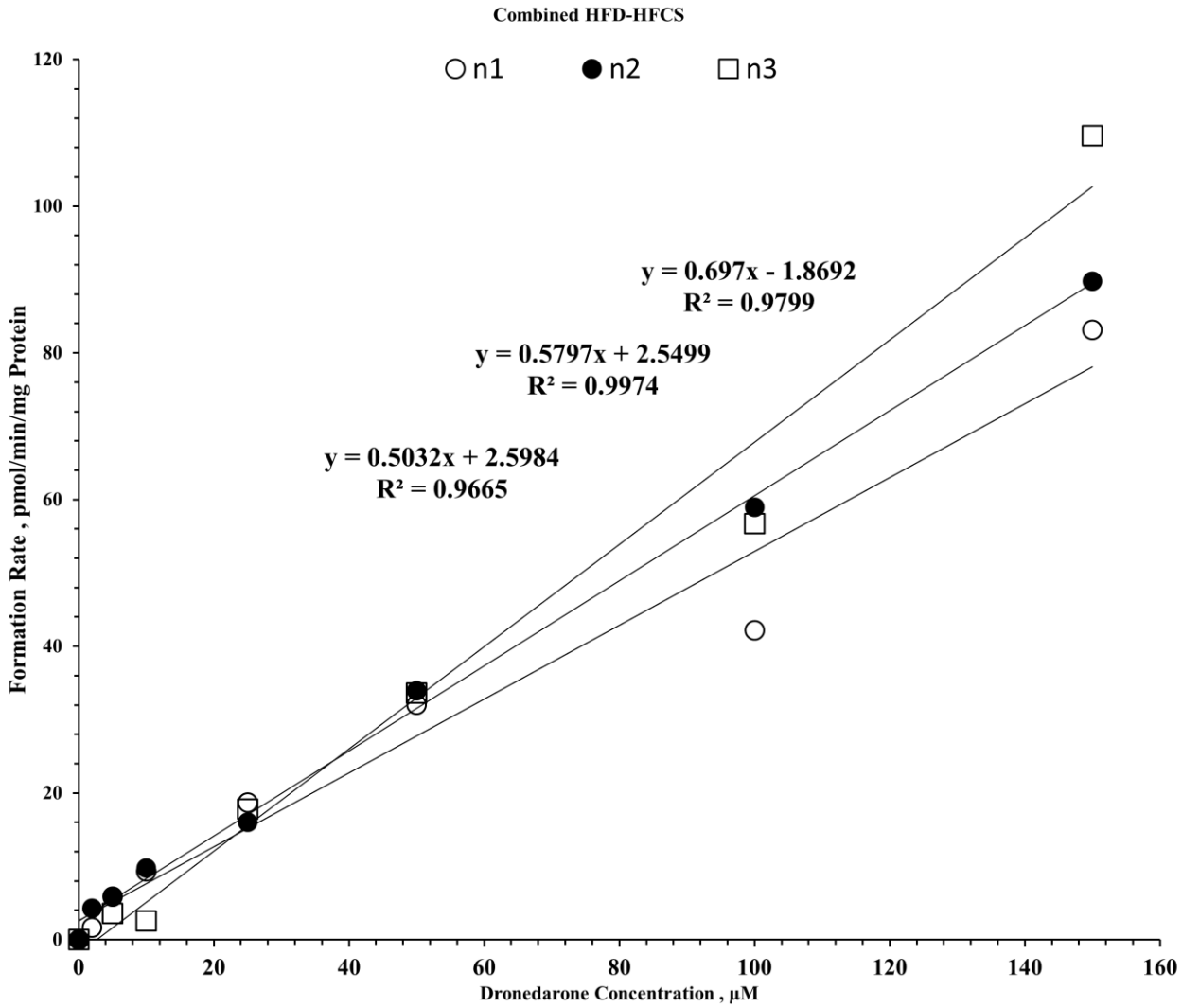

Figure 33: Velocity of DBD formation vs. dronedarone concentration by liver microsomes in Combined HFD-HFCS rat microsomes.

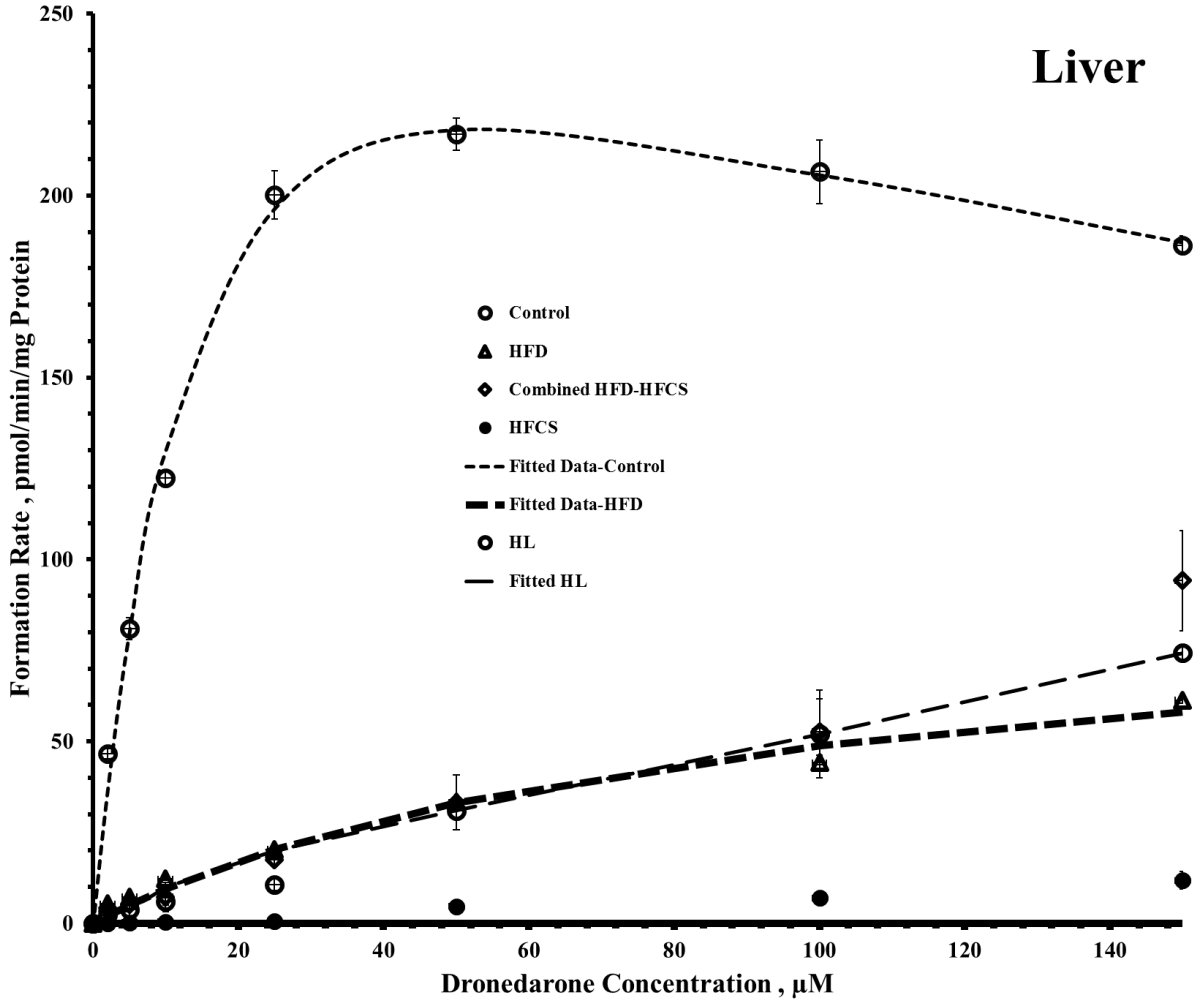

Figure 34: Velocity of DBD formation vs. dronedarone concentration by liver microsomes in all groups (Mean±SD).

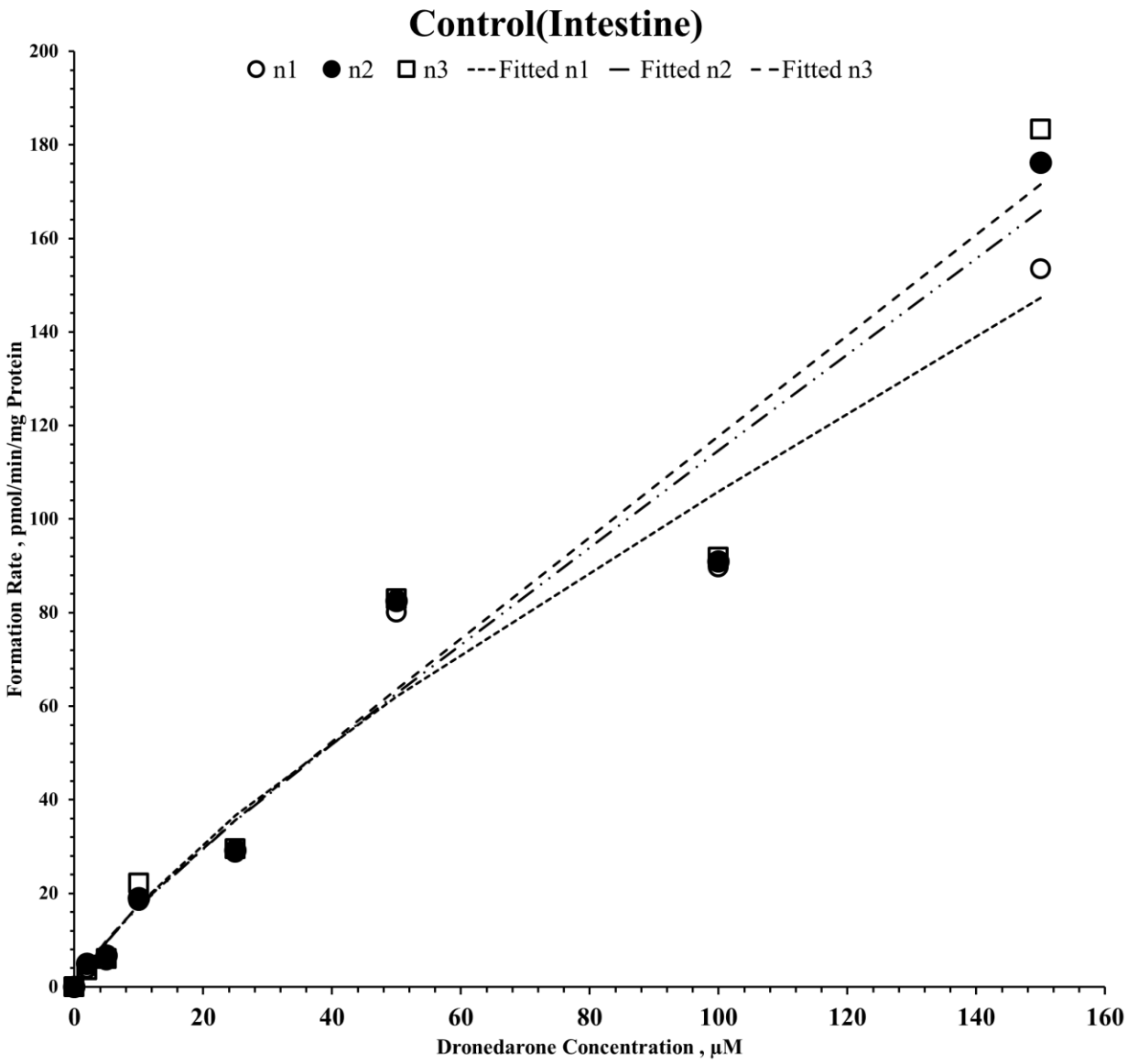

Figure 35: Velocity of DBD formation vs. dronedarone concentration by intestine microsomes in control rats.

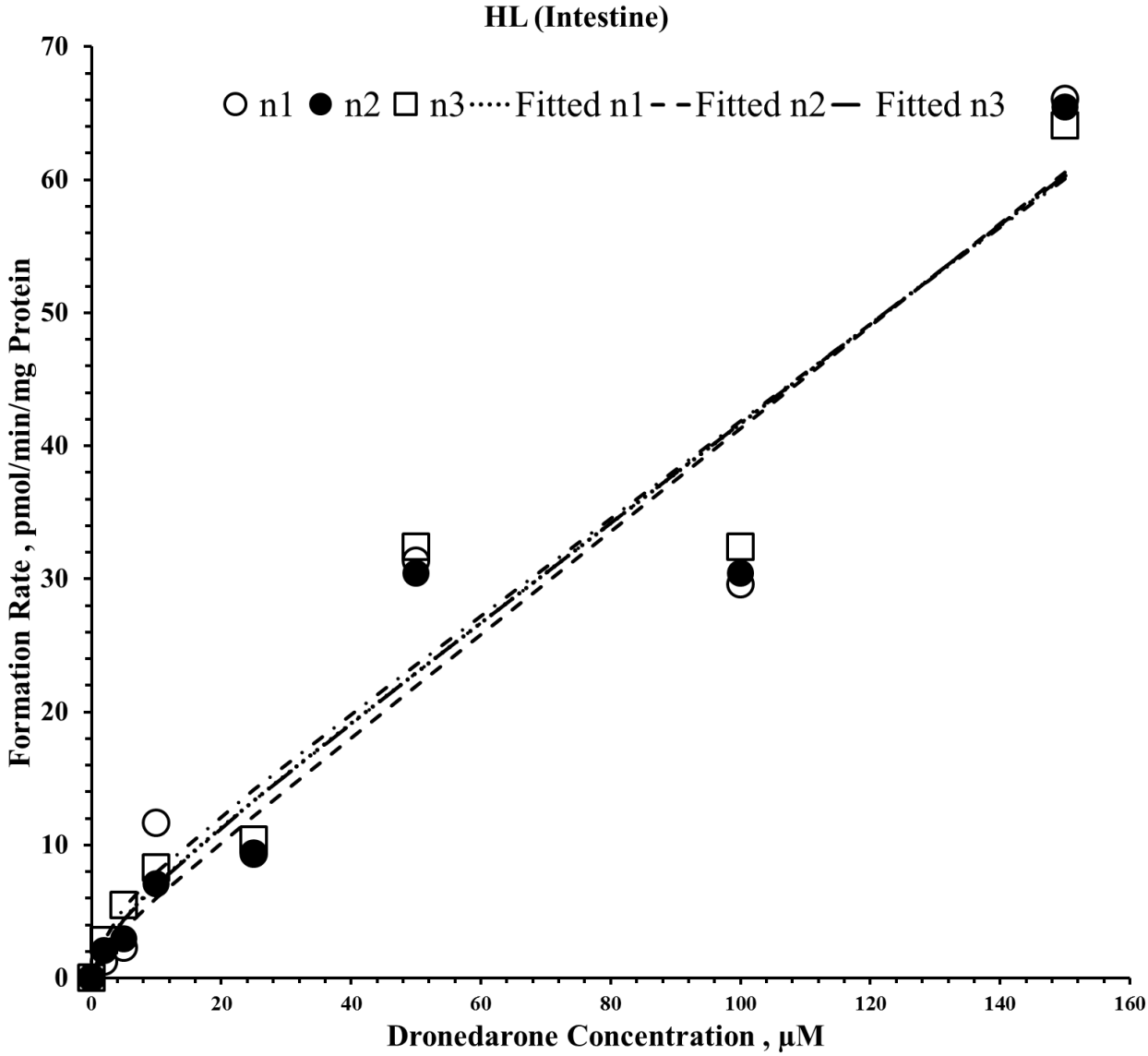

Figure 36: Velocity of DBD formation vs. dronedarone concentration by intestine microsomes in HL rats.

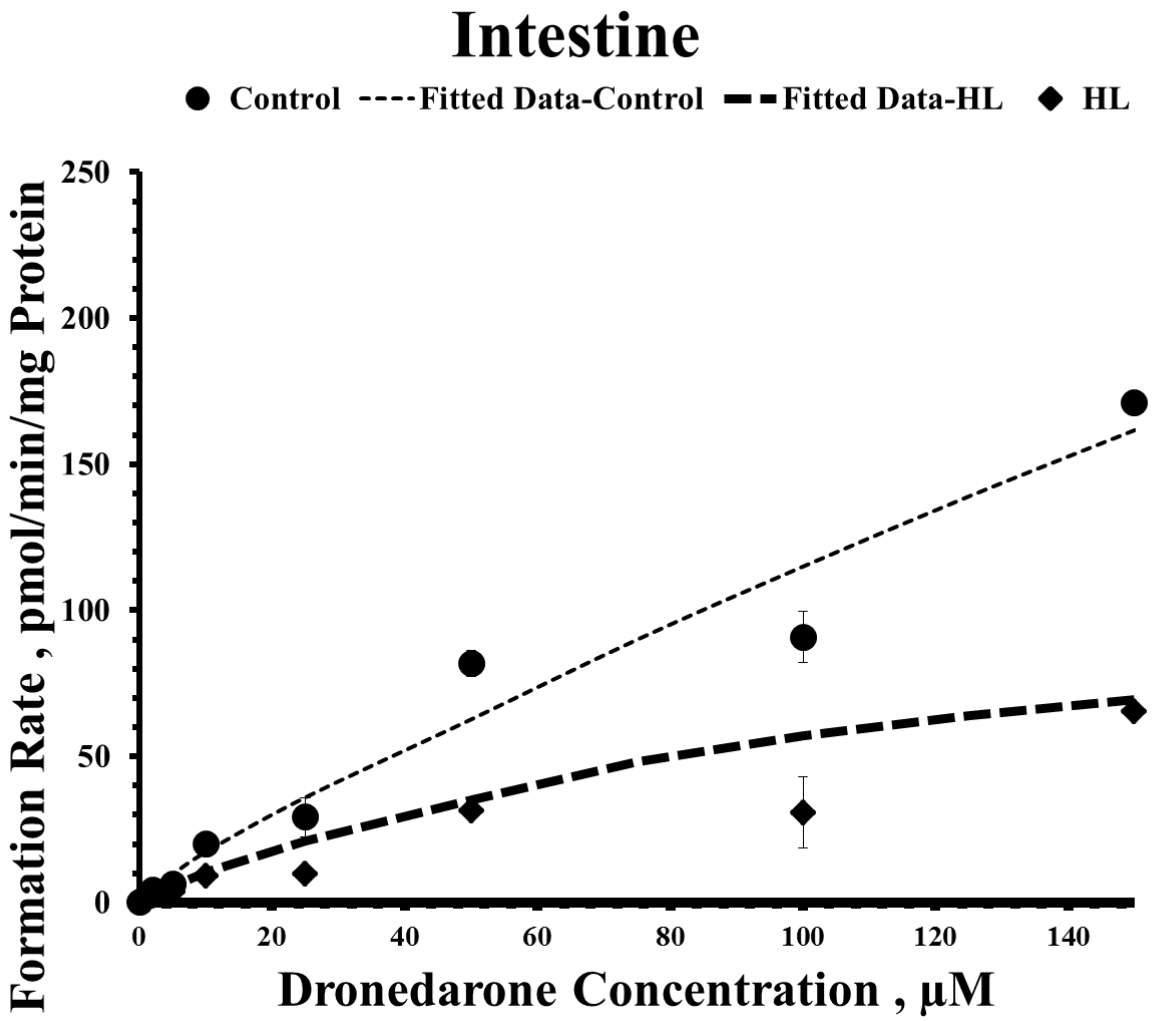

Figure 37: Velocity of DBD formation vs. dronedarone concentration by intestinal microsomes in all groups (Mean±SD).

Table 15: Enzyme kinetic parameters for desbutyldronedarone (DBD) formation by liver and intestine microsomes, n=6.

	Liver		
Group	***V_{max} , pmol/min /mg protein***	***K_m, µM***	***CL_{int}, µL/min/ mg protein***
Control	210.8±3.4	6.7±2.5	33.6±9.6
HL	359.7±85.2†	567.6±182.4†	0.65±0.1†
HFD	95.4±17.4†	96.2±41.5†	1.1±0.23†
HFCS	ND	ND	0.074±0.005†
HFD-HFCS	ND	ND	0.593±0.048†
	Intestine		
	V_{max1} , pmol/mg protein/min	***K_{m1}, µM***	***CL_{int2}, µL/min/ mg protein***
Control	20±12.10	14.40±9.31	0.96±0.15
HL	4.5±1.47	3.55±0.66	0.37±0.01†

Data are expressed as mean ± SD.

†Significant difference from control group ($p<0.05$)

ND: Not determined

3.5.3. Total CYP 450 measurement

The total CYP content was significantly lower in microsomal protein from HFD (0.44±0.06) and HL (0.01±0.011) than control (1.12±0.22 nmol/mg protein). On the other hand, the total CYP content was significantly higher in microsomal protein from Combination (HFD-HFCS) (1.37±0.06) than control. There was no significant change in HFCS group (1.15±0.02) compared to control (Figure 38).

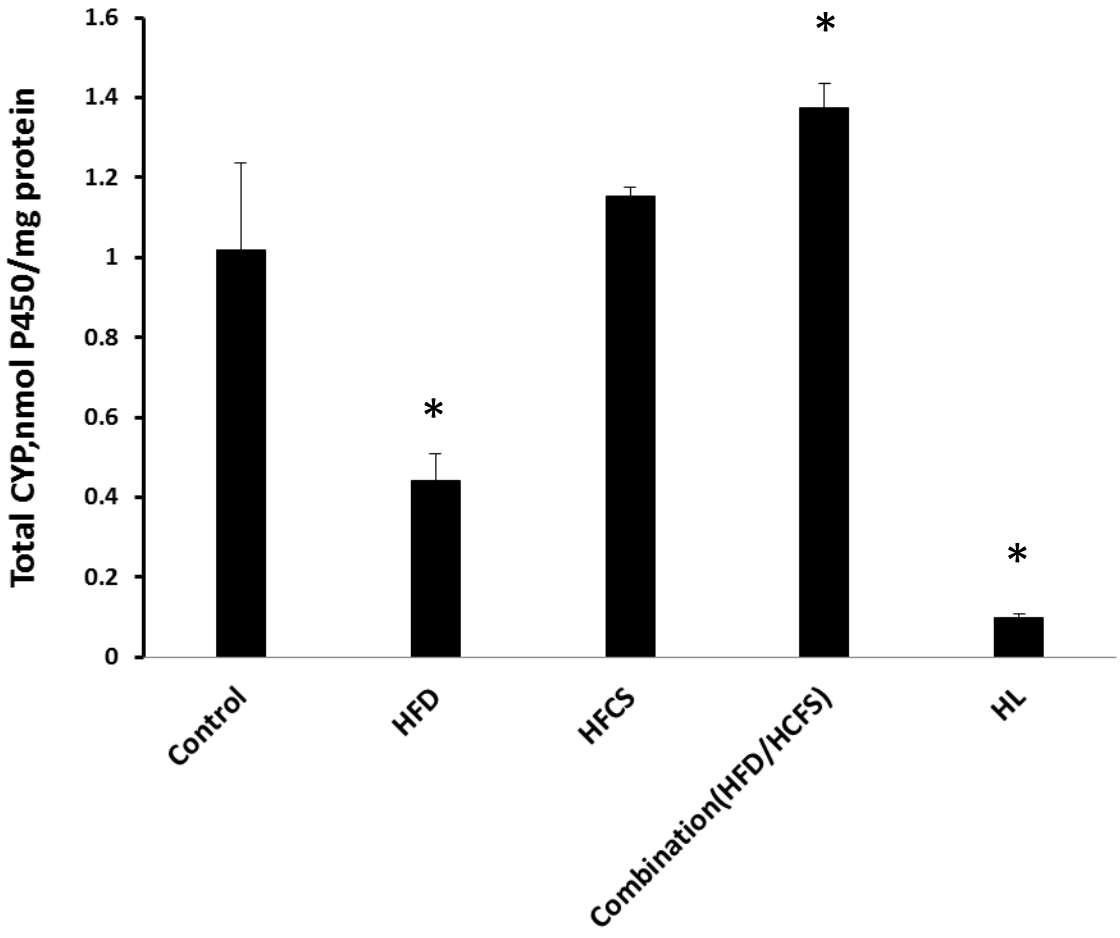

Figure 38: Comparison the levels of total hepatic CYP 450 content in all groups (Mean ±S.D.)

*Significant difference from Control ($p<0.05$)

3.5.4.TG and TC measurement

TG levels were significantly higher in HL rats compared to NL at 1, 3, 6 and at 24 h post oral dose of dronedarone (55mg/kg) (Figure 39). Also, the levels of cholesterol were significantly higher in HL rats compared to NL at 1, 6 and 9 h post oral dose of dronedarone (55mg/kg) (Figure 40).

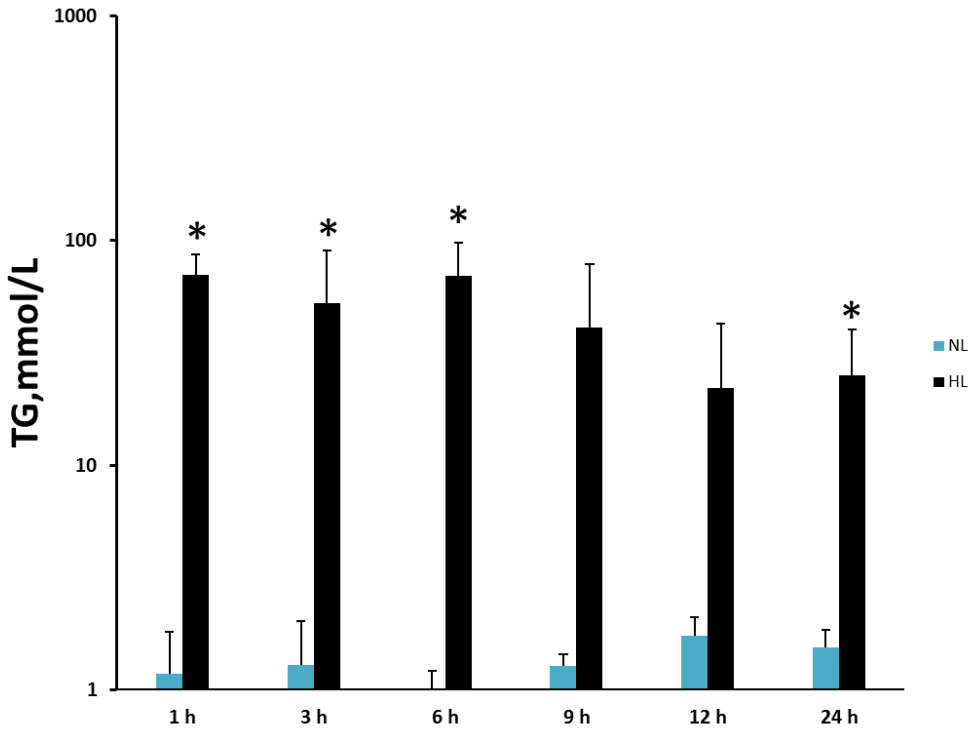

Figure 39: Levels of Triglycerides at different time points in NL and HL rats received an oral dose (55mg/kg of DR) (Mean ±S.D.) *Significant difference from NL ($p<0.05$)

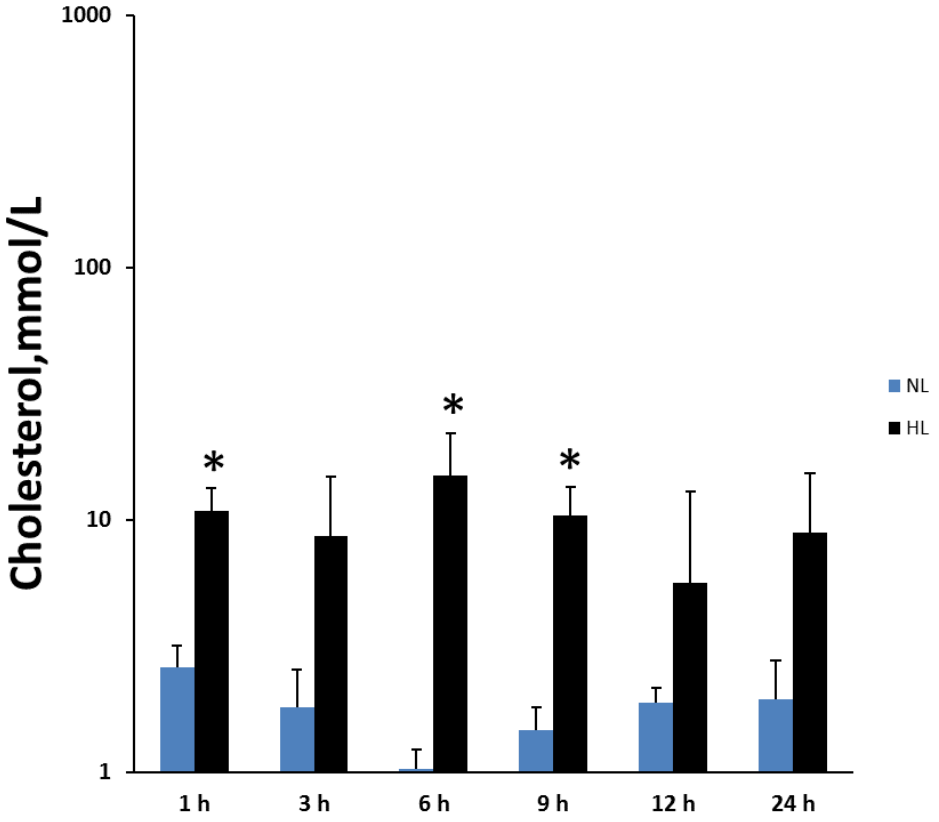

Figure 40: Levels of Cholesterol at different time points in NL and HL rats received an oral dose (55mg/kg of DR) (Mean ±S.D.) *Significant difference from NL ($p<0.05$)

Chapter 4: Discussion

As was highlighted above, dronedarone is a recently approved antiarrhythmic agent used mainly for the treatment of cardiac arrhythmias. Although amiodarone is a widely-used drug, its use is limited due to several toxicities involving the thyroid, lung, and liver. Dronedarone can reduce arrhythmias by blocking potassium, sodium and calcium channels. Due to lack of information regarding its pharmacokinetic and metabolism profile and behaviour in animal species in the peer-review literature, it is important to study and report on the pharmacokinetic profile in animal species and compare it to human data in order to maximize its safe and effective clinical use.

There is a relative dearth of detailed published methods and data about the analytical methods to measure dronedarone concentrations in human and animal biological matrices. As described above, we were able to develop two applicable, sensitive and rapid methods that meet the regulatory guidelines for drugs in biological samples to measure dronedarone concentration in the rat. Moreover, we conducted a detailed pharmacokinetic assessment of dronedarone after single doses by different routes of administration. Also, we have reported the pharmacokinetic profile in HL after a single oral dose in rat as HL widespread in large population of the society. There are some hepatotoxicity and pulmonary toxicity cases reported in clinical practices related to administration of dronedarone in humans. Thus, we have studied the distribution of dronedarone in three important organs in both NL and HL. Furthermore, we could study the metabolism of dronedarone in both HL and DIO in rat as well.

4.1. Development of an HPLC-UV assay for the determination of dronedarone in rat plasma.

This HPLC method was precise, accurate, and able to determine dronedarone concentrations in rat plasma sufficiently to depict the pharmacokinetic profile of the drug. To our knowledge, there have been no HPLC methods published to determine dronedarone concentrations in plasma utilizing a small sample volume such that it could be used in small animal species such as rats. The assay performed well and provided reliable estimates of dronedarone at concentrations as low as 25 ng/mL. Below this concentration, the variation in assay measures became unreliable (it was also tested at concentrations of both 5 and 10 ng/mL). There was no discernible decrease in the measured concentrations when frozen at −20°C for up to 28 days; this is as reported previously by others [120]. Recovery was relatively consistent from low to higher concentrations. During assay development two types of reversed-phase stationary phases, C8 and C18, were examined. The C18 column showed optimum resolution of dronedarone and IS peaks in a reasonable run time, with no interfering peaks. The extraction step was simple and rapid, using a commercially available IS.

Preparation of a set of 30 samples took about 2 h from the first step of extraction until the reconstituted extracts were placed in the HPLC autosampler tray. Ethopropazine exhibited a reasonable retention time and good sensitivity and was be eluted at an earlier time than dronedarone. The total analytical run time per sample was about 20 min (Figure 7). We tried to shorten the analysis run time by adding more organic phase into the mobile phase composition, but this was met with coelution of interfering peaks and loss of specificity. Only a few methods have been reported for the quantitation of dronedarone. One was specific for measurement of the drug in pharmaceutical dosage forms, with two others being intended for measurement of drug

from biological matrices [121-124]. Damy et al. described a liquid chromatography–mass spectrometry method with a lower limit of quantification of 0.50 ng/mL but the procedure and validation data were not disclosed [123]. Bolderman et al. reported a HPLC-UV method for determination of dronedarone and amiodarone in human plasma, goat plasma and myocardial tissue. Their reported lower limit of quantification was similar to ours (40 ng/mL). However, the extraction procedure was multi-step and required a larger volume of plasma (0.4 mL) than what we used [121]. Xie et al. reported a liquid chromatography–tandem spectrometry method with a much lower limit of quantification of 0.20 ng/mL, but the method has some disadvantages in terms of availability of instrumentation and acquisition cost [124]. The lower limit of quantification for our method was 25 ng/mL, which made this method applicable for use in the pharmacokinetic studies involving the rat. It is worth mentioning that during development of this method, we experienced some difficulties in determination of the drug concentration in blood samples due to interfering peaks in the chromatograms which resulted in inconsistent data. Moreover, the metabolite (desbutyldronedarone) was expensive and difficult to purchase commercially. However, in subsequent studies our lab was able to determine, report and validate the metabolite concentration in rat samples [114].

4.2. Development of a liquid chromatography-mass spectrometry (LC-MS) assay method for the quantification of dronedarone in rat plasma.

During the development of the HPLC-UV method, we began as well to attempt to develop an assay for dronedarone using our in-house LC-MS system. This work was delayed because of technical issues with the instrument. In the meantime, the studies were progressed using the developed HPLC-UV assay. Eventually the instrument problems were rectified, and we were able to successfully develop and assay using MS detection. The LC-MS method was precise and showed utility for dronedarone measurements in small volumes of rat plasma. For the LC-MS assay we used the same extraction step which was simple and rapid with a commercially available internal standard (ethopropazine). The internal standard exhibited a reasonable retention time. The analytical run time was 16 min (Figure 15).

During the development of this method we tried to achieve a lower limit of quantitation of <5 ng/ml but the data was not consistent leaving us with a validated LLQ of 5 ng/mL based on 100 μL of specimen. Still the method represented a 5-fold improvement in assay sensitivity over the HPLC-UV method.

There was an LC–MS method with a lower limit of quantification of 0.50 ng/mL but the procedure and validation data were not shown [123]. Also, Xie et al published a validated LC-MS/MS method with a very low limit of quantification of 0.2 ng/ml using a small sample volume but the method used tandem-mass spectrometry which was not available in our lab [124]. Our method was successfully used to monitor plasma concentrations of dronedarone for up to 24 h after dosing of 55 mg/kg (Figure 18).

4.3. Pharmacokinetics of dronedarone in normolipidemic and hyperlipidemic rats

In humans, dronedarone has a reported plasma CL of ~38.5 ml/min/kg after iv dosing, a t½ of 24 h, a high degree of binding to plasma protein, and a low oral bioavailability [125]. In the rat, the determination of F from the po doses suggested that the bioavailability is similarly low. In addition, the ip dose provided a similar measure of F to oral doses, which might reflect a high degree of hepatic first pass. It is often assumed that by injecting a drug ip, that (remove) the drug circumvents metabolism by the enterocytes. This, however, is an assumption about the mode of administration. Dronedarone has a large Vdss (Table 9) in rats, which might indicate a potential for its uptake from the mesenteric blood to the enterocytes during its residence in the mesenteric capillaries. As such, although there may be a rapid and high degree of hepatic first pass, it is not possible to rule out a contribution of intestinal metabolism even after ip injection of dronedarone.

The Vdss of dronedarone in the rat, similar to amiodarone, is higher than total body mass, indicating an extensive distribution of the drug to the tissues of the body. Limited human data [125] suggests a Vdss of ~18 L/kg, a value similar to but slightly higher than that observed in our NL rats (Table 9). Based on the compartmental analysis, the drug would appear to be widely distributed to a variety of tissues differing in their rate of blood perfusion. In comparison, the Vdss of amiodarone in rat was still higher (21-47 L/kg) than dronedarone. The combination of a lower CL and Vdss for dronedarone would account for the substantially shorter t½ of dronedarone (<8 h) compared to amiodarone (>22 h) in the rat, and in humans. Given that the plasma protein binding of the drug was high in the rat, the binding affinity of dronedarone to tissue proteins is apt to be much higher than to plasma proteins, which is consistent with other weakly basic compounds. It is crucial to mention that during protein binding experiments, we tried to use an

ultrafiltration kit but, unfortunately, we found that dronedarone bound to the kit membranes making this method impossible for using for both NL and HL rat plasma. As a result, we determined the protein binding of dronedarone by using an erythrocyte method which provides consistent and reliable data. It is worth mentioning that at the beginning of the pharmacokinetic studies, we gave a dose of 20 mg/kg dronedarone as iv to one rat and found this dosage was high and toxic as the rat died immediately. So, we reduced the dosage to be 4 mg/kg.

Klieber et al. recently reported that dronedarone has many metabolites (desbutyldronedarone, propanoic acid- dronedarone, phenol-dronedarone and dealkyl-dronedarone) after incubation of the drug with human microsomes [126]. At the time of assay, we did not possess purified standards of metabolites to assess for their presence. We are aware of no published information of dronedarone metabolism in the rat. In humans, it was reported that numerous CYP isoforms are involved in the metabolism of the drug, most notably CYP3A4 and 3A5 [99]. Later, we were able to determine the metabolite (desbutyldronedarone) concentration in metabolism studies. Our HPLC-UV method was sensitive and valid for determination both the drug and metabolite with slight extraction method modification.

Poloxamer 407 was used to test for the effects of HL in the rats (Table 13, Figure 23). This model has been shown to exert a profound effect on the pharmacokinetics of its structurally related analogue amiodarone, with substantial increases of ~10-fold in the AUC compared to NL rats[74] .

This can be explained by increasing plasma protein binding and decreasing CL (including direct enzyme expression downregulation, reduction in enzymes function and activity) and Vdss[74] . Indeed, for other drugs such as tadalafil [127], halofantrine [111], docetaxel [64] and clomipramine [65], a decrease in plasma fu could account for a number of the changes seen in the drug pharmacokinetics in the presence of HL. At the same time, HL can lead to selective changes in amiodarone concentrations in specific tissues in either an upwards or downwards direction [62]. For the study of dronedarone, po dosing was used in the HL rats because of the possible rapid hepatic CL of dronedarone, which meant that F would be the parameter expected to be most affected by a change in fu and/or hepatic intrinsic CL. Although the mean AUC values were higher in the HL rats, the magnitude of difference was much less (only 2.5-fold higher) than what we had previously observed with amiodarone. Furthermore, the lack of a significant difference in the plasma fu in the HL rats is in stark contrast to what we had seen with amiodarone where the plasma fu was ~25-fold lower [74] . This suggests that the higher plasma AUC in HL rats was attributable to a direct decrease in metabolism and/or possibly changes in intestinal drug transport. We had previously determined that in HL there was a decrease in the expression and function of some CYP from samples obtained after HL and in metabolizing activity and possibly P-glycoprotein in hepatocytes exposed to HL serum [33,57,62,127-130]. Another drug where there was no decrease in unbound fraction, but a greater AUC, is carbamazepine [33]. It was worth mentioning that we conducted a blood to plasma ration study in order the hepatic extraction ratio in both humans and rats by using fresh blood drawn on the day of experiment. Unluckily, our HPLC assay was not able to yield consistent data on the concentration of dronedarone in blood. We noticed that the chromatograms of blood samples were messy and had a lot of interfering peaks at dronedarone and IS retention times. It important to mention that in this study, we used only the

HPLC-UV method to determine drug concentration because the LC-MS method was in development process.

4.4. Tissue distribution of dronedarone in rat

Because of the organ-related toxicities of dronedarone appearing in the literature involving liver [131,132] and lung [133-135], and its antiarrhythmic effects in the heart, it was deemed crucial to study the biodistribution of dronedarone in these organs. Furthermore, AM distribution was previously found to be selectively affected by experimental HL [62]. Hence, we were also interested in understanding the effects of HL on dronedarone biodistribution.

As expected based on the large Vdss noted in the pharmacokinetic study, tissue dronedarone concentrations were overall much higher than those in the plasma. Variability in tissue concentrations was also large in the measured samples. There are several possible explanations, including perhaps the manner of dosing (oral). The order of mean dronedarone AUC among NL rat tissues from highest to lowest was heart > lung > liver > plasma. In contrast, the order in mean AM AUC among NL rats tissues from highest to lowest was lung > liver > heart > plasma [62]. In HL groups, the order for dronedarone was lung > heart > liver > plasma and for AM was liver > lung > heart > plasma [62].

Our results found a significant increase in the plasma AUC of dronedarone in HL rats compared with NL rats (Table 14). The increase in arithmetic mean plasma AUC of HL:NL was exaggerated in the tissue distribution experiment (ratio = 7.92) compared to the geometric mean HL:NL ratio of 2.31 in the pharmacokinetic study. This may in part, be attributed to a different sampling

schedule where more samples were taken to arrive at the AUC in the pharmacokinetic study [110]. However, there was also a great deal of variability present in the concentrations measured in the HL animals used in the tissue distribution study. As can be seen in (Figure 24) of the plasma samples in the tissue distribution study, the arithmetic mean vs. time curve showed a substantial secondary peak at about 9 h after the dose in the HL animals.

The Bailer's method relies on the arithmetic mean to ascertain differences in AUC between groups (Table 14). When the geometric mean was applied to the concentration vs. time data in the biodistribution study, the plasma AUC_{0-24} ratio of HL:NL AUC_{0-24} were lower (4.98) than when the arithmetic means were compared (7.92) and somewhat nearer the ratio determined in the pharmacokinetic study using the geometric means. It is also of note that for each time point, only four points were available whereas for the pharmacokinetic study a total of 6 to 8 animals were used for the HL vs NL comparison.

The levels of dronedarone in HL rats were higher in heart, its site of action, and lung, than in NL rats, but even in NL rats lung concentrations were substantial. One of the main reasons why dronedarone was developed was to allow for a Class III antiarrhythmic agent with reduced organ toxicity compared to AM. The high affinity of the drug for pulmonary tissue may be cause for concern given that reports have emerged suggesting that dronedarone, like AM, can cause pulmonary toxicity [133].

The higher concentrations in HL lung and heart cannot be definitively be explained from these descriptive results. However, an increased lipoprotein load in the plasma might have bound dronedarone more so than in NL animals, possibly leading to an increased organ uptake owing to the action of LDL receptors. It is known that mRNA and/or protein of certain CYP isoforms and

transport proteins can have altered expression in P407-induced HL, or exposure of hepatocytes to hyperlipidemic plasma from P407 treated rats [57,95,136]. The transport proteins involved in dronedarone distribution are not known at present. However, HL-related changes in expression of any such proteins might explain in part the differences seen between NL and HL tissue distribution in our rats.

For AM, it was found that HL to NL Kp ratio values AUC were higher in liver and heart than in lung (0.31, 0.24 and 0.065, respectively) [62]. These findings were not exactly like what we found for dronedarone. We found that HL to NL Kp values were higher in lung and liver than in heart (0.27, 0.11 and 0.06, respectively). Normalization of the AUC values has an advantage of correcting for the bioavailability and the clearance of the drug. The relative differences between the two drugs may be reflective of differences in the lipoprotein uptake and distribution to lipoprotein fractions and possibly transporters involved in drug tissue influx and efflux.

4.5. Microsomal metabolism of dronedarone in rat to desbutyldronedarone

Modification of the HPLC-UV assay allowed us to measure concentrations of desbutyldronedarone, the major dealkylated metabolite of dronedarone. CYP3A4, CYP2D6, and CYP3A5 are reportedly the CYP isoforms responsible for dronedarone metabolism in humans[126]. It has been shown that in HL rats, significant decreases in metabolism of AM has been reported. Considering the higher concentrations of dronedarone seen in the HL rats, it was important to understand if a decrease in metabolism could help explain the finding. Hence, we optimized the microsomal metabolism conditions by incubating a known concentration of dronedarone with various concentrations of liver and intestinal microsomal protein ranging, from 0.25 up to 1 mg/mL. We found a linear relationship in this range for desbutyldronedarone formation. Based on that, we concluded that 0.5 mg/ml protein concentration would be the optimum concentration to be used. The reaction time of 10 min was found to provide desbutyldronedarone formation in the linear range of formation vs. time.

The data indicated that the CL_{int} of dronedarone was reduced in the microsomal protein derived from the livers of HL and DIO groups compared to NL and lean controls. Interestingly, there were significant increased changes in both V_{max} (enzyme capacity and amount for reaction) and K_m (enzyme affinity) in the HL group. An increase the population of metabolizing enzymes responsible for metabolism of the drug, but involving a selective increase in enzymes with lower rather than higher affinity for dronedarone metabolism, could explain these kinetic changes.

It is clear that HL affects the expression and functional activity of metabolizing enzymes as previously reported for amiodarone and carbamazepine [33,62]. Interestingly, although Cl_{int} behaved the same way in DIO rats, the Vmax decreased (unlike HL) and the Km increased (like HL). These changes in Vmax in the DIO groups were consistent in the reduction of total CYP 450 as shown (Figure 38).

For HFCS and combined HFCS-HFD, we were not able to determine the kinetic parameters of V_{max} and k_m as the velocity of formation was linear over the dronedarone concentration range used. In this case, only CL_{int} was determined. This finding of dronedarone metabolism was in line with what has been reported for AM [62]. AM is metabolized by CYP1A1,3A4 and 2D6 in human and CYP2D1,2C11,2C6 and 3A1 in rats [94]; a thorough assessment for dronedarone in rat has not been determined.

Our research group previously found a decreased expression of hepatic metabolizing enzymes at mRNA and protein levels in a diet-induced group which is in agreement with several previously reported studies [44,137]. As expected, in intestine, we found that formation of desbutyldronedarone was less than in the liver of control and HL groups. The CL_{int} was significantly lower in the HL group compared to control. These findings would be consistent with a lower availability and expression of metabolizing enzymes in intestine compared to the main site of metabolism (liver).

In liver, it is important to mention that the control group followed the substrate-inhibition kinetic model. In this model, the velocity and the formation rates of DBD are increased as incubated dronedarone concentration increased, after a such point, the velocity curve of DBD formation reached the maximum (plateau) and start to decline as the concentration of dronedarone increased further. Notably, this unusual pattern was also observed previously in humans for desbutyldronedarone formation [138]. Hong et al found that dronedarone autoinhibited CYP 3A4 and 3A5 in human hepatic microsomes [138]. For HFD and HL groups, this autoinhibition was not seen, and Michalis-Menten kinetics provided the best fit to the data. On the other hand, determination of V_{max} and K_m values in HFCS and combined HFCS-HFD groups were not possible to determine as the velocity of desbutyldronedarone formation was linear over the concentration range studied. We could however determine estimates of the CL_{int} from the slope value of the depletion rate of dronedarone incubated with microsomes for 30 min. These reported data agree with previous studies on humans and rats which found a decrease in the metabolic activity or the expression of mRNA or reduction in protein levels of CYP3A in obesity induced by diet [137]. In line with this, the total P450 was lower in the HL group due to the HL effect on the metabolizing enzymes in the liver. In this study, we used the HPLC-UV method to determine the drug and the metabolite concentrations.

The CL_{int} formation of DBD was found to be much lower than the overall depletion CL_{int} of dronedarone in each of the HFCS and HFCS-HFD liver microsomal incubations. This suggests that there are many other metabolites of dronedarone that are formed in the rat. Nevertheless, DBD is still significant compared to parent drug, and is worthy of measure (many of the other metabolites have much less pharmacological activity compared to DBD)[126].

Chapter 5: Conclusion

Dronedarone is a recently approved antiarrhythmic agent used mainly for the treatment of cardiac arrhythmias. It is a benzofuran derivative that was developed to reduce the toxicity profile of amiodarone In our lab, we have successfully developed a rapid and simple HPLC assay for dronedarone using a reverse phase C18 column with liquid-liquid extraction method. The assay was the first to be validated for the determination of dronedarone in plasma based on 0.1 mL sample volume and with a LLQ of 25 ng/mL as dronedarone base. Moreover, our lab developed a very sensitive LC/MS method as well with 5 ng/ml as LLQ. Both methods had high sensitivity and were able to be used in dronedarone pharmacokinetic studies in rats. We found that dronedarone is extensively distributed with a high Vd in the rat. The drug showed poor bioavailability (<20%) after oral and ip administration. The higher plasma concentrations after oral dosing to hyperlipidemic rats might be because of a direct effect on metabolizing enzymes or transport proteins. This is the first study to explore pk of dronedarone in rat and the effect of HL on its pharmacokinetic profile. The tissue distribution and hepatic and intestinal microsomal metabolism of dronedarone were studied in normolipidemic and hyperlipidemic rats.

Dronedarone was detected and measured in all specimens at quantifiable concentrations in all tissues. In heart, the site of action of the drug, dronedarone higher concentrations than other organs in NL rats . In contrast, lung has the highest concentration of dronedarone in HL rats. It is worth noting that high concetration of the drug in heart, lung and liver compared to plasma in both NL and HL rats might explain the cases of toxicity reported in the literature. Moreover, the reduction of desbutyldronedarone formation was observed in liver and intestine metabolic

efficiency. It is clear that the HL model affected the expression and functional activity of metabolizing enzyme as previously reported for different drugs. Also, DIO has an impact on hepatic metabolsim of dronedarone by altering the enzymes' capacities and affinifties.

Chapter 6: Future direction

The results and data obtained from this thesis determined how dronedarone disposes in rat, and how it changed the pharmacokinetic parameters and metabolism. It important to advance these finding into higher levels by conducting the following research experiments:

1. ***To investigate the correlation between high concentration and changes in the electrocardiogram to assess the efficacy or toxicity of dronedarone in heart in vivo.***

   Rationale: In the tissue distribution study, we found increased uptake of dronedarone in the heart. It would be worth to see if higher concentration in heart is associated with pharmacodynamics effect.

   Suggested experimental design and expectation: A study similar to those done previously examining amiodarone and halofantrine effects in HL could be undertaken [59,107]. Repeated oral doses of dronedarone could be given to the rats and the ECG of each rats should be recorded before and after starting the treatment. We expect some changes in cardiac ECGs after giving dronedarone to rats.

2. ***Involvement of some other CYP isoenzymes by using either chemical or immunological inhibitors.***

   Rationale: This study raised some questions that are unanswered, pertaining to the CYP isoforms that are involved in the metabolism of dronedarone to its main dealkylated metabolite. In human, it has been reported that CYP 3A4/5 are the main responsible enzymes for dronedarone metabolism [126]. Moreover, AM metabolized by CYP 3A2 and 1A1 in rat [95].

Suggested experimental design and expectation: 1. *In vitro*, incubation of dronedarone with hepatic and intestinal microsomes with addition of antibodies to selected CYP (immunological) or use of a specific inhibitor e.g. ketoconazole (chemical) could be used to determine the enzymes involved in dronedarone metabolism in the rat. 2. *In vivo*, doses of dronedarone to be given to the rats with and without administration of chemical inhibitor (ketoconazole). After that, collecting plasma samples and assaying them for dronedarone and metabolite. We expect reduction in formation of desbutyldronedarone in microsomes group with incubated with inhibitors. Also, plasma levels of dronedarone would be expectedly higher combined (depending on the enzyme involved in metabolite metabolism) might be lower in groups given the inhibitor [95].

3. Conducting in vitro drug uptake of dronedarone studies in NL and HL by using heart (H9c2), liver (hepG2) and lung (A549) cell-lines and to assess the dronedarone concentration-toxicity related incidences.

Rationale: We found changes in the concentration of dronedarone among tissue in NL and HL rats. Also, there were some clinical cases of dronedarone–organ associated toxicity. It is possible that HL affects the intracellular levels of dronedarone owing to the effects of lipoprotein or other specific drug transporters.

Suggested experimental design and expectation: Pre-incubation of cell-lines with media only, NL and HL plasma (1-10%) for 24 h could be performed. After incubation, cells would be exposed to dronedarone for several time points. Cells would be ruptured and dronedarone concentration determined. We expect concentration of dronedarone will be different in cell exposed to media only, NL and HL plasma [57,130].

4. Study the effect of DIO on dronedarone PK in rat.

Rationale: We determined a reduction in formation of desbutyldronedarone in DIO groups rats.

Suggested experimental design and expectation: Rats will be fed with different diet for 14 weeks. On the last day, oral dose of dronedarone will be administered. Plasma, heart, liver and lung collected and assayed for dronedarone and metabolite. We expect concentration of dronedarone and AUC in DIO group will be higher with changes in Vd and CL.

Bibliography

1. J.E. Hall GaH. 2001. text book of medical physiology. Eleventh ed. ed.: ElSERVIER,.

2. Shen H, Howles P, Tso P 2001. From interaction of lipidic vehicles with intestinal epithelial cell membranes to the formation and secretion of chylomicrons. Advanced drug delivery reviews 50 Suppl 1:S103-125.

3. Wasan KM, Brocks DR, Lee SD, Sachs-Barrable K, Thornton SJ 2008. Impact of lipoproteins on the biological activity and disposition of hydrophobic drugs: implications for drug discovery. Nature reviews Drug discovery 7(1):84-99.

4. DiPiro JT, Talbert RL, Yee GC, Matzke GR, Wells BG, Posey LM, Streetman DS, Streetman D-AD. Pharmacotherapy: A Pathophysiologic Approach, 8th Edition. ed.

5. Olson RE 1998. Discovery of the lipoproteins, their role in fat transport and their significance as risk factors. The Journal of nutrition 128(2 Suppl):439S-443S.

6. Shayeganpour A, Lee SD, Wasan KM, Brocks DR 2007. The Influence of Hyperlipoproteinemia on in Vitro Distribution of Amiodarone and Desethylamiodarone in Human and Rat Plasma. Pharmaceutical Research 24(4):672-678.

7. Takahashi S, Sakai J, Fujino T, Hattori H, Zenimaru Y, Suzuki J, Miyamori I, Yamamoto TT 2004. The very low-density lipoprotein (VLDL) receptor: characterization and functions as a peripheral lipoprotein receptor. Journal of atherosclerosis and thrombosis 11(4):200-208.

8. Brown MS, Goldstein JL 1986. A receptor-mediated pathway for cholesterol homeostasis. Science 232(4746):34-47.

9. Eliot LA, Jamali F 1999. Pharmacokinetics and pharmacodynamics of nifedipine in untreated and atorvastatin-treated hyperlipidemic rats. The Journal of pharmacology and experimental therapeutics 291(1):188-193.

10. Wasan KM, Looije NA 2005. Emerging pharmacological approaches to the treatment of obesity. Journal of pharmacy & pharmaceutical sciences : a publication of the Canadian Society for Pharmaceutical Sciences, Societe canadienne des sciences pharmaceutiques 8(2):259-271.

11. Fredrickson DS 1971. An international classification of hyperlipidemias and hyperlipoproteinemias. Annals of internal medicine 75(3):471-472.

12. Fredrickson DS, Lees RS 1965. A System for Phenotyping Hyperlipoproteinemia. Circulation 31:321-327.

13. H.N. Ginsberg YA, I.J. Goldberg. Pathophysiology and therapy of hyperlipidemia. Cardiovascular Pharmacology, Antoaccio MJ(ed). , pp. 485-513. ed., .Raven: New York, .

14. Manolio TA, Pearson TA, Wenger NK, Barrett-Connor E, Payne GH, Harlan WR 1992. Cholesterol and heart disease in older persons and women. 2(1-2):161-176.

15. Austin MA 1999. Epidemiology of hypertriglyceridemia and cardiovascular disease. (9B):13F-16F.

16.Steinberg D 2005. Hypercholesterolemia and inflammation in atherogenesis: two sides of the same coin. Molecular nutrition & food research 49(11):995-998.

17. Guo F, Huang C, Liao X, Wang Y, He Y, Feng R, Li Y, Sun C 2011. Beneficial effects of mangiferin on hyperlipidemia in high-fat-fed hamsters. Molecular nutrition & food research 55(12):1809-1818.

18. Wang W, He B, Shi W, Liang X, Ma J, Shan Z, Hu Z, Danesh FR 2012. Deletion of scavenger receptor A protects mice from progressive nephropathy independent of lipid control during diet-induced hyperlipidemia. Kidney international 81(10):1002-1014.

19. Holt PR, Dominguez AA 1980. Triton-induced hyperlipidemia: a model for studies of intestinal lipoprotein production. The American journal of physiology 238(5):G453-457.

20. Johnston TP, Palmer WK 1993. Mechanism of Poloxamer 407-Induced Hypertriglyceridemia in the Rat. Biochem Pharmacol 46(6):1037-1042.

21. Levine S, Saltzman A 2007. A procedure for inducing sustained hyperlipemia in rats by administration of a surfactant. Journal of pharmacological and toxicological methods 55(2):224-226.

22. Watanabe Y 1980. Serial inbreeding of rabbits with hereditary hyperlipidemia (WHHL-rabbit). Atherosclerosis 36(2):261-268.

23. Fazio S, Linton MF 2001. Mouse models of hyperlipidemia and atherosclerosis. Frontiers in bioscience : a journal and virtual library 6:D515-525.

24. Gawronska-Szklarz B, Drozdzik M, Wojcicki J, Zakrzewski J 1994. Effect of experimental hyperlipidemia on the pharmacokinetics of digoxin. Acta poloniae pharmaceutica 51(3):271-274.

25. Johnston TP 2004. The P-407-induced murine model of dose-controlled hyperlipidemia and atherosclerosis: a review of findings to date. Journal of cardiovascular pharmacology 43(4):595-606.

26. Standeven AM, Beard RL, Johnson AT, Boehm MF, Escobar M, Heyman RA, Chandraratna RA 1996. Retinoid-induced hypertriglyceridemia in rats is mediated by retinoic acid receptors. Fundamental and applied toxicology : official journal of the Society of Toxicology 33(2):264-271.

27. Garcia-Sainz JA, Juarez-Ayala J, Valles VE 1987. Pertussis toxin induces fatty liver, hyperlipemia and ketosis in hamsters. Toxicon : official journal of the International Society on Toxinology 25(6):603-609.

28. Oda H, Matsushita N, Hirabayashi A, Yoshida A 1990. Hyperlipoproteinemia in rats fed polychlorinated biphenyls. Journal of nutritional science and vitaminology 36(2):117-122.

29. Blonder JM, Baird L, Fulfs JC, Rosenthal GJ 1999. Dose-dependent hyperlipidemia in rabbits following administration of poloxamer 407 gel. Life sciences 65(21):PL261-266.

30. Palmer WK, Emeson EE, Johnston TP 1998. Poloxamer 407-induced atherogenesis in the C57BL/6 mouse. Atherosclerosis 136(1):115-123.

31. Li C, Palmer WK, Johnston TP 1996. Disposition of poloxamer 407 in rats following a single intraperitoneal injection assessed using a simplified colorimetric assay. Journal of pharmaceutical and biomedical analysis 14(5):659-665.

32. Chaudhary HR, Brocks DR 2013. The Single Dose Poloxamer 407 Model of Hyperlipidemia; Systemic Effects on Lipids Assessed Using Pharmacokinetic Methods, and its Effects on Adipokines. Journal of Pharmacy & Pharmaceutical Sciences 16(1):65.

33. Lee YS, Kim YW, Kim SG, Lee I, Lee MG, Kang HE 2012. Effects of poloxamer 407-induced hyperlipidemia on the pharmacokinetics of carbamazepine and its 10,11-epoxide metabolite in rats: Impact of decreased expression of both CYP3A1/2 and microsomal epoxide hydrolase. Eur Neuropsychopharmacol 22(6):431-440.

34. Wout ZG, Pec EA, Maggiore JA, Williams RH, Palicharla P, Johnston TP 1992. Poloxamer 407-mediated changes in plasma cholesterol and triglycerides following intraperitoneal injection to rats. Journal of parenteral science and technology : a publication of the Parenteral Drug Association 46(6):192-200.

35. Wasan KM, Subramanian R, Kwong M, Goldberg IJ, Wright T, Johnston TP 2003. Poloxamer 407-mediated alterations in the activities of enzymes regulating lipid metabolism in

rats. Journal of pharmacy & pharmaceutical sciences : a publication of the Canadian Society for Pharmaceutical Sciences, Societe canadienne des sciences pharmaceutiques 6(2):189-197.

36. Brocks DR, Ben-Eltriki M, Gabr RQ, Padwal RS 2012. The effects of gastric bypass surgery on drug absorption and pharmacokinetics. Expert opinion on drug metabolism & toxicology 8(12):1505-1519.

37. Haslam DW, James WP 2005. Obesity. Lancet 366(9492):1197-1209.

38. Jain R, Chung SM, Jain L, Khurana M, Lau SW, Lee JE, Vaidyanathan J, Zadezensky I, Choe S, Sahajwalla CG 2011. Implications of obesity for drug therapy: limitations and challenges. Clinical pharmacology and therapeutics 90(1):77-89.

39. Maury E, Ehala-Aleksejev K, Guiot Y, Detry R, Vandenhooft A, Brichard SM 2007. Adipokines oversecreted by omental adipose tissue in human obesity. American journal of physiology Endocrinology and metabolism 293(3):E656-665.

40. Lago F, Gomez R, Conde J, Scotece M, Gomez-Reino JJ, Gualillo O 2011. Cardiometabolic comorbidities and rheumatic diseases: focus on the role of fat mass and adipokines. Arthritis care & research 63(8):1083-1090.

41. Christian-Kopp S, Sinha M, Rosenberg DI, Eisenhart AW, McDonald FW 2010. Antibiotic dosing for acute otitis media in children: a weighty issue. Pediatric emergency care 26(1):19-25.

42. Muluke M, Gold T, Kiefhaber K, Al-Sahli A, Celenti R, Jiang H, Cremers S, Van Dyke T, Schulze-Spate U 2016. Diet-Induced Obesity and Its Differential Impact on Periodontal Bone Loss. Journal of dental research 95(2):223-229.

43. Bocarsly ME, Powell ES, Avena NM, Hoebel BG 2010. High-fructose corn syrup causes characteristics of obesity in rats: increased body weight, body fat and triglyceride levels. Pharmacology, biochemistry, and behavior 97(1):101-106.

44. Abdussalam A, Elshenawy OH, Bin Jardan YA, El-Kadi AO, Brocks DR 2017. The obesogenic potency of various high caloric diet compositions in male rats, and their effects on expression of liver and kidney proteins involved in drug elimination. Journal of pharmaceutical sciences.

45. Lutz TA, Woods SC 2012. Overview of animal models of obesity. Current protocols in pharmacology Chapter 5:Unit5 61.

46. Fedder DO, Koro CE, L'Italien GJ 2002. New National Cholesterol Education Program III guidelines for primary prevention lipid-lowering drug therapy: projected impact on the size, sex, and age distribution of the treatment-eligible population. Circulation 105(2):152-156.

47. Maji D, Shaikh S, Solanki D, Gaurav K 2013. Safety of statins. Indian journal of endocrinology and metabolism 17(4):636-646.

48. Pahan K 2006. Lipid-lowering drugs. Cellular and molecular life sciences : CMLS 63(10):1165-1178.

49. Seabra MC 1998. Membrane association and targeting of prenylated Ras-like GTPases. Cellular signalling 10(3):167-172.

50. Barter PJ, Rye KA 2016. New Era of Lipid-Lowering Drugs. Pharmacol Rev 68(2):458-475.

51. Ahmed SM, Clasen ME, Donnelly JE 1998. Management of dyslipidemia in adults. American family physician 57(9):2192-2204, 2207-2198.

52. Wadden TA, Neiberg RH, Wing RR, Clark JM, Delahanty LM, Hill JO, Krakoff J, Otto A, Ryan DH, Vitolins MZ, Look ARG 2011. Four-year weight losses in the Look AHEAD study: factors associated with long-term success. Obesity 19(10):1987-1998.

53. Wadden TA, Volger S, Tsai AG, Sarwer DB, Berkowitz RI, Diewald LK, Carvajal R, Moran CH, Vetter M, Group P-UR 2013. Managing obesity in primary care practice: an overview with perspective from the POWER-UP study. Int J Obes (Lond) 37 Suppl 1:S3-11.

54. Aguilar-Olivos NE, Almeda-Valdes P, Aguilar-Salinas CA, Uribe M, Mendez-Sanchez N 2016. The role of bariatric surgery in the management of nonalcoholic fatty liver disease and metabolic syndrome. Metabolism 65(8):1196-1207.

55. Sweeting AN, Hocking SL, Markovic TP 2015. Pharmacotherapy for the treatment of obesity. Molecular and cellular endocrinology 418 Pt 2:173-183.

56. Gilbert EW, Wolfe BM 2012. Bariatric surgery for the management of obesity: state of the field. Plastic and reconstructive surgery 130(4):948-954.

57. Brocks DR, Hamdy DA, Ben-Eltriki M, Patel JP, El-Kadi AO 2013. Effect of rat serum lipoproteins on mRNA levels and amiodarone metabolism by cultured primary rat hepatocytes. Journal of pharmaceutical sciences 102(1):262-270.

58. Brill MJ, Diepstraten J, van Rongen A, van Kralingen S, van den Anker JN, Knibbe CA 2012. Impact of obesity on drug metabolism and elimination in adults and children. Clinical pharmacokinetics 51(5):277-304.

59. Patel JP, Brocks DR 2010. Effect of experimental hyperlipidaemia on the electrocardiographic effects of repeated doses of halofantrine in rats. Br J Pharmacol 161(6):1427-1440.

60. McIntosh MP, Batey AJ, Coker SJ, Porter CJ, Charman WN 2004. Evaluation of the impact of altered lipoprotein binding conditions on halofantrine induced QTc interval prolongation in an anaesthetized rabbit model. The Journal of pharmacy and pharmacology 56(1):69-77.

61. Aliabadi HM, Spencer TJ, Mahdipoor P, Lavasanifar A, Brocks DR 2006. Insights into the effects of hyperlipoproteinemia on cyclosporine A biodistribution and relationship to renal function. The AAPS Journal 8(4):E672-E681.

62. Shayeganpour A, Korashy H, Patel JP, El-Kadi AO, Brocks DR 2008. The impact of experimental hyperlipidemia on the distribution and metabolism of amiodarone in rat. International journal of pharmaceutics 361(1-2):78-86.

63. Fukushima K, Kobuchi S, Shibata M, Takada K, Sugioka N 2011. Decrease in brain distribution of fluvoxamine in experimental hyperlipidemic rats. Journal of pharmacy & pharmaceutical sciences : a publication of the Canadian Society for Pharmaceutical Sciences, Societe canadienne des sciences pharmaceutiques 14(3):414-424.

64. Lee JH, Oh JH, Lee YJ 2011. Effects of experimental hyperlipidaemia on the pharmacokinetics of docetaxel in rats. Xenobiotica 41(9):797-804.

65. Kobuchi S, Fukushima K, Shibata M, Ito Y, Sugioka N, Takada K 2011. Pharmacokinetics of clomipramine, an antidepressant, in poloxamer 407-induced hyperlipidaemic model rats. The Journal of pharmacy and pharmacology 63(4):515-523.

66. Cheymol G 2000. Effects of obesity on pharmacokinetics implications for drug therapy. Clinical pharmacokinetics 39(3):215-231.

67. Bowman SL, Hudson SA, Simpson G, Munro JF, Clements JA 1986. A comparison of the pharmacokinetics of propranolol in obese and normal volunteers. British journal of clinical pharmacology 21(5):529-532.

68. Cheymol G, Weissenburger J, Poirier JM, Gellee C 1995. The pharmacokinetics of dexfenfluramine in obese and non-obese subjects. British journal of clinical pharmacology 39(6):684-687.

69. Clauson PG, Linde B 1995. Absorption of rapid-acting insulin in obese and nonobese NIDDM patients. Diabetes care 18(7):986-991.

70. Sanderink GJ, Le Liboux A, Jariwala N, Harding N, Ozoux ML, Shukla U, Montay G, Boutouyrie B, Miro A 2002. The pharmacokinetics and pharmacodynamics of enoxaparin in obese volunteers. Clinical pharmacology and therapeutics 72(3):308-318.

71. Sugioka N, Haraya K, Fukushima K, Ito Y, Takada K 2009. Effects of obesity induced by high-fat diet on the pharmacokinetics of nelfinavir, a HIV protease inhibitor, in laboratory rats. Biopharmaceutics & drug disposition 30(9):532-541.

72. Goodman LS BL, Chabner B, Knollman BC. Goodman & Gilman's the pharmacological basis of therapeutics: New York : McGraw-Hill, 2011.

73. Chung EK, Cheatham SC, Fleming MR, Healy DP, Shea KM, Kays MB 2015. Population pharmacokinetics and pharmacodynamics of piperacillin and tazobactam administered by prolonged infusion in obese and nonobese patients. Journal of clinical pharmacology 55(8):899-908.

74. Shayeganpour A, Jun AS, Brocks DR 2005. Pharmacokinetics of Amiodarone in hyperlipidemic and simulated high fat-meal rat models. Biopharmaceutics & drug disposition 26(6):249-257.

75. Brocks DR, Ala S, Aliabadi HM 2006. The effect of increased lipoprotein levels on the pharmacokinetics of cyclosporine A in the laboratory rat. Biopharmaceutics & drug disposition 27(1):7-16.

76. Imaoka S, Hashizume T, Funae Y 2005. Localization of rat cytochrome P450 in various tissues and comparison of arachidonic acid metabolism by rat P450 with that by human P450 orthologs. Drug Metab Pharmacokinet 20(6):478-484.

77. Lewis DF 2003. Human cytochromes P450 associated with the phase 1 metabolism of drugs and other xenobiotics: a compilation of substrates and inhibitors of the CYP1, CYP2 and CYP3 families. Current medicinal chemistry 10(19):1955-1972.

78. Patoine D, Levac X, Pilote S, Drolet B, Simard C 2013. Decreased CYP3A expression and activity in guinea pig models of diet-induced metabolic syndrome: is fatty liver infiltration involved? Drug metabolism and disposition: the biological fate of chemicals 41(5):952-957.

79. Kim MS, Wang S, Shen Z, Kochansky CJ, Strauss JR, Franklin RB, Vincent SH 2004. Differences in the pharmacokinetics of peroxisome proliferator-activated receptor agonists in genetically obese Zucker and sprague-dawley rats: implications of decreased glucuronidation in obese Zucker rats. Drug metabolism and disposition: the biological fate of chemicals 32(9):909-914.

80. Chaudhary IP, Tuntaterdtum S, McNamara PJ, Robertson LW, Blouin RA 1993. Effect of genetic obesity and phenobarbital treatment on the hepatic conjugation pathways. The Journal of pharmacology and experimental therapeutics 265(3):1333-1338.

81. Abernethy DR, Greenblatt DJ, Divoll M, Smith RB, Shader RI 1984. The influence of obesity on the pharmacokinetics of oral alprazolam and triazolam. Clinical pharmacokinetics 9(2):177-183.

82. Durham D, Worthley LI 2002. Cardiac arrhythmias: diagnosis and management. The tachycardias. Critical care and resuscitation : journal of the Australasian Academy of Critical Care Medicine 4(1):35-53.

83. Connolly SJ 1999. Evidence-based analysis of amiodarone efficacy and safety. Circulation 100(19):2025-2034.

84. Naccarelli GV, Wolbrette DL, Dell'Orfano JT, Patel HM, Luck JC 2000. Amiodarone: what have we learned from clinical trials? Clinical cardiology 23(2):73-82.

85. Mason JW, Hondeghem LM, Katzung BG 1984. Block of inactivated sodium channels and of depolarization-induced automaticity in guinea pig papillary muscle by amiodarone. Circulation research 55(3):278-285.

86. Singh BN 1997. Amiodarone: the expanding antiarrhythmic role and how to follow a patient on chronic therapy. Clinical cardiology 20(7):608-618.

87. Kramer SD, Gautier JC, Saudemon P 1998. Considerations on the potentiometric log P determination. Pharmaceutical research 15(8):1310-1313.

88. Lalloz MR, Byfield PG, Greenwood RM, Himsworth RL 1984. Binding of amiodarone by serum proteins and the effects of drugs, hormones and other interacting ligands. The Journal of pharmacy and pharmacology 36(6):366-372.

89. Latini R, Bizzi A, Cini M, Veneroni E, Marchi S, Riva E 1987. Amiodarone and desethylamiodarone tissue uptake in rats chronically treated with amiodarone is non-linear with the dose. The Journal of pharmacy and pharmacology 39(6):426-431.

90. Wyss PA, Moor MJ, Bickel MH 1990. Single-dose kinetics of tissue distribution, excretion and metabolism of amiodarone in rats. The Journal of pharmacology and experimental therapeutics 254(2):502-507.

91. Nattel S, Davies M, Quantz M 1988. The antiarrhythmic efficacy of amiodarone and desethylamiodarone, alone and in combination, in dogs with acute myocardial infarction. Circulation 77(1):200-208.

92. Trivier JM, Libersa C, Belloc C, Lhermitte M 1993. Amiodarone N-deethylation in human liver microsomes: involvement of cytochrome P450 3A enzymes (first report). Life sciences 52(10):PL91-96.

93. Fabre G, Julian B, Saint-Aubert B, Joyeux H, Berger Y 1993. Evidence for CYP3A-mediated N-deethylation of amiodarone in human liver microsomal fractions. Drug metabolism and disposition: the biological fate of chemicals 21(6):978-985.

94. Elsherbiny ME, El-Kadi AO, Brocks DR 2008. The metabolism of amiodarone by various CYP isoenzymes of human and rat, and the inhibitory influence of ketoconazole. Journal of pharmacy & pharmaceutical sciences : a publication of the Canadian Society for Pharmaceutical Sciences, Societe canadienne des sciences pharmaceutiques 11(1):147-159.

95. Shayeganpour A, El-Kadi AO, Brocks DR 2006. Determination of the enzyme(s) involved in the metabolism of amiodarone in liver and intestine of rat: the contribution of cytochrome P450 3A isoforms. Drug metabolism and disposition: the biological fate of chemicals 34(1):43-50.

96. Elsherbiny ME, Brocks DR 2010. The effect of CYP1A induction on amiodarone disposition in the rat. Journal of pharmaceutical sciences 99(1):539-548.

97. Pamukcu B, Lip GY 2011. Dronedarone as a new treatment option for atrial fibrillation patients: pharmacokinetics, pharmacodynamics and clinical practice. Expert opinion on pharmacotherapy 12(1):131-140.

98. 2011. Safety of dronedarone (Multaq). The Medical letter on drugs and therapeutics 53(1379-1380):103-104.

99. Dorian P 2010. Clinical pharmacology of dronedarone: implications for the therapy of atrial fibrillation. Journal of cardiovascular pharmacology and therapeutics 15(4 Suppl):15S-18S.

100. De Ferrari GM, Dusi V 2012. Drug safety evaluation of dronedarone in atrial fibrillation. Expert opinion on drug safety 11(6):1023-1045.

101. Patel C, Yan GX, Kowey PR 2009. Dronedarone. Circulation 120(7):636-644.

102. Jahn S, Zollner G, Lackner C, Stauber RE 2013. Severe toxic hepatitis associated with dronedarone. Current drug safety.

103. Felser A, Blum K, Lindinger PW, Bouitbir J, Krahenbuhl S 2013. Mechanisms of hepatocellular toxicity associated with dronedarone--a comparison to amiodarone. Toxicological sciences : an official journal of the Society of Toxicology 131(2):480-490.

104. Goldschlager N 2012. Dronedarone use and fatal lung toxic effects? Archives of internal medicine 172(6):517.

105. Voth ARH, Catalan JS, Manas PDB, Martinez RJA, Paolini CLP, Rodriguez MJDD 2012. A 73-Year-Old Man with Interstitial Lung Disease Due to Dronedarone. Am J Resp Crit Care 186(2):201-202.

106. Siu CW, Wong MP, Ho CM, Lam CL, Tse HF 2012. Fatal Lung Toxic Effects Related to Dronedarone Use. Archives of internal medicine 172(6):516-517.

107. Hamdy DA, Brocks DR 2009. Experimental hyperlipidemia causes an increase in the electrocardiographic changes associated with amiodarone. Journal of cardiovascular pharmacology 53(1):1-8.

108. Matuszewski BK, Constanzer ML, Chavez-Eng CM 2003. Strategies for the assessment of matrix effect in quantitative bioanalytical methods based on HPLC-MS/MS. Analytical chemistry 75(13):3019-3030.

109. Matuszewski BK 2006. Standard line slopes as a measure of a relative matrix effect in quantitative HPLC-MS bioanalysis. Journal of chromatography B, Analytical technologies in the biomedical and life sciences 830(2):293-300.

110. Jardan YA, Brocks DR 2016. The pharmacokinetics of dronedarone in normolipidemic and hyperlipidemic rats. Biopharmaceutics & drug disposition 37(6):345-351.

111. Brocks DR, Wasan KM 2002. The influence of lipids on stereoselective pharmacokinetics of halofantrine: Important implications in food-effect studies involving drugs that bind to lipoproteins. Journal of pharmaceutical sciences 91(8):1817-1826.

112. Schuhmacher J, Buhner K, Witt-Laido A 2000. Determination of the free fraction and relative free fraction of drugs strongly bound to plasma proteins. Journal of pharmaceutical sciences 89(8):1008-1021.

113. Lowry OH, Rosebrough NJ, Farr AL, Randall RJ 1951. Protein measurement with the Folin phenol reagent. J Biol Chem 193(1):265-275.

114. Ali Abdussalam. Drug Discovery and Development in the Post-Genomic Era A joint conference of: Canadian Society for Pharmaceutical Sciences Canadian Chapter of Controlled Release Society, Toronto,ON. Canada, May 26-28, 2015

115. Omura T, Sato R 1964. The Carbon Monoxide-Binding Pigment of Liver Microsomes. I. Evidence for Its Hemoprotein Nature. J Biol Chem 239:2370-2378.

116. Gibaldi M and Perrier D. City. 1982. Pharmacokinetics. ed.

117. Zhang Y, Huo M, Zhou J, Xie S 2010. PKSolver: An add-in program for pharmacokinetic and pharmacodynamic data analysis in Microsoft Excel. Computer methods and programs in biomedicine 99(3):306-314.

118. Bailer AJ 1988. Testing for the equality of area under the curves when using destructive measurement techniques. J Pharmacokinet Biopharm 16(3):303-309.

119. Venkatakrishnan K, von Moltke LL, Obach RS, Greenblatt DJ 2003. Drug metabolism and drug interactions: application and clinical value of in vitro models. Curr Drug Metab 4(5):423-459.

120. Xie C, Yang S, Zhong D, Dai X, Chen X 2011. Simultaneous determination of dronedarone and its active metabolite debutyldronedarone in human plasma by liquid chromatography–tandem mass spectrometry: Application to a pharmacokinetic study. Journal of Chromatography B 879(28):3071-3075.

121. Bolderman RW, Hermans JJR, Maessen JG 2009. Determination of the class III antiarrhythmic drugs dronedarone and amiodarone, and their principal metabolites in plasma and myocardium by high-performance liquid chromatography and UV-detection. Journal of Chromatography B 877(18-19):1727-1731.

122. Dabhi B 2013. Method Development and Validation of a Stability-Indicating RP-HPLC Method for the Quantitative Analysis of Dronedarone Hydrochloride in Pharmaceutical Tablets. Scientia Pharmaceutica 81(1):115-122.

123. Damy T, Pousset F, Caplain H, Hulot JS, Lechat P 2004. Pharmacokinetic and pharmacodynamic interactions between metoprolol and dronedarone in extensive and poor CYP2D6 metabolizers healthy subjects. Fundamental & clinical pharmacology 18(1):113-123.

124. Xie C, Yang S, Zhong D, Dai X, Chen X 2011. Simultaneous determination of dronedarone and its active metabolite debutyldronedarone in human plasma by liquid chromatography-tandem mass spectrometry: application to a pharmacokinetic study. Journal of

chromatography B, Analytical technologies in the biomedical and life sciences 879(28):3071-3075.

125. 2013. Multaq ® Product Monograph Sanofi, ed.

126. Klieber S, Arabeyre-Fabre C, Moliner P, Marti E, Mandray M, Ngo R, Ollier C, Brun P, Fabre G 2014. Identification of metabolic pathways and enzyme systems involved in the in vitro human hepatic metabolism of dronedarone, a potent new oral antiarrhythmic drug. Pharmacology research & perspectives 2(3):e00044.

127. Lee JH, Oh JH, Lee YJ 2012. Effects of experimental hyperlipidemia on the pharmacokinetics of tadalafil in rats. Journal of pharmacy & pharmaceutical sciences : a publication of the Canadian Society for Pharmaceutical Sciences, Societe canadienne des sciences pharmaceutiques 15(4):528-537.

128. Patel JP, Hamdy DA, El-Kadi AO, Brocks DR 2012. Effect of serum lipoproteins on stereoselective halofantrine metabolism by rat hepatocytes. Chirality 24(7):558-565.

129. Choi MR, Kwon MH, Cho YY, Choi HD, Kim YC, Kang HE 2014. Pharmacokinetics of tolbutamide and its metabolite 4-hydroxy tolbutamide in poloxamer 407-induced hyperlipidemic rats. Biopharmaceutics & drug disposition 35(5):264-274.

130. Brocks DR, Chaudhary HR, Ben-Eltriki M, Elsherbiny ME, El-Kadi AO 2014. Effects of serum lipoproteins on cyclosporine A cellular uptake and renal toxicity in vitro. Canadian journal of physiology and pharmacology 92(2):140-148.

131. Felser A, Stoller A, Morand R, Schnell D, Donzelli M, Terracciano L, Bouitbir J, Krahenbuhl S 2014. Hepatic toxicity of dronedarone in mice: role of mitochondrial beta-oxidation. Toxicology 323:1-9.

132. (Multaq). USFDA drug report. 2011.

133. Stack S, Nguyen DV, Casto A, Ahuja N 2015. Diffuse alveolar damage in a patient receiving dronedarone. Chest 147(4):e131-133.

134. Hernandez Voth AR, Catalan JS, Benavides Manas PD, Avila Martinez RJ, Penalver Paolini CL, Diaz de Atauri Rodriguez MJ 2012. A 73-year-old man with interstitial lung disease due to dronedarone. Am J Respir Crit Care Med 186(2):201-202.

135. Quaglino D, Ha HR, Duner E, Bruttomesso D, Bigler L, Follath F, Realdi G, Pettenazzo A, Baritussio A 2004. Effects of metabolites and analogs of amiodarone on alveolar macrophages: structure-activity relationship. American journal of physiology Lung cellular and molecular physiology 287(2):L438-447.

136. Gabr RQ, El-Sherbeni AA, Ben-Eltriki M, El-Kadi AO, Brocks DR 2017. Pharmacokinetics of metformin in the rat: assessment of the effect of hyperlipidemia and evidence for its metabolism to guanylurea. Canadian journal of physiology and pharmacology 95(5):530-538.

137. Yoshinari K, Takagi S, Yoshimasa T, Sugatani J, Miwa M 2006. Hepatic CYP3A expression is attenuated in obese mice fed a high-fat diet. Pharmaceutical research 23(6):1188-1200.

138. Hong Y, Chia YM, Yeo RH, Venkatesan G, Koh SK, Chai CL, Zhou L, Kojodjojo P, Chan EC 2016. Inactivation of Human Cytochrome P450 3A4 and 3A5 by Dronedarone and N-Desbutyl Dronedarone. Molecular pharmacology 89(1):1-13.